Operational limits of 2XL monopile installation

A comparative analysis of side and stern installation

A.M. (Anke Marij) Elzinga

Delft University of Technology

TU Delft

ULSTEIN®

Thesis for the degree of MSc in Marine Technology in the specialisation of *Ship Design*

Operational limits of 2XL monopile installation

A comparative analysis of side and stern installation

by

A.M. (Anke Marij) Elzinga

Performed at

Ulstein Design & Solutions B.V.

to obtain the degree of Master of Science in Marine Technology at Delft University of Technology,
to be defended publicly on March 4, 2024 at 14:00.

Report number:	**MT.23/24.022.M**
Student number:	4594983
Thesis exam committee:	
Chair - TU Delft:	Dr. A.A. Kana
Supervisor - TU Delft:	Ir. J.L. Gelling
Supervisor - Ulstein Design & Solutions B.V.	Ir. J.D. Stroo
Project Duration:	February 16, 2023 - March 4, 2024
Faculty:	Faculty of Mechanical Engineering (ME)
Department:	Maritime and Transport Technology

An electronic version of this thesis is available at `https://repository.tudelft.nl/`

Cover: Artist impression of stern installation of monopiles by a heavy lift crane vessel

TU Delft

ULSTEIN®

Preface

This thesis marks the end of the years as a bachelor and master student of Marine Technology in Delft, which after high school graduation felt as a natural choice with my nautical family background. During the past year, this project allowed me to work on the interface of ship design and ship hydromechanics, a field which has a particular interest to me. This project dives into the operational limits of side and stern installation methods of large monopiles by heavy lift crane vessels, which are incredibly relevant with the development of offshore wind farms worldwide. This development of the offshore wind farms comes with the trend of designing larger offshore wind turbines, and therefore larger foundations of these turbines. The installation of large monopiles by floating vessels, such as heavy lift crane vessels, induces coupled dynamic behaviour and might cause pendulum effects and resonance behaviour, which is the focus of this project as a comparative analysis between side and stern installation.

This project is carried out at Ulstein Design & Solutions in Rotterdam and would not have been possible without the help of multiple people. I would like to thank Jaap Gelling for his feedback and guidance throughout the thesis, Ko Stroo for his time to help me with my questions and give advice on the approach of different problems, Cristian Rossetti for all the support with OrcaFlex, and finally Austin Kana for his new perspectives during discussions. Additionally, I would like to thank my family and friends for all the support and valuable advice.

A.M. (Anke Marij) Elzinga
Delft, February 2024

Abstract

The offshore wind energy sector is rapidly growing with an increase in the capacity of offshore wind turbines (OWT). This implies an increase in size and weight of OWTs. The commonly applied fixed-bottom foundation, the monopile (MP), is therefore also increasing in dimensions. MPs are widely applied due to their relatively low costs, simplicity, and easy installation. MPs used to be installed from jack-up vessels, but are nowadays installed from floating vessels. The vessel forms a multi-body system with the MP and crane, inducing coupled dynamic behaviour. Pendulum effects of the MP might occur. During lowering, hydrodynamic wave loads induce motion on the multi-body system. The MP can be installed at the side or stern of the vessel. Stern installation with the MP longitudinally on deck is in development. Currently, the dominant method is side installation with the MP placed transversely on deck. Therefore, this research focuses on the dynamic behaviour of XXL (2XL) MPs for water depths up to 70 metres and eventually the comparison in terms of operational limits between side and stern installation.

A case study is performed for an UDSBV (Ulstein Design and Solutions B.V.) heavy lift crane vessel including a crane with a capacity of 5000 tonnes and a pile gripper. The MP is installed at offshore wind farm (OWF) Hornsea on the North Sea. The MP has a mass of 2300 tonnes with a diameter of 11 metres and a length of 100 metres. The hindcast data of the North Sea are applied in combination with a JONSWAP spectrum. Steady-state time-domain simulations for side and stern installation are performed using an implicit time-integration scheme for 5 loading conditions: horizontal position of the MP, 45° upended MP, fully upended MP, the MP halfway water depth, and lastly the MP 3 metres above seabed.

In OrcaFlex, the partly submerged 2XL MP is modelled hybridly: it consists of a vessel object, a 6 degrees of freedom (6D) buoy and a line object, to model respectively hydrodynamic damping, the buoyancy, and the contact with the pile gripper ring. The hydrodynamic damping includes the tip vortex damping derived by Computational Fluid Dynamics (CFD) tests of Ulstein and Heerema. Other hydrodynamic properties, such as added mass and damping matrices and load, displacement, and sea state Response Amplitude Operators (RAO) are generated from HydroD. The MP is modelled as a line object in case of a horizontal position and a 45° upended position. The contact with the MP and the pile gripper ring is modelled by 4 rollers. The applied model is validated using partial validation using design values for the radii of gyration resulting from the loading conditions and face and graphical validation for the numerical simulations. Finally, the behaviour of the MP and the rigging is validated by modal analyses provided by OrcaFlex and by analytical pendulum calculations applying the mathematical models of the simple, physical and double pendulum.

The assessment of operational limits during marine operations is required in the planning phase. The operational limits are expressed as the dynamic amplification factor (DAF) and the dynamic utilisation factor (DUF) for the vertical crane tip force, and the roll and pitch angle of the crane tip. Additionally, a new DUF is defined for the lateral pile gripper interface loads. It is found that the pitch angle is generally governing the operational limits for side and stern installation except during upending the MP with stern installation. For stern installation, during upending, the roll angle can be governing, due to the longitudinal position of the monopile. During the lowering stage, both installation sequences show a similar course in the operational limits plotted against the spectral peak periods (T_p). For the fully upended MP, the T_p around 7.2 seconds is critical due to the natural period of the MP. Additionally, these shorter T_p occur regularly on the North Sea. However, the most critical loading condition is the MP halfway the water depth: the operational limits are most exceeded for both installation sequences. In the T_p range of $12.0 - 15.0$ seconds, the natural period of the double pendulum of the falls and MP coincides with the natural period of the vessel and the T_p. This T_p range corresponds with long waves which do not occur frequently on the North Sea. When the monopile is almost at the seabed, the operational limits are not limiting the operation for both side and stern installation. In conclusion, in terms of the set operational limits, stern installation provides a larger operability window during upending. During the lowering phase, side and stern installation show a comparable performance.

Contents

Preface i

Abstract ii

List of Figures vii

List of Tables viii

Nomenclature ix

1 Introduction 1
- 1.1 Offshore wind farm development . . . 1
- 1.2 Problem statement . . . 2
- 1.3 Research objective . . . 2
  - 1.3.1 Research questions . . . 3
  - 1.3.2 Scope . . . 3
- 1.4 Societal and scientific relevance . . . 3
- 1.5 Company introduction . . . 4
- 1.6 Content description . . . 4

2 Background 5
- 2.1 Offshore wind turbines . . . 5
- 2.2 Operational limits . . . 8
  - 2.2.1 Planning phase . . . 10
  - 2.2.2 Decision making . . . 11
- 2.3 Conclusion . . . 11

3 State-of-the-art monopile installation 13
- 3.1 Monopiles . . . 13
- 3.2 Vessels . . . 15
  - 3.2.1 Jack-up vessels . . . 15
  - 3.2.2 Floating vessels . . . 16
- 3.3 Installation steps . . . 18
  - 3.3.1 Transportation to the offshore wind farm . . . 18
  - 3.3.2 Storage on deck . . . 19
  - 3.3.3 Upending methods . . . 20
  - 3.3.4 Lowering process . . . 21
  - 3.3.5 Driving/ drilling operations . . . 23
  - 3.3.6 Stern installation . . . 23
- 3.4 Conclusion . . . 24

4 Method 26
- 4.1 Methodology . . . 26
- 4.2 Tools . . . 28
  - 4.2.1 HydroD . . . 28
  - 4.2.2 OrcaFlex . . . 28
- 4.3 Input data . . . 29
  - 4.3.1 Monopile data . . . 29
  - 4.3.2 Vessel data . . . 29
  - 4.3.3 Environmental data . . . 32
- 4.4 Conclusion . . . 35

5 Model set-up **36**
5.1 Installation sequences . . . 36
5.1.1 Side installation . . . 36
5.1.2 Stern installation . . . 36
5.2 Loading conditions . . . 38
5.2.1 Side installation . . . 39
5.2.2 Stern installation . . . 39
5.2.3 Free surface moment . . . 39
5.3 Hydrodynamic properties . . . 40
5.4 OrcaFlex model . . . 41
5.4.1 Monopile . . . 41
5.4.2 Mission equipment . . . 43
5.4.3 Wave shielding . . . 44
5.4.4 DP system . . . 44
5.5 Hydrodynamic damping . . . 44
5.6 Conclusion . . . 45

6 Numerical simulations **46**
6.1 Static simulation . . . 46
6.2 Dynamic simulation . . . 46
6.2.1 Implicit time-domain simulation . . . 47
6.2.2 Explicit time-domain simulation . . . 47
6.2.3 Simulation approach . . . 47
6.3 Conclusion . . . 50

7 Validation and verification **51**
7.1 Loading conditions . . . 51
7.2 Hydrodynamic properties . . . 53
7.3 Wave shielding . . . 53
7.4 Numerical simulation . . . 54
7.5 Pendulum calculations . . . 54
7.5.1 Modal analysis . . . 54
7.5.2 Analytical approach . . . 55
7.6 Conclusion . . . 57

8 Operational limits **58**
8.1 Crane tip forces . . . 59
8.2 Pile gripper interface loads . . . 60
8.3 Results . . . 60
8.3.1 Side installation . . . 60
8.3.2 Stern installation . . . 62
8.3.3 Comparison side and stern installation . . . 62
8.3.4 Change of maximum roll and pitch angle . . . 63
8.4 Conclusion . . . 64

9 Discussion **65**
9.1 Relevance of the results . . . 65
9.2 Limitations of the results . . . 65
9.3 Recommendations for further research . . . 65
9.3.1 Installation sequences . . . 65
9.3.2 Model set-up . . . 66
9.3.3 Numerical simulations . . . 66

10 Conclusion **67**

References **71**

A Modal analysis **77**

B Additional results **78**
B.1 Side installation 78
B.2 Stern installation 80
B.3 Side installation - max. pitch angle of 6 ° 82
B.4 Stern installation - max. pitch angle of 6 ° 83

C Load and displacement RAOs **84**

List of Figures

1.1 World non-fossil energy supply by source [3] . . . 1

2.1 Offshore wind turbine [12] . . . 5
2.2 Fixed foundations for offshore wind turbines [19] . . . 6
2.3 Globally installed fixed foundations based on the data of 4C Offshore (2022) . . . 7
2.4 Globally planned fixed foundations in FEED and tender or EPCI phase based on the data of 4C Offshore (2022) . . . 7
2.5 Floating foundations for offshore wind turbines [24] . . . 8
2.6 Flowchart of DNV to determine whether the operation is weather (un)restricted [26] . . . 9
2.7 Multi-body system of vessel, monopile and mission equipment during the lowering phase 10
2.8 General methodology to establish the allowable limits of sea states [25] . . . 12

3.1 Orion of DEME installing monopiles with a diameter of 9.5 metres at Arcadis Ost in June 2022 [42] . . . 14
3.2 Categorisation of dimensions and weight of monopiles by Ulstein . . . 14
3.3 Expected market development for L, XL, 2XL, 3XL MPs in period $2000 - 2040$ by Ulstein (J.D. Stroo, 2023) . . . 15
3.4 Development of monopile projects for water depth against foundation weight [1] . . . 15
3.5 Angle definition for wave direction and slewing angle for the crane boom . . . 16
3.6 Jack-up vessel: Vole au Vent (by M. Ibeler, Ørsted) . . . 17
3.7 Heavy lift vessel: catamaran Svanen [65] . . . 17
3.8 Heavy lift vessel: Bokalift 2 [66] . . . 17
3.9 Alfa Lift [67] . . . 17
3.10 Heavy lift crane vessel: Aegir [68] . . . 18
3.11 Transport vessel with longitudinal storage of monopiles [71] . . . 19
3.12 Concept design of a foundation installation vessel with vertical storage [72] . . . 20
3.13 Monopile upending and lifting tool of SpanSet Axzion [76] . . . 21
3.14 Flanged Pile Upending Tool by Iqip [77] . . . 21
3.15 3D structure of the cam-type clamp tool for upending monopiles [78] . . . 22
3.16 Upending tool placed on a monopile [78] . . . 22
3.17 Motion compensated pile gripper [79] . . . 22
3.18 Pile driving of a monopile [18] . . . 23
3.19 Shielding analysis for stern and side installation for different headings by Huisman Equipment [84] . . . 24
3.20 U-stern concept by Ulstein . . . 24

4.1 Flowchart of the applied methodology to establish the operational limits: from definition of installation sequences and loading conditions to analysis of responses at relevant locations and comparison of installation sequences. *Note: the colours indicate the path to be followed. Follow the colour at the start and finish the entire path, switching to another colour in between is not allowed.* . . . 27
4.2 HX118 with Huisman TMC crane, upending a MP in the U-stern (Ulstein, 2023) . . . 29
4.3 Recess in stern (Ulstein, 2023) . . . 30
4.4 Axis convention for respectively a thick-walled cylinder and cylinder . . . 31
4.5 Mass [tonnes] of mission equipment and monopile . . . 32
4.6 Local VCG [m] of mission equipment and monopile . . . 32
4.7 Seasonal mean H_s in metres during respectively January, April, July, and October on the North Sea using MetOcean View Hindcast ([97], [98]) . . . 33

4.8 Probability function and cumulative probability of H_s [m] based on empirical data of nautical zone 11 (North Sea) [96] . . . 33
4.9 Wave scatter diagram based on empirical data of nautical zone 11 (North Sea) [96] . . . 34
4.10 Nautical zones used for estimating long-term wave distribution parameters [96] . . . 34

5.1 Stages of upending and lowering of a monopile towards the seabed for side installation 37
5.2 Stages of upending and lowering of a monopile towards the seabed for stern installation 38
5.3 Modelling of monopile in OrcaFlex as line object for horizontal and upended monopile . 41
5.4 Modelling of monopile in OrcaFlex as hybrid buoy-vessel-line object for partly submergence of monopile . . . 42
5.5 Wave slope estimation of OrcaFlex to calculate buoyancy based on [105] . . . 42
5.6 Modelling of pile gripper contact with monopile in OrcaFlex by four (pink) rollers with constraint . . . 44
5.7 Assessment of tip vortex damping by model tests and CFD calculations . . . 45

6.1 Simulation time of the time-domain simulations solved with the generalised-α integration scheme . . . 48
6.2 Dynamic x at the crane tip [m] . . . 48
6.3 Dynamic y at the crane tip [m] . . . 48
6.4 Dynamic z at the crane tip [m] . . . 49
6.5 Dynamic x at the monopile tip [m] . . . 49
6.6 Dynamic y at the monopile tip [m] . . . 50
6.7 Dynamic z at the monopile tip [m] . . . 50

7.1 Schematic representation of the simple and physical pendulum with the characteristics of the 2XL MP . . . 55
7.2 Schematic representation of the double pendulum with the characteristics of the falls, the crane hook, and the 2XL MP . . . 56
7.3 Natural periods for multiple levels of submergence of the monopile . . . 57

8.1 Locations for response analysis with the position of the pile gripper ring at starboard of the vessel for side installation and at the recess for stern installation . . . 58
8.2 Pitch angle [°] for H_s = 2 metres for side and stern installation with a maximum allowable limit of 3.5 ° . . . 63
8.3 Pitch angle [°] for H_s = 2 metres for side and stern installation with a maximum allowable limit of 6 ° . . . 63

B.1 Roll angle [°] for side installation . . . 78
B.2 Pitch angle [°] for side installation . . . 78
B.3 DAF of crane tip [-] for side installation . . . 79
B.4 DUF of crane tip [-] for side installation . . . 79
B.5 DUF of pile gripper in x-direction [-] for side installation . . . 79
B.6 DUF of pile gripper in y-direction [-] for side installation . . . 79
B.7 Roll angle [°] for stern installation . . . 80
B.8 Pitch angle [°] for stern installation . . . 80
B.9 DAF of crane tip [-] for stern installation . . . 80
B.10 DUF of crane tip [-] for stern installation . . . 81
B.11 DUF of pile gripper in x-direction [-] for stern installation . . . 81
B.12 DUF of pile gripper in y-direction [-] for stern installation . . . 81
B.13 Roll angle [°] for side installation . . . 82
B.14 Pitch angle [°] for side installation . . . 82
B.15 DUF of crane tip [-] for side installation . . . 82
B.16 Roll angle [°] for stern installation . . . 83
B.17 Pitch angle [°] for stern installation . . . 83
B.18 DUF of crane tip [-] for stern installation . . . 83

List of Tables

3.1 Examples of jack-up vessels ([47], [48], [49], [50]) . . . 16
3.2 Examples of monohulls ([53], [54], [55], [56], [57], [58], [59]) . . . 16
3.3 Examples of SSCVs ([61], [62], [63]) . . . 17
3.4 Relative characteristics of jack-up vessels, monohulls, SSCVs, and sheerlegs ([60], [64]) 18

4.1 2XL monopile characteristics . . . 29
4.2 Characteristics of heavy lift crane vessel HX118 . . . 29
4.3 Crane characteristics based on [93] . . . 30
4.4 Simulated peak period T_p [s] based on hindcast data of Hornsea Wind Farm ([97], [99]) 35

5.1 Reference loading conditions for side installation . . . 39
5.2 Reference loading conditions for stern installation . . . 39
5.3 Sloshing periods based on [103] and [104] . . . 40

7.1 Difference [%] due to exclusion of buoyancy for the loading condition with a partly submerged, tapered monopile for side and stern installation . . . 51
7.2 Ratio of radii of gyration and main dimension of the reference vessel for the loading conditions for side and stern installation . . . 52

8.1 Operability with a maximum roll angle and pitch angle of $3.5°$, maximum crane tip DAF of 1.15, crane tip DUF of 1 and pile gripper DUF for x- and y-direction of 1 for range of T_p between 5.0 and 15.0 seconds for a fully upended 2XL MP, a 2XL MP halfway water depth, and 2XL MP 3 metres above seabed for side installation . . . 61
8.2 Operability with a maximum roll and pitch angle of 3.5 °, maximum crane tip DAF of 1.15, and crane tip DUF of 1 for range of T_p between 5.0 and 15.0 seconds for a horizontal placed and $45°$ upended 2XL MP for side installation and stern installation . . . 61
8.3 Operability with a maximum roll and pitch angle of $3.5°$, maximum crane tip DAF of 1.15, crane tip DUF of 1 and pile gripper DUF for x- and y-direction of 1 for range of T_p between 5.0 and 15.0 seconds for a fully upended 2XL MP, a 2XL MP halfway water depth, and 2XL MP 3 metres above seabed for stern installation . . . 62

Nomenclature

Abbreviations

Abbreviation	Definition
2D	Two-dimensional
2XL	XXL
3D	Three-dimensional
3XL	XXXL
6D	Six degrees of freedom
BV	Bureau Veritas
CFD	Computational Fluid Dynamics
CoG	Centre of Gravity
DAF	Dynamic Amplification Factor
DNV	Det Norske Veritas
DP	Dynamic Positioning
DUF	Dynamic Utilisation Factor
EPCI	Engineering, Procurement, Construction, and Installation
FEED	Front-end Engineering Design
FSM	Free Surface Moment
GE	General
GRG	Generalised Reduced Gradient
GW	Gigawatt
HLV	Heavy Lift Vessel
IEA	International Energy Agency
JONSWAP	Joint North Sea Wave Observation Project
KC	Keulegan-Carpenter
kW	Kilowatt
LCG	Longitudinal Centre of Gravity
LI	Lifting
MP	Monopile
MPM	Most Probable Maximum
MW	Megawatt
MWL	Mean Water Level
NPD	Norwegian Petroleum Dictorate
OCIMF	Oil Companies International Marine Forum
OWF	Offshore Wind Farm
OWFA	Offshore Wind Foundations Alliance
OWT	Offshore Wind Turbine
PM	Pierson-Moskowitz
QTF	Quadratic Transfer Function
RAO	Response Amplitude Operator
SHL	Static Hook Load
SSCV	Semi-submersible Crane Vessels
TCG	Transverse Centre of Gravity
TLP	Tension Leg Platform
TMC	Tube Mounted Crane
TP	Transition Piece
TWH	Terrawatt-hour
UDSBV	Ulstein Design and Solutions B.V.

Abbreviation	Definition
VCG	Vertical Centre of Gravity
WLL	Working Load Limit
WTG	Wind Turbine Generator

Symbols

Symbol	Definition	Unit
A	Drag area	[m^2]
a	Amplitude	[m]
A_a	Drag area for axial direction	[m^2]
A_n	Drag area for normal direction	[m^2]
B_{recess}	Breadth of recess	[m]
$B_{tip\ linear}$	Linearised tip vortex damping	[kNs/m]
$B_{tip\ quadratic}$	Quadratic tip vortex damping	[kNs/m^2]
B_{vessel}	Breadth of vessel	[m]
C	System damping load	[N]
C_a	Added mass coefficient	[-]
C_d	Drag coefficient	[-]
C_{Da}^f	Drag force coefficient for axial direction	[-]
C_{Dn}^f	Drag force coefficient for normal direction	[-]
C_m	Inertia coefficient	[-]
D	Diameter	[m]
D_{MP}	Diameter of monopile	[m]
D_{recess}	Depth of recess	[m]
f	Frequency	[Hz]
F	Fluid force on a body	[N]
f_{Dx}	Drag force in local x-direction	[N]
f_{Dy}	Drag force in local y-direction	[N]
f_{Dz}	Drag force in local z-direction	[N]
F_E	External load	[N]
f_m	Peak frequency	[Hz]
F_x	Crane tip force in global x-direction	[kN]
F_y	Crane tip force in global y-direction	[kN]
F_z	Crane tip force in global z-direction	[kN]
g	Gravity acceleration	[m/s^2]
h	Height cylinder	[m]
h	Height above mean water level	[m]
h	Water column height in the moonpool	[m]
H_s	Significant wave height	[m]
I	Inertia matrix	[t] and [tm^2]
${}^cI_h$	Hull inertia matrix relative to global origin	[t] and [tm^2]
I_s	Structure inertia matrix	[t] and [tm^2]
I_{xx}	Mass moment of inertia about x-axis	[tm^2]
I_{yy}	Mass moment of inertia about y-axis	[tm^2]
I_{zz}	Mass moment of inertia about z-axis	[tm^2]
J_n	Coefficient for sloshing risk assessment	[-]
k	Ratio maximum tank breadth and tank height	[-]
K	System stiffness load	[N]
k	Stiffness	[N/m]
K_L	Linear tip vortex damping coefficient	[kNs/m$^{3.5}$]
K_Q	Quadratic tip vortex damping coefficient	[kNs^2/m^4]
K_{xx}	Radius of gyration about x-axis	[m]
K_{yy}	Radius of gyration about y-axis	[m]
K_{zz}	Radius of gyration about z-axis	[m]
KC	Keulegan Carpenter number	[-]
L	Length	[m]
L_{boom}	Length of crane boom	[m]
L_{MP}	Length of monopile	[m]
L_{recess}	Length of recess	[m]

Symbol	Definition	Unit
L_{vessel}	Length of vessel	[m]
m	Mass	[kg]
m_h	Mass hull	[t]
M	System inertia load	[N]
M_{boom}	Mass crane boom	[t]
M_{fs}	Free surface moment	[mt]
M_{MP}	Mass monopile	[kg] or [t]
$M_{rigging}$	Mass rigging and crane hook	[kg] or [t]
$M_{slewing\ column}$	Mass slewing column	[t]
n	Number of wave length contained by the moonpool	[-]
n	Node number	[-]
p	Proportion of the submerged cylinder volume	[-]
r	Radius	[m]
r_i	Inner radius	[m]
r_o	Outer radius	[m]
R	Rotation matrix	[-]
Re	Reynolds number	[-]
$S(f)$	Wave spectrum	[m^2/Hz]
T	Draught of monopile	[m]
T	Oscillation period	[s]
t	Thickness monopile wall	[m]
t	Time step	[s]
T_C	Estimated maximum contingency time	[h]
T_n	Natural period	[s]
$T_{l/r}$	Sloshing period	[s]
T_l	Longitudinal period	[s]
T_p	Spectral peak period	[s]
T_{POP}	Planned operation period	[h]
T_R	Reference period	[h]
T_z	Zero up-crossing period	[s]
T_t	Tranversal period	[s]
u	Fluid velocity relative to the earth	[m/s]
V	Tip velocity of monopile	[m/s]
V	Volume	[m^3]
v	Velocity of object	[m/s]
v_n	Component of object's velocity normal to cylinder axis	[m/s]
v_w	Wind speed	[m/s]
v_x	X-component of v_n	[m/s]
v_y	Y-component of v_n	[m/s]
v_z	Component of object's velocity in z-direction relative to the fluid	[m/s]
x	Position of node	[m]
α	Safety factor	[-]
α	Spectral energy parameter	[-]
β	Ratio between Re and KC	[-]
γ	Peak enhancement factor	[-]
δ	Permeability of tank	[%]
Δ	Offset	[m]
$\vec{\Delta}_{hc}$	Centre of Gravity of hull relative to global origin	[m]
θ	Pitch angle	[rad]
θ_1	Angle of inclination	[degrees]
θ_2	Angle of inclination	[degrees]
θ_{crane}	Pitch angle at crane tip	[degrees]

Symbol	Definition	Unit
Θ	Rotation matrix for pitch	[-]
λ	Wavelength	[m]
λ	Eigenvalue	
ν	Kinematic viscosity	[m^2/s]
ρ_{tank}	Density fluid in tank	[kg/m^3]
ρ_w	Density of water	[kg/m^3]
σ	Standard deviation of spectrum	[m or rad]
σ_a	Spectral width parameter	[-]
σ_b	Spectral width parameter	[-]
ϕ	Roll angle	[rad]
ϕ_{crane}	Roll angle at crane tip	[degrees]
Φ	Rotation matrix for roll	[-]
ψ	Yaw angle	[rad]
Ψ	Rotation matrix for yaw	[-]
ω	Angular frequency	[rad/s]
ω_n	Natural angular frequency of moonpool or recess	[rad/s]

1 Introduction

This chapter introduces this thesis about the operational limits of 2XL monopile installation. Therefore, there is an elaboration on the scientific and societal relevance and the problem statement with the research gap. This results in a research objective and a corresponding main research question with subquestions. Lastly, the content description of this thesis is presented.

1.1. Offshore wind farm development

Since the commissioning of the first offshore wind farm, Vindeby, in 1991 in Denmark, offshore wind energy is a rapidly growing energy sector. Nowadays, there is a need to swiftly expand the potential of offshore wind energy. This growth is expected to occur mainly in Europe and China [1]. The International Energy Agency (IEA) predicts that by 2050, offshore wind energy will be the dominant technology of electricity generation in the European Union [2]. The wind energy supply is predicted to be 13 % in the global primary energy supply, which is the second largest after the predicted 15 % share of solar energy supply, as presented in Figure 1.1 [3]. The European Union aims at having installed 450 Gigawatt (GW) by the end of 2050, and globally the installed offshore capacity is expected to be 630 GW by 2050 [4]. Where the first offshore wind turbines had a capacity of 450 kilowatt (kW), currently developed OWTs have a capacity of 10 Megawatt (MW). Within 5 years, a capacity per OWT of more than 15 MW is expected to be available [4]. This capacity growth implies an increase in the size and weight of the OWTs.

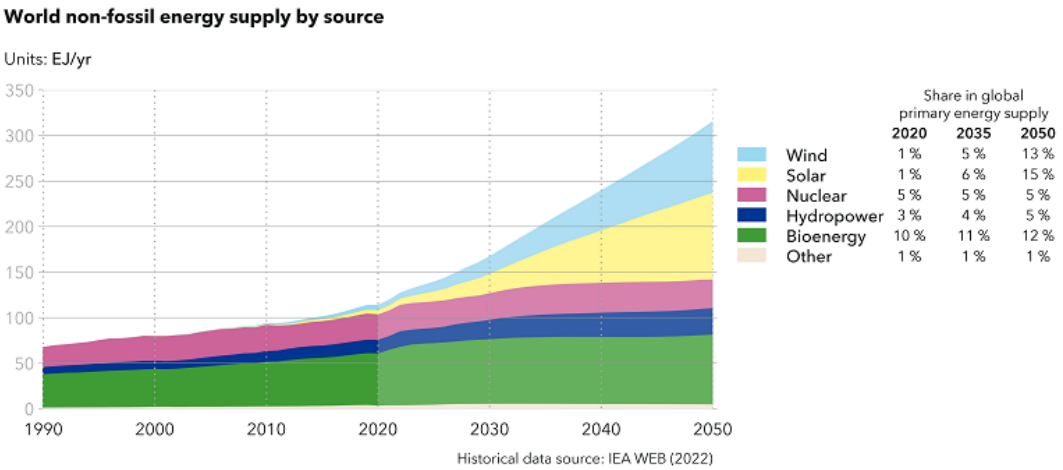

Figure 1.1: World non-fossil energy supply by source [3]

In addition, there is a tendency to locate offshore wind farm sites further offshore. Further offshore, there are more consistent wind speeds, and therefore better quality wind resources, more space, and less interaction with shipping. In most cases, sites with a water depth of less than 70 metres are suitable for OWT-fixed bottom foundations, based on 4C Offshore data, whereas floating foundations are required in deeper water [2]. For the sites with a water depth of less than 60 metres, the technical potential is 87.000 terrawatt-hour (TWh) per year, whereas for deep water this potential is 330.000 TWh per year [2]. It is expected to observe a decrease in the number of wind farms installed up to a water depth of 40 metres, while the number of turbines for water depths greater than 40 metres will increase [1].

The increasing capacity and greater water depth at OWF locations result in increasing OWTs [1]. These increasing OWTs result in larger foundations as well. A commonly applied type of fixed-bottom foundation is an MP. Different types of foundations and their applications are elaborated in Chapter 2. The boundaries of monopile design are constantly being pushed, leading to ever-growing monopiles. In 2020, the average monopile weight was 1000 tons with a diameter of 8 metres and a length of 80 metres, however, current monopiles can have a diameter of about $10 - 12$ metres with a weight of up to 2500 tonnes [1]. These mega monopiles are referred to as XL, 2XL, or XXXL (3XL) monopiles [1].

1.2. Problem statement

The mega monopiles, as described in the previous paragraph, are installed from floating vessels, which induces dynamic behaviour and coupled motions between the monopile and the vessel. Due to the growth of the dimensions and weight of the mega monopiles, the natural frequencies of the monopiles change as well. This change in characteristics influences the dynamic behaviour of the coupled system during the installation of the monopile. Therefore, it is important to investigate monopile installations.

Several studies investigated offshore operations, such as installation methods of monopiles from floating vessels ([5], [6], [7]), and the lifting and installation of jackets [8]. The lowering stage and passing the splash zone are of particular interest, due to the multi-body system and coupled dynamic behaviour. For monopile installation, the splash zone is of less interest because the buoyancy is considered small. For assets such as subsea spool pieces and subsea templates, this zone is more important. For monopiles, the splash zone can be relevant when the monopile is upended and partly submerged. However, the lowering stage is more interesting for monopiles. Monopiles are partly submerged, and wave and wind conditions both play a role: pendulum effects and damping need to be taken into account. The influence of potential damping of the MP during lowering is simulated in the time domain by Li et al. (2015) [5]. In 2016, Li conducted research on lowering an MP focusing on radiation damping and including wave short-crestedness and shielding effects with a coupled Heavy Lift Vessel (HLV) - MP approach. The considered monopile had an outer diameter of 5.7 metres. Furthermore, research on the lowering of jackets modelled in the time domain is also conducted [8]. More recent research focused on improving the time-domain simulations by developing a constant parameter time-domain model for dynamic modelling of multi-body systems [9].

The increase in length and weight of the MP influences the dynamic behaviour, such as the natural frequency. Pile model drag tests performed at Huisman Equipment in cooperation with Heerema and Ulstein show the importance of aspects of non-linear damping and tip damping ([10], [11]). The model tests have been scaled to MP with a diameter of 11 metres in reality. These damping aspects are not incorporated in previous works studied in this literature research.

In conclusion, the problem statement is twofold: firstly, the induced coupled dynamic behaviour of the ever-growing monopiles and the floating vessels, possibly resulting in resonance behaviour, which has not been studied in detail before. Secondly, the incorporation of the hydrodynamic damping of the monopile including tip vortex damping.

1.3. Research objective

The increasing dimensions of monopiles and the newly derived damping for large monopiles are neither separately nor combined studied in terms of operational limits during the upending and lowering phase

for side and stern installation for water depths between 40 and 70 metres. However, these two aspects are relevant when analysing the induced coupled behaviour of the monopile, crane, and floating vessel. Additionally, the assessment of operational limits for the mission equipment and for both side and stern installation for various environmental conditions is not explicitly found in literature. The shielding effects and wave direction are taken into account as well since these effects are considered to influence the dynamic behaviour of the multi-body system. This is done to obtain the operational limits of the offshore operation. Eventually this thesis contributes to a better understanding and estimation of monopile installation, which adds to the development of specific mission equipment and to the acceleration of the renewable energy use.

1.3.1. Research questions

The research gap results in the following research question, which is the main question throughout this master thesis:

How do side and stern installation of 2XL monopiles from heavy lift crane vessels compare in terms of operational limits during the upending and lowering stage?"

To answer this question, supporting subquestions are formulated:

1. Why are monopiles widely applied as foundation for offshore wind turbines, and which physical phenomena are relevant concerning the operational limits of monopile installation?
2. What are the state-of-the-art installation methods for 2XL monopile installation?
3. What is a suitable method for the assessment of operational limits for 2XL monopile installation?
4. Which installation sequences are preferred for 2XL monopile installation?
5. How is the applied model verified and validated?
6. What are the operational limits per installation sequence?

1.3.2. Scope

The scope of this thesis is limited by the following aspects:

- Only the installation of 2XL monopiles is considered, since these monopiles are installed from floating vessels. Smaller monopiles are installed from jack-up vessels.
- The considered type of installation vessel is a heavy lift crane vessel. These floating vessels induce dynamic behaviour.
- The installation sequence of monopiles consists of different stages, however only the upending and lowering stage are considered. Other aspects, like the transport to the site or the pile hammering phase, are excluded. The upending and lowering stage is relevant for the assessment of the dynamic behaviour of the vessel and the monopile.
- Regarding the environmental conditions, the spectral peak period T_p and the significant wave height H_s are varied. The wave direction is fixed for both installation methods, and no directional spreading is applied. The current is also excluded from the analysis.
- The operational limits of only the mission equipment are considered. Operational limits regarding human safety are excluded.

1.4. Societal and scientific relevance

The societal relevance of this research is characterised by its contribution to the energy transition. The aim of this thesis is a better understanding and estimation of the operational limits of 2XL monopile installation. This adds to the acceleration of the use of renewable energy.

In practice, the development of (the installation of) large monopiles is in full swing. However, scientifically limited literature is available about the installation of these large monopiles and the corresponding mission equipment, like monopile grippers. This thesis provides a better insight in dynamic behaviour and thus the corresponding operational limits of the mission equipment. The results and conclusion form a basis for further extensive research of even larger monopiles and the development of mission equipment.

1.5. Company introduction

This research is carried out in cooperation with Ulstein Design and Solutions B.V., located in Rotterdam. Ulstein develops vessels for offshore energy industries such as wind farm installations vessel, heavy lift crane vessels, rock installation vessels, and cable installation vessels.

1.6. Content description

Firstly, Chapter 2 zooms in on the relevant background information of OWT foundations and operational limits during marine operations such as monopile installation. This chapter is a product of the previously performed literature study, and answers the subquestion: *Why are monopiles widely applied as foundation for offshore wind turbines, and which physical phenomena are relevant concerning the operational limits of monopile installation?*.

Chapter 3 answers the subquestion: *"What are the state-of-the-art installation methods for 2XL monopile installation?"*. This chapter covers the different installation methods, installation vessels, and installation stages.

The methodology to assess the main research question is described in Chapter 4, and therefore answers the subquestion *"What is a suitable method for the assessment of operational limits for 2XL monopile installation?"*. It includes a description of the used tools and the input data of the case study.

In Chapter 5 the preferred installation sequences based on the state-of-the-art installation methods of subquestion 2 are presented, including the corresponding model set-up. Additionally, the implementation of the loading conditions of the installation sequences in the software OrcaFlex are described. The model set-up forms the basis for the time-domain simulations, which are described in Chapter 6.

The fifth subquestion: *"How is the applied model verified and validated?"* is answered in Chapter 7, which discusses the partial validation of the thesis.

Chapter 8 describes the applied operational limits and discusses the sixth subquestion: *"What are the operational limits per installation sequence?"*. It includes a definition of the operational limits and the results for both installation methods.

Chapter 9 emphasizes the relevance, the limitations and the recommendations for further research. Finally, Chapter 10 states the conclusion of the thesis, by answering the subquestions and the main research question.

2

Background

Monopiles are a type of fixed-bottom foundations for offshore wind turbines. The choice of the type of foundation depends on different aspects. Depending on the type of foundation, different installation sequences exist. During the installation, the foundation is exposed to environmental loads. These loads influence the operability of the marine operation. This chapter provides background literature on offshore wind turbines and operational limits during marine operations such as monopile installation, and therefore answers the subquestion: *"Why are monopiles widely applied as foundation for offshore wind turbines, and which physical phenomena are relevant concerning the operational limits of monopile installation?"*.

2.1. Offshore wind turbines

Offshore wind turbines consist of different parts: the support structure, the nacelle, and the rotor. The support structure is composed of a foundation, a substructure, and a tower. According to the definitions of DNV, a schematic representation of a three-bladed offshore wind turbine with a monopile foundation is depicted in Figure 2.1 [12]. The tower, nacelle, hub, and blades are also referred to as a Wind Turbine Generator (WTG).

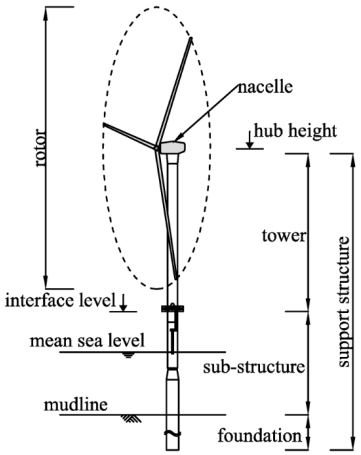

Figure 2.1: Offshore wind turbine [12]

The design of the foundation of an OWT depends on conditions at the location of the offshore wind farm. The soil type, water depth, maximum wind speed and wave height currents influence the design of a foundation [13]. The foundation of an OWT is prefabricated on the shore and transported to the installation site. Possible transportation methods are described in more detail in Section 3.3.1.

The foundation of an offshore wind turbine is a fixed-bottom or floating foundation. Examples of fixed foundations are gravity-based foundations, suction bucket monopiles, monopiles, tripods, and jackets, which are shown in Figure 2.2. Both gravity-based foundations and suction buckets depend on the seabed condition and are best suited in areas that are not suitable for monopiles. Gravity-based foundations use their own weight to resist wind and wave loading [13]. Those foundations are mostly applied in areas with shallow water where pile driving is difficult [7]. However, the related total supply and installation costs are high ([13], [7]). Tripods are suitable at locations with a water depth of up to 60 metres [14]. Jackets are structures with truss frames, which are robust and heavy. Jackets are also used as supports of oil and gas production facilities, with a water depth of up to 300 metres [15]. The transportation to the wind farm is expensive and is more widely applied in areas with deeper water (more than 50 metres) [13]. Tripods consist of three tubes at the bottom of the sea, connected to each other by a central shaft. These three tubes are tightly secured on the bottom of the sea and are therefore more robust than monopiles [13]. Monopiles are tubular structures that are the most widely applied support structures. Approximately 65% of the fixed foundations are monopiles, due to their simplicity, ease of installation, the beneficial ratio of price and quality, low production and installation costs ([2], [16], [17]). They have been installed in areas up to $40 - 60$ metres ([2], [16], [17]). Between the monopile and the wind turbine, a transition piece (TP) is placed, which has functionalities such as access to maintenance and connection to the turbine power cable [18]. In some cases, the TP is integrated with the MP which is called a TP-less monopile.

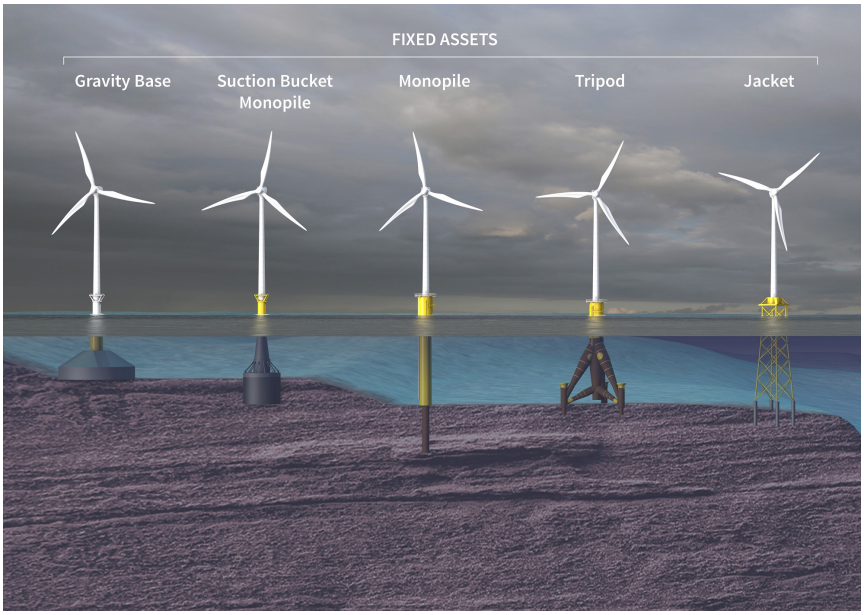

Figure 2.2: Fixed foundations for offshore wind turbines [19]

In Figure 2.3, the globally installed fixed foundations are depicted, which shows that approximately 65 % of the installed fixed foundations are monopiles. In Figure 2.4, the planned fixed foundations around the world are shown. The percentage of monopiles in the preliminary stages of a project before winning a tender or contract is about 88 % of the fixed foundations. The preliminary stages consists of a Front-End Engineering Design (FEED) stage and an Engineering, Procurement, Construction, and Installation (EPCI) stage. The FEED stage consists of planning and definitions of all the elements of the project. The scope of the FEED stage becomes part of the technical scope of the Engineering, Procurement, Construction, and Installation (EPCI) contracts [20]. These stages are relevant to consider since they provide information about trends of types of fixed foundations in the near future.

Floating foundations are upcoming and different types have been developed recently. In Figure 2.5 an offshore wind turbine on a floating barge, a semi-submersible floating foundation, an articulated multi-spar, a spar, and a tension-leg platform (TLP) are presented. These foundations are attached to the sea bottom by anchors with mooring lines. Floating foundations are particularly interesting in locations with a large water depth (60 metres or deeper) [7]. These foundations are considered cost-beneficial

for water depths larger than 100 metres [2]. In 2022, three floating offshore wind turbine farms were operational off the coasts of Scotland and Portugal. Several projects of these wind farms are planned or under construction ([21], [22]). Based on the data of 4C Offshore (2022), the percentage of floating foundations over both fixed and floating foundations is growing: 0.21 % of the installed foundations are floating, while 1.16 % of the foundations in the EPCI phase are floating, and 14.6% of the foundations in the planning phase are floating. Nevertheless, floating foundations are costly and in order to be cost-competitive with fixed foundations, technology needs to be further developed [23].

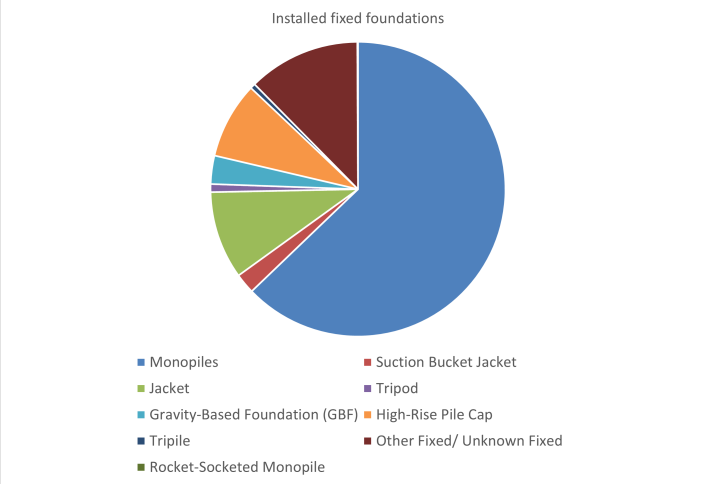

Figure 2.3: Globally installed fixed foundations based on the data of 4C Offshore (2022)

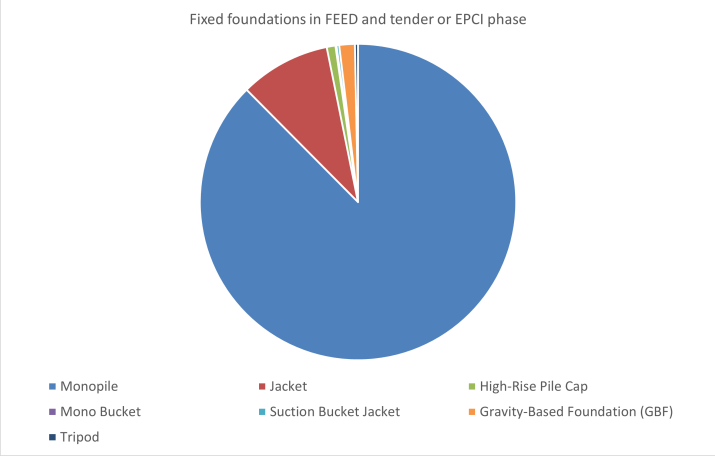

Figure 2.4: Globally planned fixed foundations in FEED and tender or EPCI phase based on the data of 4C Offshore (2022)

Figure 2.5: Floating foundations for offshore wind turbines [24]

2.2. Operational limits

Marine operations, such as installation of fixed-bottom foundations, are influenced by wave, wind, and current loads. These loads induce motion responses of the asset being installed, and the vessel installing it. The operational limits are the allowable limits of sea states and motion responses. During the preparation and execution of a marine operation, only the values of sea states and motion responses are accepted the allowable limits [25]. Other effects related to wind and wave loads, such as shielding, wave direction, and shallow water, also affect the operational limits. During a marine operation, several activities are taken into account to assess operational limits, such as the duration of the activity, continuity, and sequential execution [25].

A marine operation can either be a weather-restricted operation or a weather-unrestricted operation. A weather-restricted operation cannot exceed the duration of a reliable weather forecast, which is typically 72 hours [26]. This period is called the planned operation period (T_{POP}). In addition, the reference period (T_R) must be less than 96 hours [26]. The reference period is the sum of the operation reference period and the estimated maximum contingency time (T_C). The environmental criteria of an unrestricted operation should be based on extreme value statistics according to DNV [26]. DNV presented a flowchart to determine whether an operation is weather restricted or not (Figure 2.6) [26]. Operability represents the time available for operating in a given period and in a safe way [25]. Operational limits are used during different stages of the operation: during the planning phase as risk management of critical events, in the monitoring phase prior to execution as decision-making whether to start the operation or not, or these limits can be monitored during the execution of the operation. The planning phase and decision making are elaborated in more detail in respectively Section 2.2.1 and Section 2.2.2.

These operational limits can be based on different criteria such as personnel safety, shipping water, or slamming [27]. Safety can for example be assessed by vertical motions of, for instance, a crane tip during certain stages of the operation. Another operational limit is the station keeping capability of the vessel regarding dynamic positioning (DP) and the environmental footprint (J.D. Stroo, personal communication, April 20 2023).

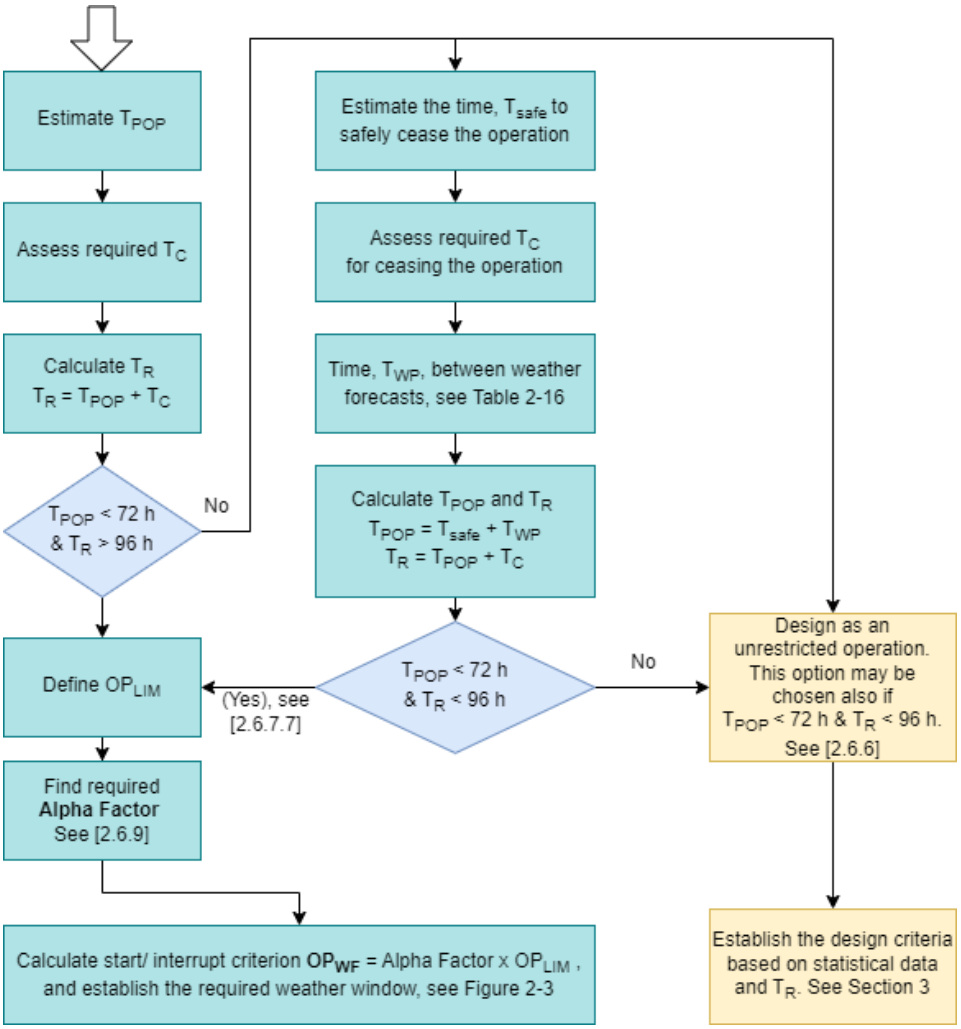

Figure 2.6: Flowchart of DNV to determine whether the operation is weather (un)restricted [26]

2.2.1. Planning phase

Risk management of critical events during the planning phase is obligatory by DNV to identify critical events of offshore activities that can lead to failures [28]. It involves the corresponding response parameters, quantification of associated risks, and suggestions for mitigation actions. The decision of whether to start the operation is based on the responses of the vessel, weather forecasts, and operational limits provided in the operational procedure [25]. These limits are then compared with the measurable sea state parameters, where the decision is made. DNV states that in the operational manual parameters such as wind speed, wave conditions, and relative motions must be provided. Therefore, the operational limits need to include both allowable limits of sea states and allowable limits of the vessel's responses. The limits are given as significant wave height (H_s), spectral peak period (T_p), and wave direction. To account for uncertainties, a safety factor α must be included, as recommended by DNV and the International Organisation for Standardisation (ISO) ([26], [29]). The alpha factor is applied for the uncertainty of weather forecasts by reducing of the limits of H_s [26].

According to Acero et al. [25], traditionally operational limits are set based on industry experience. In studies, only the critical events of marine operations are considered under certain sea states. A methodology for systematic derivation of response-based operational limits and assessment of the operability of weather-restricted marine operations for offshore wind turbine installation activities is provided, which is illustrated in Figure 2.8 [25]. This methodology is then applied to a case of installing an MP using a HLV. It is recommended that other sources of uncertainty, such as human decisions, weather forecasts, and numerical models, be addressed in future studies. Several examples of the application of this general methodology can be found in [30], [31] and [32].

The lowering phase (Figure 2.7) of an installation operation is found to be a critical event of a marine operation in multiple studies ([5], [6], [25], [33], [30], [8]). During the lowering, the vessel and the monopile form a multi-body system which creates interaction between both structures. When the monopile is hanging freely, pendulum effects might occur. The monopile acts as a pendulum with forced oscillations due to the crane tip motion. The crane tip moves with the motion of the vessel. When the forced oscillations are close to the natural frequency of the monopile, resonance occurs. Resonance causes large motions of the MP which are undesirable. The distance between the Centre of Gravity (CoG) of the monopile and the crane tip changes during the lifting operation, which influences the potential resonance motions. Therefore, the system needs to be analysed during different stages of operation.

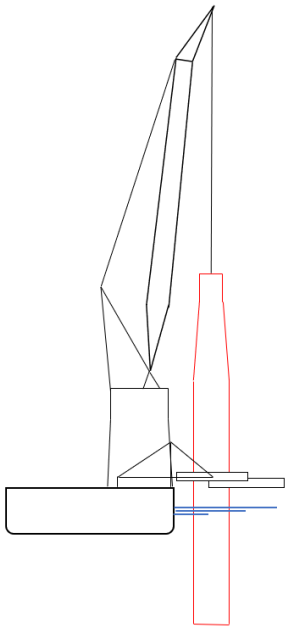

Figure 2.7: Multi-body system of vessel, monopile and mission equipment during the lowering phase

Furthermore, rocking motions can also occur. These motions are a result of cyclic loads due to wind and waves. Rocking around the CoG implies that the load will tilt until the CoG is directly under the crane hook. The angle of tilt is affected by the height of the CoG as well, and therefore changes during the lifting operation.

When an MP or another asset passes the splash zone, two criteria must be considered: the potential damage caused by slamming and the potential for snapping forces acting on the lift wire and the slings [34]. A snap force is a dynamic force within a short duration, related to sudden changes in the velocity of the lifted asset [35]. The magnitude of this force can be many times greater than the dynamic tension of the steady-state response of the system [36].

2.2.2. Decision making

Onboard decision-making is critical because safety is affected by the dynamic responses caused by certain environmental conditions. In combination with weather forecasts, operational limits can be used for on-board decision-making during marine operations [37].

Tools to monitor the motions of the vessel are developed industry wide in the past decades to improve decision-making on board and therefore ensure a safe voyage or operation of several types of vessels, for instance, offshore vessels or heavy lift transport vessels ([38], [39], [40]). Dynamic characteristics of the vessel are used in combination with 5-day weather forecasts and design limits to provide information for the crew to decide on a safe heading, speed, and route during the voyage or marine operation. This increases safety on board. The tool is based on the vessel's response characteristics in combination with the daily predicted weather conditions.

2.3. Conclusion

This chapter discusses the subquestion: *"Why are monopiles widely applied as foundation for offshore wind turbines, and which physical phenomena are relevant concerning the operational limits of monopile installation?"*. Monopiles are the most widely applied support structures because of relatively low costs, simplicity and ease of installation. Approximately 88% of the planned fixed foundations are monopiles. However, the water depth is a limiting factor. The identification of critical events during marine operations, such as monopile installation, is obligatory in the planning phase by classification societies. The critical events are identified by assessing the operational limits. These limits are the allowable limits of sea states and motion responses and therefore include H_s, T_p, and wave direction. A critical event of an installation operation is the lowering phase of the asset. The multi-body system of the vessel, crane, and monopile induces interaction between the structures and pendulum effects of the asset might occur. Rocking motions and slamming and snap forces while passing the splash zone are also possibly critical effects. Relevant physical phenomena during installation are resonance behaviour, and therefore pendulum effects, rocking motions, and slamming and snap forces. In conclusion, monopiles are known for their simplicity which makes them a commonly applied type of bottom-fixed foundations. However, particularly the lowering of a monopile during installation should be carefully assessed because of possible resonance behaviour.

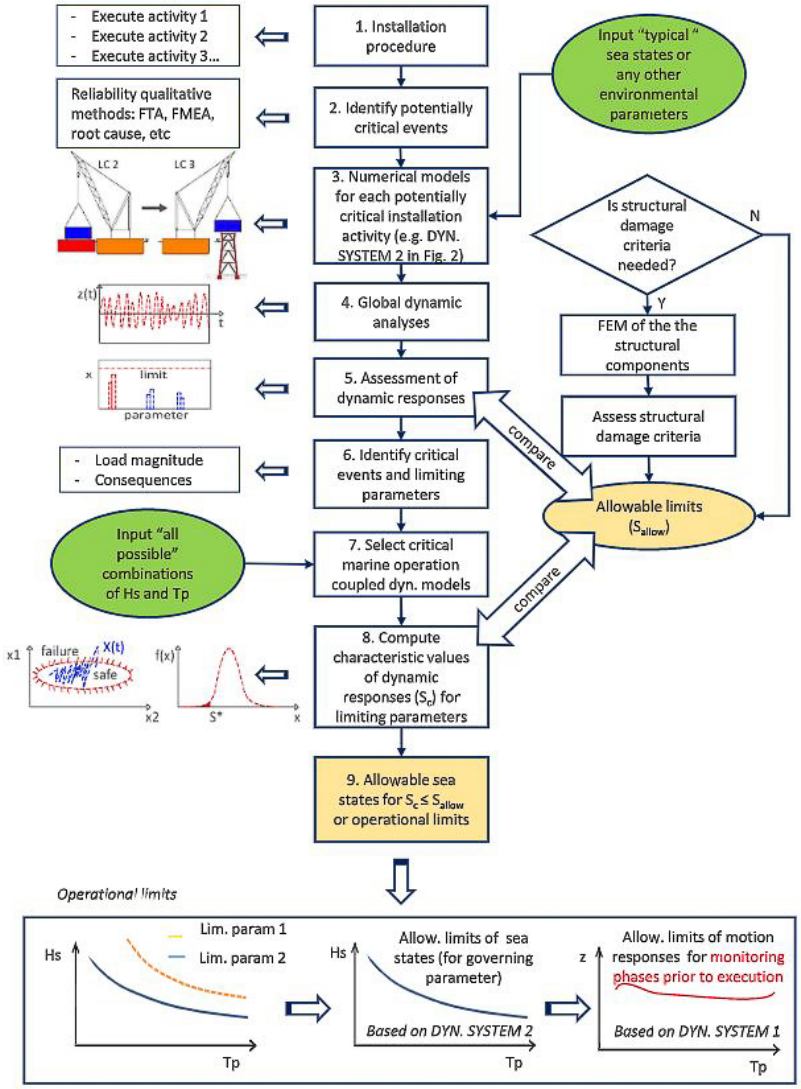

Figure 2.8: General methodology to establish the allowable limits of sea states [25]

3

State-of-the-art monopile installation

Various methods exist to install a monopile. The installation of a monopile consists of the following stages: transportation to the installation site, storage on deck, upending of the monopile to vertical position, lowering to the sea bed and driving the monopile into the sea bed. For every step, multiple options are available, and the choice depends, on among others the monopile and environment. This chapter describes the current monopile installation methods. Therefore, the definition of monopiles and various types of installation vessels are covered. At the end of the chapter the following subquestion is answered: *"What are the state-of-the-art installation methods for 2XL monopile installation?"*.

To install a fixed support structure, there are mainly three methods: component installation method, partially integrated method, and integrated method [41]. The component method implies that each component is separately manufactured, loaded and transported to the installation site where it is assembled and installed. Components can sometimes already be integrated partially, for example the tower and wind turbine, or fully integrated before it is transported to the installation site. In the integrated method the foundation, tower and turbine are assembled at a construction site and transported in once to the offshore wind farm. The component method is mainly applied for OWTs with a monopile as a foundation, whereas the partially integrated and integrated methods are currently used for gravity and suction bucket foundations [41]. The construction and installation costs of foundations are about $35 - 55\%$ of the total development costs of an offshore wind farm, as analysed by Guo et al. (2022). The installation technology directly influences the economy and safety. Each component of the OWT undergoes the following steps: onshore manufacturing, loading at the dock, maritime transportation, offshore assembly, and installation operation. This chapter covers these steps.

3.1. Monopiles

Monopiles are widely applied as fixed-bottom foundations of OWTs. The boundaries of monopile design are constantly being pushed, leading to ever-growing monopiles. In 2020, the average monopile weight was 1000 tons with a diameter of 8 metres and a length of 80 metres, however, current monopiles are able to have a diameter of about $10 - 12$ metres with a weight of up to 2500 tonnes. In June 2022, the Orion of DEME installed monopiles with a diameter of 9.5 metres at the offshore wind farm Arcadis Ost [42] as shown in Figure 3.1. Les Alizés, a heavy lift vessel of Jan de Nul with a crane capacity of 5000 tonnes, started installation of 107 monopiles with a diameter of almost 10 metres in August 2023 at Gode Wind 3 and Borkum Riffgrund 3 ([43], [44]). In the long term, the weight is expected to increase to 3000 tonnes with a monopile length of 120 metres [1]. Additionally, Ulstein predicts a trend towards larger MPs with weights around maximum 3500 tonnes and a diameter of maximum 15 metres in the coming years (up to 2040) as presented in Figure 3.3. Offshore Wind Foundations Alliance (OWFA) predicts monopile diameters to be upon 13 metres in the future [45]. OWFA is a coalition of five European companies, Bladt Industries, EEW, SiF, Smulders Projects, and Steelwind Nordenham. These mega monopiles are referred to as XL, XXL (2XL), or XXXL (3XL) monopiles, although there is no clear definition when a monopile is an XL, 2XL, or 3XL monopile. Ulstein uses for 2XL and 3XL MPs the definition presented in Figure 3.2. In addition, the X and XL MPs are depicted in Figure 3.3.

Figure 3.1: Orion of DEME installing monopiles with a diameter of 9.5 metres at Arcadis Ost in June 2022 [42]

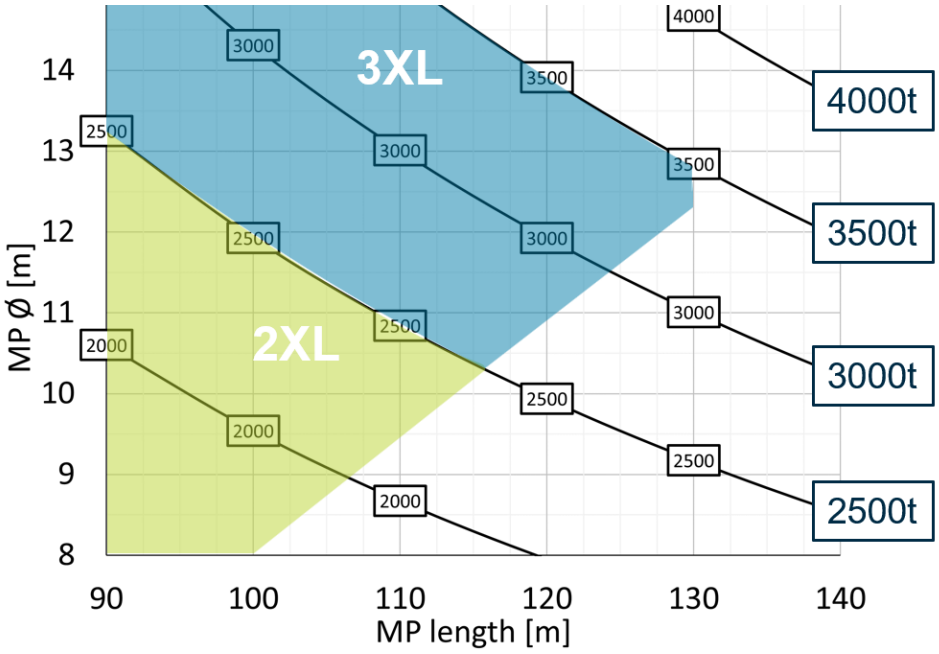

Figure 3.2: Categorisation of dimensions and weight of monopiles by Ulstein

The trend of installing heavier monopiles in deeper water is visually represented in Figure 3.4. Larger monopiles create the possibility of installing OWTs in deeper water, about 65 metres deep. The water depth in Northern Europe is mostly approximately 60 metres or less, particularly along the coast [46]. Therefore, monopiles are a suitable type of foundation, combined with the reasons described in Section 2.1, and are preferred over floating foundations, which are more likely to be cost-beneficial in water depths of more than 100 metres [7]. However, those ever-growing monopiles create extra challenges to safely install the foundations and therefore extra attention needs to be paid to for instance storage, transportation, and pile handling.

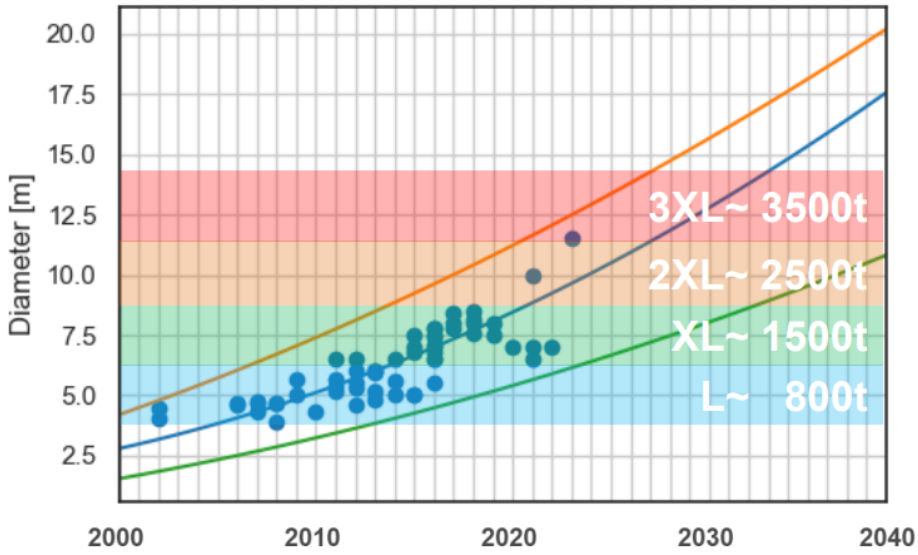

Figure 3.3: Expected market development for L, XL, 2XL, 3XL MPs in period $2000 - 2040$ by Ulstein (J.D. Stroo, 2023)

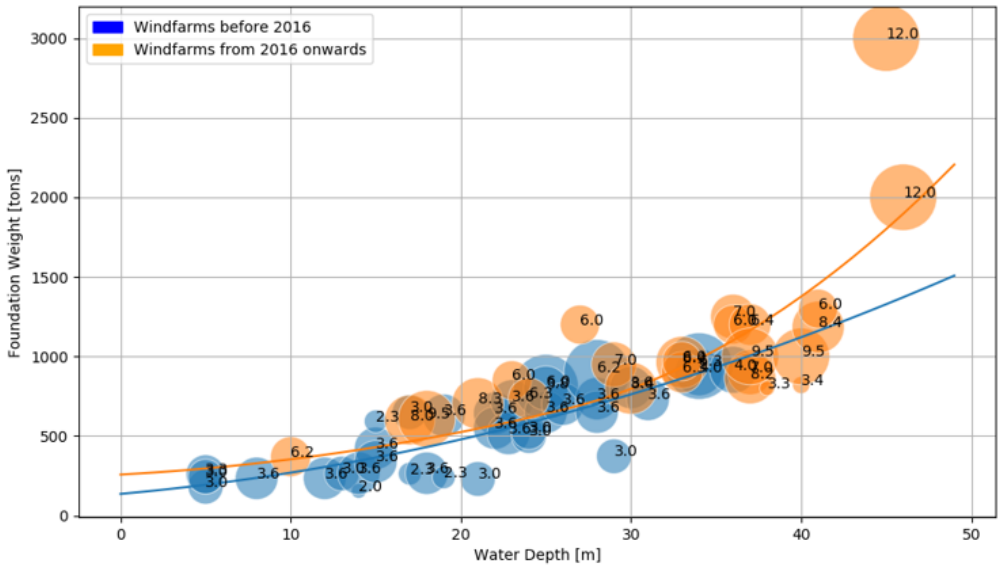

Figure 3.4: Development of monopile projects for water depth against foundation weight [1]

3.2. Vessels

The lifting operation of monopiles is performed by either floating crane vessels or jack-up vessels.

3.2.1. Jack-up vessels

The jack-up vessel provides a stable platform: the entire vessel is lifted by multiple extendable legs. The legs of the jack-up vessel require a limited water depth and suitable sea bottom. These vessels are designed for operations that require minimal motions, thus for the installation of OWTs. Furthermore, the positioning of the jack-up vessels causes downtime which adds up to the cycle time of the jack-up vessel. The monopiles can either be stored on the deck of the jack-up vessel or be transported

by a feeder vessel. These differences in monopile transportation will be elaborated more in detail in Section 3.3.1. Examples of jack-up vessels are described in Table 3.1. The Vole au Vent of Jan de Nul is depicted in Figure 3.6.

Table 3.1: Examples of jack-up vessels ([47], [48], [49], [50])

Vessel	Length [m]	Breadth [m]	Length of legs [m]	Crane capacity [tonnes]	Construction year
Aeolus - Van Oord	140	44	81	1600	2014
Innovation - DEME	148	42	89	1500	2015
Vole au Vent - Jan de Nul	140	41	90	1500	2013
Wind Orca - Cadeler	161	49	105	1200	2012

3.2.2. Floating vessels

Another type of vessel that is used to install foundations is a floating vessel. In order to maintain position during the operation, the vessel can be moored with mooring lines or use DP. In practice, DP is mostly used. Vessels with DP are not restricted to certain water depths and are able to adjust the heading during operation. Therefore, floating vessels are less sensitive to weather during positioning [51] and are able to create a shielding effect during monopile installation. The angle definition is presented in Figure 3.5. For vessels with a mooring system the installation time increases due to positioning of the mooring lines. Three types of floating vessels can be distinguished: heavy lift vessels (monohulls), semi-submersible crane vessels, and sheerlegs.

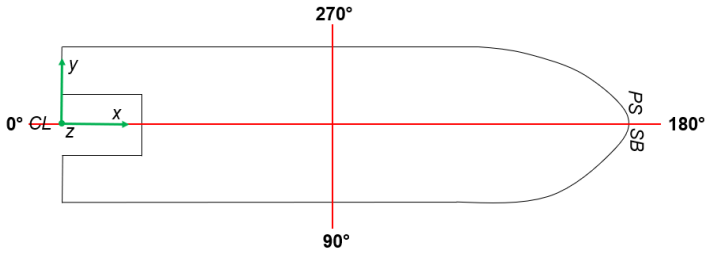

Figure 3.5: Angle definition for wave direction and slewing angle for the crane boom

Heavy lift vessels (monohull)

HLVs are less constrained to water depths and the positioning of the vessel requires less time compared to jack-up vessels. However, the dynamic behaviour of the HLV, the crane, and the monopile are significantly more important due to the larger motions. Due to the growth of large monopile installations, several companies started conversion projects [52]: for example, Boskalis converted in 2020 a 20-year-old drilling vessel into an HLV, as shown in Figure 3.8. The Aegir is depicted in Figure 3.10. Vessels, such as the Orion, are able to transport the monopiles on deck (Figure 3.1). Some examples of monohulls are presented in Table 3.2. The Alfa Lift is separately included in Table 3.2. The vessel, shown in Figure 3.9, is a combination of heavy lift vessel and a semi-submersible heavy transport vessel.

Table 3.2: Examples of monohulls ([53], [54], [55], [56], [57], [58], [59])

Vessel	Length [m]	Breadth [m]	Max. operating draft [m]	Crane capacity [tonnes]	Construction year
Aegir - Heerema	211	46	11	5000	2012
Bokalift 1 - Boskalis	43	216	9	3000	2012
Bokalift 2 - Boskalis	49	231	10	4000	2000
Les Alizés - Jan de Nul	237	52	10.5	5000	2023
Orion - DEME	217	49	11	5000	2019
Strashnov - Seaway 7	47	183	10.5	5000	2011
Alfa Lift - Seaway 7	218	56	-	3000	2023

Semi-submersible crane vessels

Semi-submersible crane vessels (SSCV) are also employed to install fixed foundations. There is a smaller number of these vessels on the market compared to heavy-lift vessels. Heerema has multiple SSCVs: the Sleipnir and the Thialf. However, the Sleipnir mostly installed and removed jackets, topsides, and modules. These vessels have the largest displacements, and the lifting capacity can reach $20,000$ tonnes [60].An overview of examples of SSCVs is presented in Table 3.3.

Table 3.3: Examples of SSCVs ([61], [62], [63])

Vessel	Length [m]	Breadth [m]	Max. operating draft [m]	Crane capacity [tonnes]	Construction year
Sleipnir - Heerema	220	102	32	10000 (2x)	2019
Saipem 7000 - Saipem	198	87	27.5	7000 (2x)	1985
Thialf - Heerema	202	88	32	7100 (2x)	1985

Sheerleg

Sheerlegs are vessels that are similar to barges. However, the crane of a sheerleg cannot rotate independently from the barge.

In Figure 3.7, the Svanen is shown, which is a crane pontoon with an overall length of 103 metres and an overall breadth of 75 metres. The maximum lifting capacity is 5705 tonnes [64]. Svanen is a crane vessel that is used to install wind turbine foundations [65]. The vessel does not transport the foundations. This transportation is done by a feeder vessel or the monopiles are being wet towed to the vessel.

In Table 3.4 the characteristics of jack-up vessels, monohulls, SSCVs, and sheerlegs (Svanen) are presented. These characteristics are expressed in relative terms to each other.

Figure 3.6: Jack-up vessel: Vole au Vent (by M. Ibeler, Ørsted)

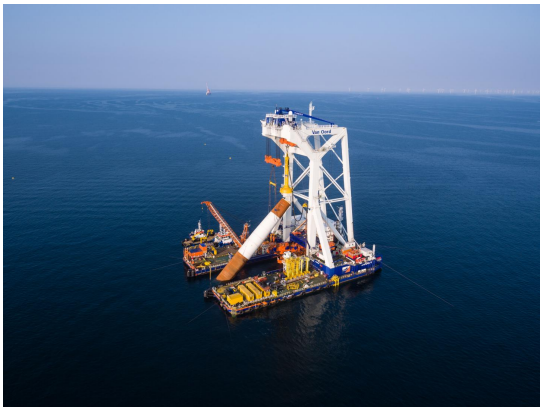

Figure 3.7: Heavy lift vessel: catamaran Svanen [65]

Figure 3.8: Heavy lift vessel: Bokalift 2 [66]

Figure 3.9: Alfa Lift [67]

Figure 3.10: Heavy lift crane vessel: Aegir [68]

Table 3.4: Relative characteristics of jack-up vessels, monohulls, SSCVs, and sheerlegs ([60], [64])

Vessel type	Deck space	Station keeping	Allowable crane load	Day rate	Transport method
Jack-up vessel	Medium	Jacking system	Low	Medium	Shuttle
Monohull	Large	DP and/or mooring system	Medium	Low	Shuttle
SSCV	Large	DP and/or mooring system	High	High	Feeder
Sheerleg (Svanen)	Small	Mooring system	Medium	Medium	Feeder

3.3. Installation steps

The installation of monopiles consists of multiple phases. Before the installation can be conducted, the monopiles need to be transported to the location of the wind farm. When the monopiles are transported by the installation vessel itself, the storage of monopiles on the deck influences the applied installation method. The installation method consists of three steps: upending the monopile into a vertical position, lowering the monopile to the sea bed, and lastly driving the monopile into the sea bed. Those phases will be elaborated and several methods for each phase will be covered.

3.3.1. Transportation to the offshore wind farm

The monopile can be transported by a vessel or a barge on deck or be wet towed to the location of the wind farm location [69]. The choice of mode of transport depends on several factors, such as the distance to the port, the size and weight of the monopile, the crane capacity of the installation vessel, and the environmental conditions [13].

On-board transportation

The transportation of monopiles to the installation site can be done by the installation vessel itself or by a feeder. In the first case, the HLV is deployed for the transportation and installation of the monopiles. The monopiles are loaded on deck by the crane of the vessel at the port. The monopiles are sea-fastened and the vessel sets sail to the installation site. At the site, the vessel performs the installation activities. After the installation of all monopiles, the HLV returns to the port to start the procedure again. This method is called the ”shuttling strategy” [70].

A second strategy is the use of a feeder vessel. The feeder is either a barge or vessel that supplies the monopiles to the HLV. The HLV is constantly at the installation location. This strategy implies the addition of two activities offshore: mooring alongside the HLV and lifting monopiles from the feeder [70]. These activities create risk. Once all the monopiles are lifted of the feeder, the feeder returns to the port to repeat the procedure. The installation vessel has now a large deck space available. The number of feeders can be adjusted to the installation operation.

Wet tow transportation
Another option is to tow the monopile to the wind farm. To provide buoyancy, the monopile is capped by two end-caps. The capped monopile is towed by a tug boat to the location of the wind farm. After upending, the end caps are removed. In theory, it is possible to have multiple monopiles moored in series towed by a tugboat. However, in practice, a tugboat tows one monopile at the time [13].

3.3.2. Storage on deck

When the shuttling strategy is applied, the monopiles need to be stored on the deck of the installation vessel. The way of storage influences the installation method later on and the motion behaviour. Monopiles can either be stalled horizontally (longitudinally or transversely) or vertically on deck. Those three methods will be briefly covered. For every method, vessel motions might cause extreme accelerations or vibrations of monopiles, which should be limited by the application of sea fastening equipment like transport frames and racks.

Longitudinal storage
Longitudinal storage of monopiles requires more deck space. An example of monopiles placed longitudinally is depicted in Figure 3.11. The monopiles are placed parallel to the vessel on a series of saddles welded to the deck.

Figure 3.11: Transport vessel with longitudinal storage of monopiles [71]

Transversal storage
As depicted in Figure 3.9, monopiles can be stored transversely. Both ends of the monopile are hanging over. This creates more available deck space for more monopiles to transport in one transit.

Vertical storage
Vertical storage of monopiles is a relatively novel method. Vuyk Engineering developed a concept that optimises the layout of the deck as shown in Figure 3.12. This concept design is a result of the growing wind turbines as well [72].

Figure 3.12: Concept design of a foundation installation vessel with vertical storage [72]

3.3.3. Upending methods

The first step in installing a monopile is upending the monopile. Upending is the transfer from the horizontal position of the monopile to a vertical position. The transportation mode to the wind farm affects the upending method. Before upending, the monopile is transported over deck to the upending tool. An example of this deck transport is a crane hoisting the monopile into the pile gripper that is also used for upending. Another option is a skidding tool that transports the monopile to the location where it can be upended (J.D. Stroo, personal communication, April 20 2023).

Upending can be done by a specialised pile gripper device, by an upending frame or by a crane, which governs the crane capacity [73]. The upper end of the monopile is lifted by a crane, while the lower end of the monopile is controlled by a pivoting upending tool mounted on the vessel [74]. The pile gripper device used for the lowering process can also be used at the lower end of the monopile as a pivoting upending tool. The hoisting tool needs to be connected to the upper end of the monopile, which is done by the crew on deck or with manhandled cables. Motion-compensated devices are integrated into the installation vessels. Another strategy is the use of an upending trolley [75]. This trolley runs on longitudinal tracks. This strategy is useful when the floating vessel has a fixed hoist, for example, the Svanen catamaran as shown in Figure 3.7.

The hoisting at the upper end of the monopile can be done with several types of lifting tools. Dual block upending, for example, a split main crane block, is a possibility to allow upending of tall and long piles [68]. Furthermore, tools are developed which are a combination of a gripper and an upending tool, as shown in Figure 3.13. This tool can lift monopiles up to 1800 tonnes [76]. Other developments are the flanged pile upending tool (Figure 3.14) and the cam-type clamp tool (Figure 3.15 and Figure 3.16) ([77], [78]). The flanged pile upending tool is stabbed into the monopile. This tool is only applicable on flanged monopiles but can be remotely controlled by operators on board. Therefore, the safety on board increases. The cam-type clamp tool is designed to overcome the difficulties of transporting and upending large-diameter monopiles [78]. The study by Zhang et al. (2021) concluded that this tool was feasible for practical applications.

Figure 3.13: Monopile upending and lifting tool of SpanSet Axzion [76]

Figure 3.14: Flanged Pile Upending Tool by Iqip [77]

3.3.4. Lowering process

In this process, the monopile is lowered to the sea bed through the wave zone. When passing through the wave zone, the hydrodynamic wave loads induce the motions of the monopile [73]. When the monopile is precisely landed, the monopile can be driven into the sea bed, as described in Section 3.3.5.

The gripper device controls the horizontal motions of the monopile during lowering and landing to support the monopile during driving operations. This device is rigidly fixed to the vessel. The gripper device is a ring-shaped structure [73]. In the case of a jack-up vessel, a fixed pile gripper can be used. For floating vessels, a motion-compensated gripper is capable of compensating the heave, roll, pitch, and yaw motion of the vessel (Figure 3.17). The frame, which is the interface between the vessel and the system, compensates the horizontal movements of the vessel as well as DP drift.

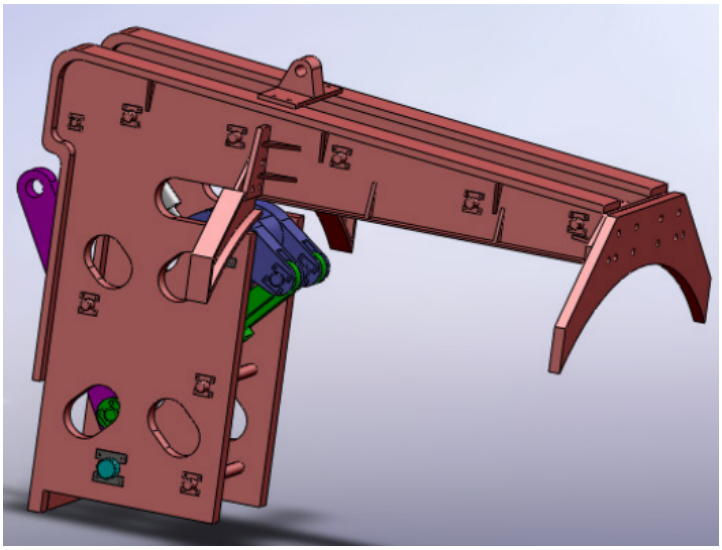

Figure 3.15: 3D structure of the cam-type clamp tool for upending monopiles [78]

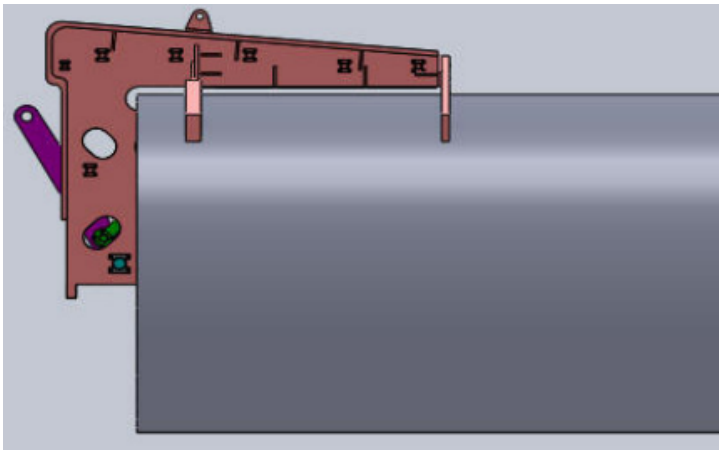

Figure 3.16: Upending tool placed on a monopile [78]

Figure 3.17: Motion compensated pile gripper [79]

3.3.5. Driving/ drilling operations

After lowering the monopile, the foundation needs to be installed into the seabed. Depending on the type of soil, the monopile is driven or drilled into the sea bed. The pile is driven into the sea bottom with typically a length of $30 - 50\%$ of the entire length [13]. After this operation, a transition piece is placed on top of the monopile, where the turbine can be placed.

Pile driving

The dominant method of driving monopiles into the sea bed is hammering, which is hydraulic impact piling [80]. A hydraulic hammer is placed on top of the pile and driven into the seabed. The time for this part of the operation is dependent on the type of soil of the sea bottom, the dimensions of the monopile, and the weight of the hammer [13]. A disadvantage of this method is the high noise levels during pile driving. An example of pile driving is shown in Figure 3.18. To reduce the high noise levels, alternatives are developed, such as vibrating pile drivers or Blue piling technology, which are drivers using the acceleration of a water column [81]. Vibrating pile drivers are compared to impact driving in a large-scale field test in Germany, the VIBRO Project [82].

Drilling operation

When the sea bottom is rocky, pile driving might not be an option and drilling must be applied. This increases the installation time of the monopile.

Figure 3.18: Pile driving of a monopile [18]

3.3.6. Stern installation

Ulstein developed a concept design which includes a recess in the stern of the vessel. The monopile is upended longitudinally in a recess in the aft in the centre line of the vessel to improve pile upending control and to enable weather vaning. Ulstein patented this U-Stern installation method in 2021 and launched it mid-April 2023 [83]. This solution for installing large monopiles on DP is shown in Figure 3.20. After a project of Ulstein with Huisman Equipment, Rosenboom (2022) investigated on behalf of Huisman Equipment the differences between the side and stern installation of monopiles. Traditionally, monopiles are installed on the side of a floating vessel. Rosenboom found that the stern installation provides significantly better dynamic performance due to the lower out-of-plane accelerations and smaller wave loads on the monopile compared to the side installation [84]. The shielding effect for side and stern installation is presented visually in Figure 3.19. The location of the crane and the pile gripper on board influences the level of shielding when side installation is applied. Depending on the weight of the monopile, the outreach of the crane changes and therefore, the shielding effect may be different.

Besides side and stern installation, other studies are carried out on new installation methods. Examples of these other methods are the use of ballasts for vertical transfer [85] and with the help of a floatable subsea structure [86].

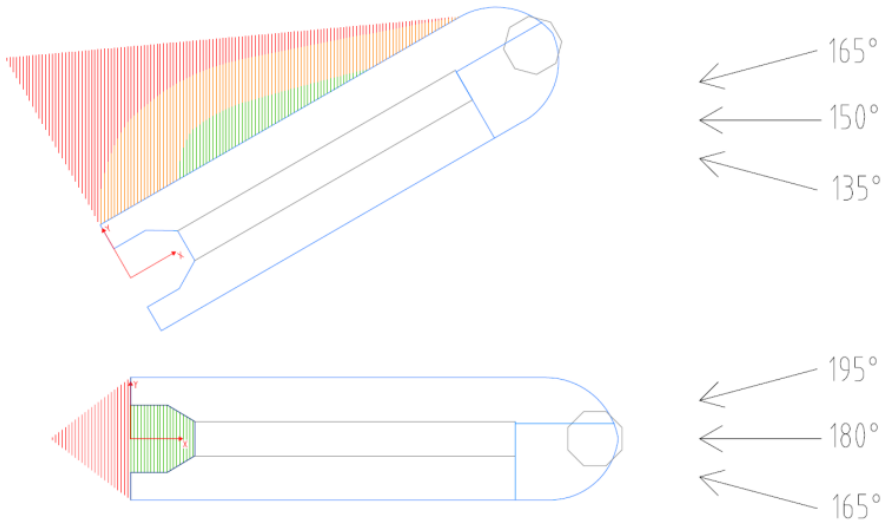

Figure 3.19: Shielding analysis for stern and side installation for different headings by Huisman Equipment [84]

Figure 3.20: U-stern concept by Ulstein

3.4. Conclusion

In this chapter, the methods for installing monopiles are elaborated. It provides an answer to the sub-question: *"What are the state-of-the-art installation methods for 2XL monopile installation?"*. Monopiles are increasing in size and weight. Current monopiles can have a diameter of $10 - 12$ metres with a weight of up to 2500 tonnes. These heavier and larger monopiles are installed in deeper water, up to 70 metres deep, which corresponds with the water depth in Northern Europe which is approximately 60 metres or less. These growing monopiles lead to extra challenges to safely install the foundations.

Multiple installation methods exist and depend on the installation vessel and transportation method. Monopiles are installed from jack-up vessels or floating vessels (monohulls, SSCVs, sheerlegs). Jack-up vessels are stable platforms, but these vessels are limited in terms of water depth, suitable sea bottom, and crane capacity. Floating vessels are less constrained to water depths and positioning requires less time compared to jack-up vessels. However, the dynamic behaviour of the vessel, crane, and monopile is more important due to the larger motions. Monopiles are transported to the location of the wind farm on board, by either the installation vessel itself (shuttling strategy) or by a feeder vessel or the monopile can be wet-towed. When the monopile is transported on board, the monopile can either be longitudinally, transversely, or vertically stored. Vertical storage of monopiles on deck is still in the

concept phase. The start of the installation of the monopile is the upending of the monopile, which can be done by a specialised pile gripper device, an upending frame, or a crane. Other strategies, such as the use of an upending trolley, are more useful for floating vessels with a fixed hoist. The hoisting of the upper end of the monopile can be done by multiple types of lifting tools, which are in constant development, such as combinations of grippers and upending tools. During the lowering of the monopile, hydrodynamic wave loads induce motion of the monopile and the vessel. The gripper device controls the horizontal motions. This gripper can be fixed or motion-compensated. The foundation is installed in the seabed by pile driving or drilling. Pile driving is mostly done by hammering. Drilling is applied in the case of rocky sea bottoms. Other concepts of installation methods exist, such as stern installation, ballasting for vertical transfer, or floatable subsea structures, although these methods are not regularly applied and . Stern installation with the monopiles longitudinally placed on deck is in development and currently becoming the state-of-the-art installation method with multiple companies being engaged in this method. However, the dominant installation method remains side installation with the monopiles placed transversely on deck.

This chapter discussed the current state-of-the-art monopile installation methods. This overview facilitates narrowing down the preferred installation sequences and creating a methodology to assess the operational limits of these preferred installation sequences. For the assessment of installation methods both side and stern installation of 2XL MPs are taken into account. The upending and lowering part of the installation sequence are analysed due to focus on the multi-body behaviour of the floating vessel, crane, and 2XL monopile. The transport to the installation site, the storage on deck and the pile driving / drilling are excluded from the scope. In Chapter 4 the methodology, tools and input data to address the main research question are elaborated. In Chapter 5 the focus is on the preferred installation sequences and hydrodynamic damping of the monopile.

4

Method

This chapter describes the method to assess the main question. It provides an answer to the subquestion: *"What is a suitable method for the assessment of operational limits for 2XL MP installation?"*. A methodology is defined in Section 4.1 and a case study is performed for side and stern installation during upending and lowering of a 2XL monopile. The used tools are described in Section 4.2. The input data of the case study is elaborated in more detail in Section 4.3.

4.1. Methodology

The aim of this thesis is to assess the main research question: the determination of the influence of damping of monopiles, wave direction, and shielding effects during monopile installation. Therefore, the operational limits of the marine operation need to be established. The methodology of this thesis is described in general by several steps and is visually presented in Figure 2.6.

Input data includes vessel, foundation, and environmental data. Firstly, the installation sequence is defined which depends on the type of foundation and environmental circumstances at the installation site, such as water depth and soil type. These factors govern the installation vessel and mission equipment. The next steps are to define and apply the loading condition. The installation method previously defined influences the loading condition. A floating equilibrium needs to be established. When this equilibrium is realistic, the hydrodynamic properties, such as load RAOs, quadratic transfer functions (QTF), hydrostatic stiffness, added mass, and damping, can be obtained. Otherwise, the process needs to be reevaluated. This loop is repeated after the hydrodynamic properties are obtained.

The response of the multi-body system at relevant locations is analysed for every defined and applied loading condition for various environmental circumstances, such as significant wave height and peak period. This analysis results in an identification of critical combinations of key positions and environmental circumstances. These combinations are then studied in more detail, which requires a reevaluation of the loading conditions, the application of the loading conditions, and the floating equilibrium. Finally, the operational limits of the preferred loading conditions are obtained. The different installation sequences can be compared, which leads to a conclusion of the influence of the variables of choice.

Application of this approach is possible for various installation sequences and loading conditions. It is not only limited to floating monopile installation methods. However, the application of this methodology on other assets or other installation vessels, such as jack-up vessels implies other aspects that need to be taken into account. The characteristics of the installed assets lead to another installation method, such as for floating foundations, and the characteristics of the asset lead to other aspects that cannot be neglected, such as buoyancy. Therefore, the user always needs to revise which aspects are required to be incorporated and which aspects are negligible.

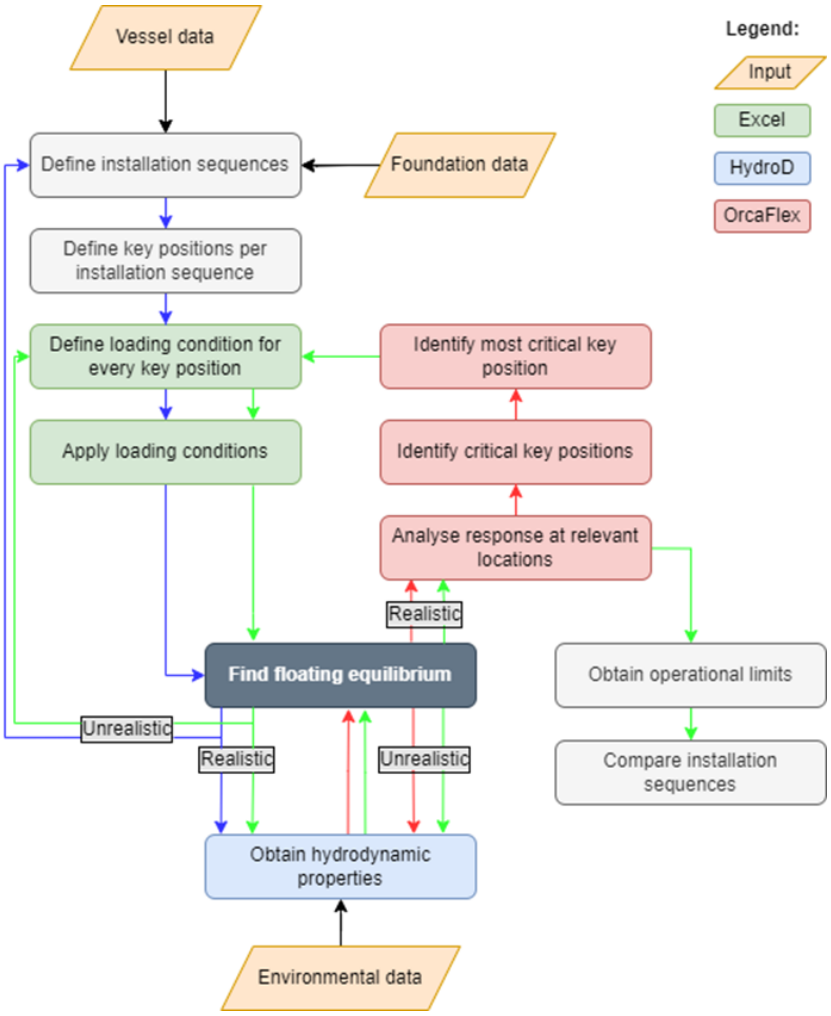

Figure 4.1: Flowchart of the applied methodology to establish the operational limits: from definition of installation sequences and loading conditions to analysis of responses at relevant locations and comparison of installation sequences.
Note: the colours indicate the path to be followed. Follow the colour at the start and finish the entire path, switching to another colour in between is not allowed.

4.2. Tools

Various programmes are used to generate results for this case study. The reason for choosing these software programmes instead of other options is also shortly covered in this paragraph. For this case study, the hydrodynamic properties are generated by the diffraction programme HydroD. To assess the operational limits, the operations are numerically simulated. These simulations are performed in the finite element programme OrcaFlex. The reference loading conditions are calculated using DELFTship, a tool for hull modelling and stability calculations [87]. Excel is used to create the loading conditions based on the reference loading conditions and to post-process results. In Section 4.2.1 and Section 4.2.2, more information regarding these programmes is provided.

4.2.1. HydroD

HydroD is a diffraction programme which calculates the load and displacement RAOs, added mass and damping matrices. It carries out a multi-body analysis. Other diffraction programmes exist, such as OrcaWave, Moses, and AQWA. OrcaWave is included in OrcaFlex and creates input for OrcaFlex. OrcaWave generates the displacement RAOs, added mass and damping matrices, and multi-body analysis identically to HydroD [88]. Both HydroD and OrcaWave are available during this thesis, so a choice is made between these two software programmes.

In HydroD, the input data is generated and the hydrodynamic analysis is performed by the programme Wadam, which is based on the programme Wasim. HydroD is chosen instead of OrcaWave, based on the estimation of roll damping. Roll damping is overestimated by potential theory. Unlike heave and pitch, the roll damping has a significant contribution of viscous effects [89]. Potential theory neglects viscous effects. Therefore the roll amplitude in resonance is overestimated and thus not accurate [90]. Orcawave, the diffraction programme related to Orcaflex, includes an extra roll damping to meet the target of the total damping for the wave period that excited the largest roll amplitude [91]. HydroD, however, numerically estimates the roll damping by a component discrete method, including lift, wave, frictional, eddy and the appendages contributions [90]. Therefore, HydroD is chosen to perform the hydrodynamic analysis instead of Orcawave.

In this thesis, the focus is not primarily on the application of this programme. The hydrodynamic properties are generated by the diffraction programme and are provided for this thesis.

4.2.2. OrcaFlex

The numerical simulations are performed in the finite element programme OrcaFlex. OrcaFlex is a software package that is used for dynamic analysis of offshore marine systems. This software solves for the time and frequency domain and can be applied to offshore wind farm installations and wind turbine modelling. Other applications include, for example, mooring, buoy systems, and installation analysis. Furthermore, OrcaFlex includes several requirements for code checks DNV.

OrcaFlex offers explicit time-domain integration, implicit time-domain integration, and frequency solutions [92]. The explicit scheme is robust and flexible, however, it possibly leads to short time steps and therefore long computational times. Implicit schemes, on the other hand, achieve stability more easily, but result in less accurate results. The frequency-domain analysis assumes that the response is linearly related to an underlying process and that this process is stationary. This type of analysis can be an accurate and efficient solution method. However, if there are nonlinearities present, the accuracy of the results decreases.

OrcaFlex offers a wide range of objects, which creates the possibility to model complicated structures. Environmental conditions, such as sea, seabed, wind, waves, and current, can be added to the simulation. The programme is a cost-effective simulation tool for companies and organisations. Other similar software is Moses of Bentley systems. Moses is an offshore simulation tool which determines model hydrostatics and hydrodynamics, and models, for example, lifting operations in the frequency and time domain. The choice for OrcaFlex is based on the availability of the OrcaFlex software within the company. Furthermore, an extensive documentation of OrcaFlex is available online, which is an advantage.

Table 4.1: 2XL monopile characteristics

Characteristics	2XL MP
Length [m]	100
Diameter [m]	11
Mass [tonnes]	2300

Table 4.2: Characteristics of heavy lift crane vessel HX118

Characteristics	HX118
Length [m]	215.60
Beam [m]	57.40
Depth [m]	16.80
Max. deadweight [tonnes]	40000

4.3. Input data

The input data for the case study is categorised into monopile data (Section 4.3.1), vessel data which includes mission equipment data (Section 4.3.2), and environmental data (Section 4.3.3).

4.3.1. Monopile data

This thesis covers the hydrodynamic behaviour of 2XL monopiles. Different definitions of 2XL monopiles exist, as described in Chapter 2. In this thesis, the definition by Ulstein is leading. The main dimensions of the monopile are shown in Table 4.1. The thickness of the steel is chosen to be 160 mm. The diameter of the monopile coincides with the diameter of the monopile corresponding to the model pile drag tests. These tests are conducted to properly assess the tip vortex damping of monopiles. These damping coefficients are applied for the 2XL MP. More information about these tests is provided in section 5.5.

4.3.2. Vessel data

The reference vessel is the heavy lift crane vessel HX118 developed by Ulstein. The main characteristics are presented in Table 4.2. A schematic representation of this vessel is shown in Figure 4.2. The vessel has a recess at the stern, which is intended for stern installation of monopiles. An impression of this is shown in Figure 4.3. This hull is used in this thesis for different installation sequences.

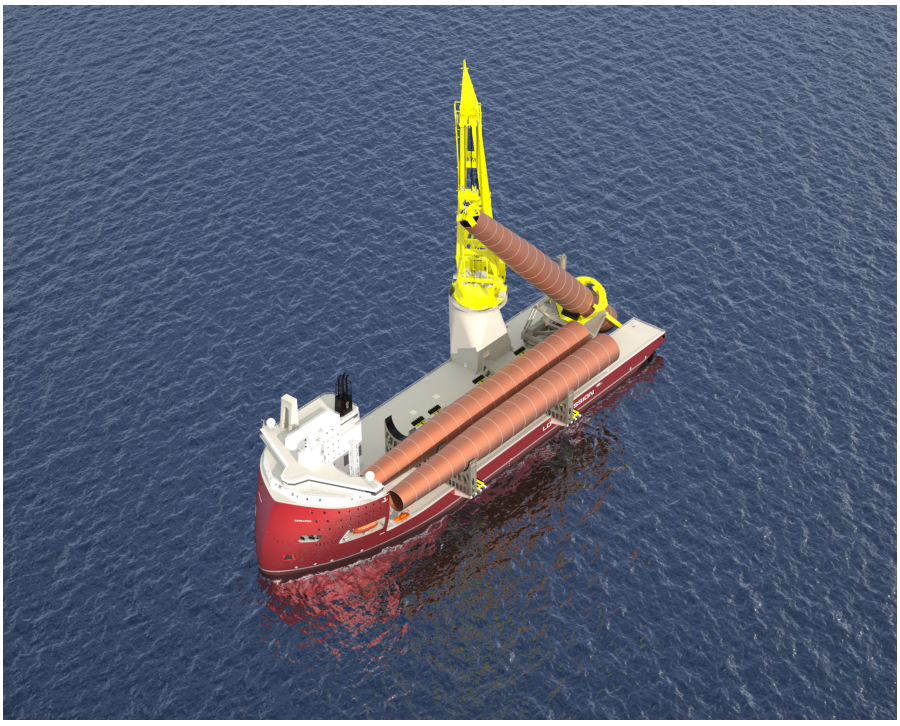

Figure 4.2: HX118 with Huisman TMC crane, upending a MP in the U-stern (Ulstein, 2023)

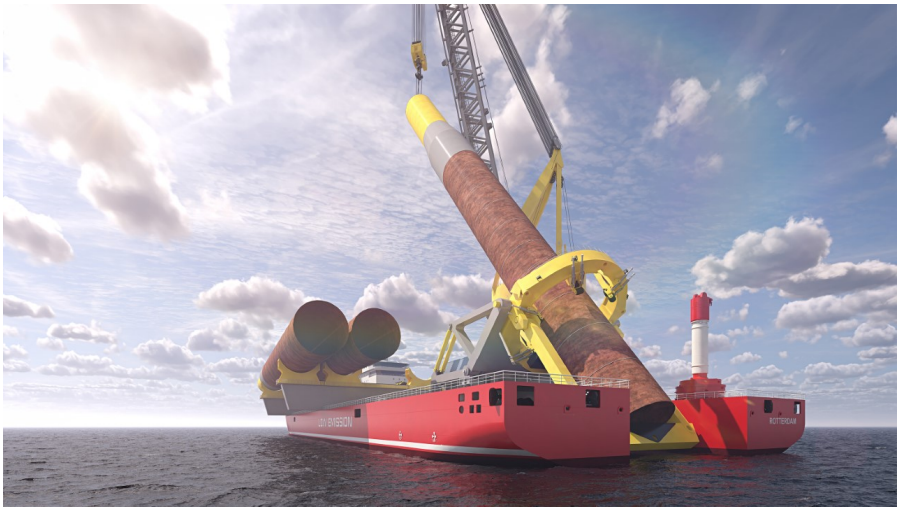

Figure 4.3: Recess in stern (Ulstein, 2023)

Mission equipment
The mission equipment considered is the main crane and the monopile gripper. The main crane is a 5000 t @ 36 m TMC (Tube Mounted Crane) with foldable A-frame of Huisman Equipment. The monopile gripper is a single ring of Huisman Equipment.

Main crane
The crane characteristics are shown in Table 4.3. The centre of mass of the crane boom is assumed to be in the centre of the hollow beam. The mass of the boom includes the mass of the falls, ropes, and hook.

Table 4.3: Crane characteristics based on [93]

5000 t TMC crane	
Crane capacity [mT]	5000 @ 36 m
Crane boom length [m]	108
Crane boom mass [t]	1932
Slewing column mass [t]	3887
Hook mass [t]	200
Fall mass per unit length (2x20 falls) [t/m]	0.924

The mass moments of inertia of the crane boom are included and approached as a thick-walled hollow cylinder at the base of the cylinder. It is assumed that the thickness is 0.45 metres to apply the thick-walled theory (Equation 4.1). This cylinder is approximated by taking the average area of a section of the crane boom, and calculated the corresponding outer radius in case of an area related to a circle. To apply the thick-walled theory, the following constraint must be satisfied.

$$t \leq \frac{D}{20} \tag{4.1}$$

The mass moments of inertia are calculated as follows:

$$I_{xx} = I_{yy} = \frac{M_{boom}}{12} \cdot (3({r_o}^2 + {r_i}^2) + 4 \cdot L_{boom}) \tag{4.2}$$

$$I_{zz} = \frac{M_{boom}}{2} \cdot ({r_o}^2 + {r_i}^2) \tag{4.3}$$

The mass moment of inertia of the slewing column is also calculated separately as a cylinder:

$$I_{xx} = I_{yy} = \frac{M_{slewing\ column}}{12} \cdot (3r^2 + h^2) \tag{4.4}$$

$$I_{zz} = \frac{M_{slewing\ column}}{2} r^2 \tag{4.5}$$

The axis convention for a thick-walled cylinder and a regular cylinder is depicted in Figure 4.4.

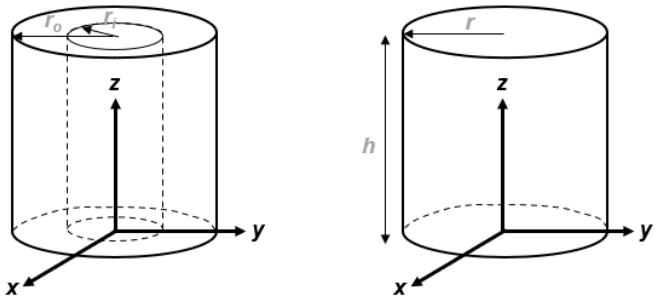

Figure 4.4: Axis convention for respectively a thick-walled cylinder and cylinder

The boom weight and slewing column weight are including a 5% design growth and 10% contingency. The weight of the boom includes the luffing ropes, the main hoist, the aux block, and the hook. In the first versions of the model, the hook mass is included in the mass of the crane boom.

Monopile gripper
The monopile gripper is a single ring and acts like a hinge. A mass of 2000 tonnes is assumed based on internal information of Ulstein. The centre of mass is assumed to be in the middle of the pile gripper, with a distance of 9 metres to the main deck. The mass moments of inertia are calculated based on the equations for a thick-walled hollow cylinder, as presented in Equation 4.3.

The masses of the crane, pile gripper, and monopile are depicted in Figure 4.5. The local Vertical Centre of Gravity (VCG) of these components are shown in Figure 4.6. The masses and VCG are identical for different installation sequences.

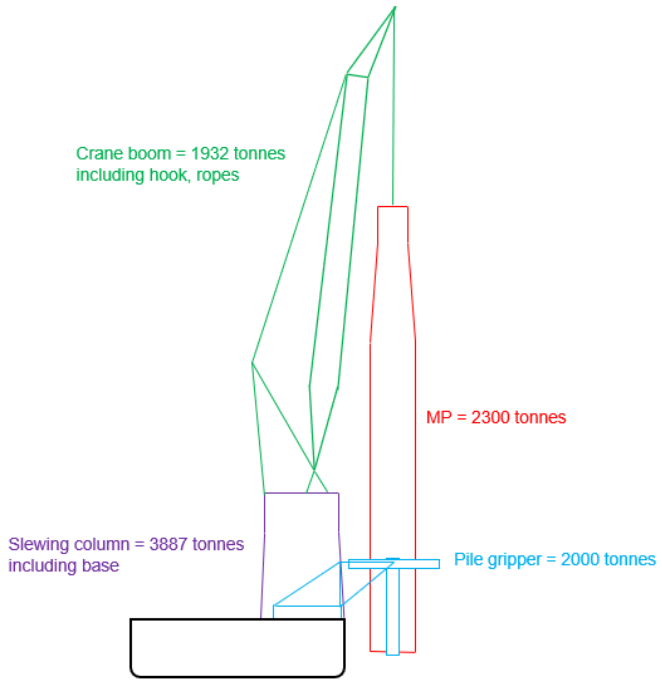

Figure 4.5: Mass [tonnes] of mission equipment and monopile

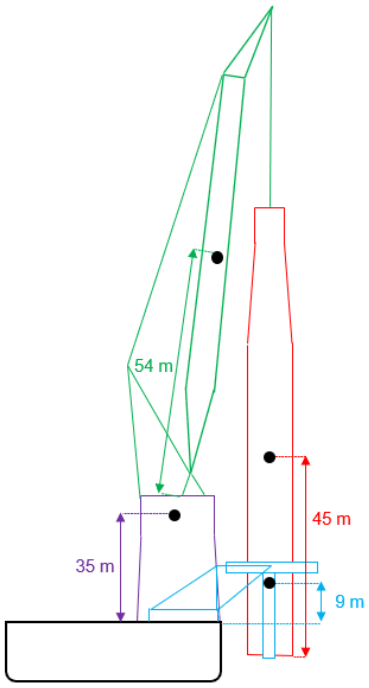

Figure 4.6: Local VCG [m] of mission equipment and monopile

4.3.3. Environmental data

Based on 4COffshore data (2022), 59% of the monopiles for water depths of $30 - 70$ metres in the planning and EPCI phase will be installed on the North Sea. The largest known water depth where monopiles will be installed is 68 metres, at Hornsea Offshore Wind Farm, United Kingdom. Therefore, Hornsea Wind Farm is chosen as the case study for this thesis. The installation of the monopiles for this wind farm will be performed by a jack-up vessel that will be delivered at the end of 2025. The environmental data is therefore based on the wind and wave characteristics of the North Sea.

Wave conditions

The JONSWAP spectrum, a standard spectrum based on data collected during the Joint North Sea Wave Observation Project, is applied. This spectrum is a modification of a Pierson-Moskowitz (PM) spectrum: it is multiplied by a peak enhancement factor γ. The JONSWAP spectrum is defined as follows [94]:

$$S(f) = \frac{\alpha g^2}{16\pi^4} f^{-5} exp[-\frac{5}{4}(\frac{f}{f_m})^{-4}]\gamma^b \tag{4.6}$$

with:

$$b = exp[-\frac{1}{2\sigma^2}(\frac{f}{f_m} - 1)^2] \tag{4.7}$$

and:

$$\sigma = \begin{cases} \sigma_a & \text{for } f \leq f_m \\ \sigma_b & \text{for } f > f_m \end{cases} \tag{4.8}$$

The parameters f and f_m are respectively the frequency and the peak frequency. The parameters γ, α, σ_a and σ_b are data items. The values of these parameters are chosen to have a standard spectrum:

$$\gamma = 3.3 \tag{4.9}$$

$$\alpha = 9.18 \cdot 10^{-4} \tag{4.10}$$

$$\sigma_a = 0.07 \tag{4.11}$$

$$\sigma_b = 0.09 \tag{4.12}$$

In Chapter 5, the installation sequences of side and stern installation are elaborated. For side installation, the wave direction is $210°$ to create a shielding effect. For the stern installation, the wave direction is $180°$. Initially, wave spreading is not taken into account to clearly observe the main physical effects of environmental conditions and the multi-body interaction of the vessel and the monopile. Similarly, no current is added to the simulation of the side and stern installation.

The significant wave height is the mean wave height of the highest third of the waves and is introduced to denote the characteristic height of random waves in a sea state [95]. In Figure 4.7, the seasonal mean significant wave height is shown. The upper red dot represents the Hornsea Wind Farm. At this wind farm the H_s is 1.5 metres during spring and summer, and a mean H_s of 2.5 metres is observed during autumn and winter. Additionally, the probability function and cumulative probability of H_s based on empirical data of the North Sea is presented in Figure 4.8 [96]. For this case study, H_s values of 2 and 3 metres are chosen. H_s of 2 metres has a probability of occurrence of 12.8 % based on Figure 4.8. Ulstein established a significant wave height of 3 metres as a goal for the development of vessels.

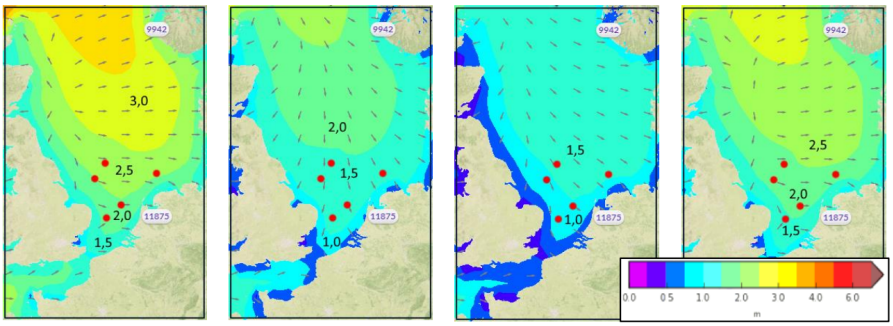

Figure 4.7: Seasonal mean H_s in metres during respectively January, April, July, and October on the North Sea using MetOcean View Hindcast ([97], [98])

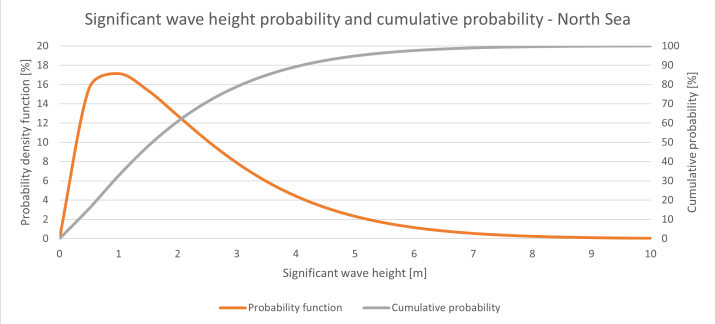

Figure 4.8: Probability function and cumulative probability of H_s [m] based on empirical data of nautical zone 11 (North Sea) [96]

The joint probability of the significant wave height and the zero up-crossing period (T_z), which is related to the spectral peak period T_p, is presented in a wave scatter diagram for the North Sea in Figure 4.9. This joint distribution is calculated by multiplying $f_{H_s}(H_s)$ and $f_{T_z|H_s}(T_z|H_s)$, which are presented in respectively Equation 4.13 and Equation 4.14. The significant wave height is modelled by a 3-parameter Weibull probability density function with shape, scale, and location parameters (β_{H_s}, α_{H_s}, and γ_{H_s}) and the zero up-crossing period depending on H_s is modelled by a log-normal distribution [96].

$$f_{H_s}(H_s) = \frac{\beta_{H_s}}{\alpha_{H_s}}\left(\frac{H_s - \gamma_{H_s}}{\alpha_{H_s}}\right)^{\beta_{H_s}-1} exp\{-\left(\frac{H_s - \gamma_{H_s}}{\alpha_{H_s}}\right)^{\beta}_{H_s}\} \tag{4.13}$$

$$f_{T_z|H_s}(T_z|H_s) = \frac{1}{\sigma T_z \sqrt{2\pi}} exp\{-\frac{(ln(T_z) - \mu)^2}{2\sigma^2}\} \tag{4.14}$$

μ and σ are distribution parameters which are dependent on H_s, and estimated by:

$$\mu = E[ln(T_z)] = a_0 + a_1 H_s^{a_2} \tag{4.15}$$

$$\sigma = std[ln(T_z)] = b_0 + b_1 exp\{b_2 H_s\} \tag{4.16}$$

The coefficients a_0, a_1, a_2, b_0, b_1, and b_2 are estimated based on empirical data for the corresponding nautical zone [96]. The nautical zones worldwide are depicted in Figure 4.10.

Percentage [%] of occurrence of joint significant wave height and zero up-crossing period for North Sea (zone 11)

Hs [m] \ Tp [s]	5,0	6,1	7,2	8,3	9,4	10,6	11,7	12,8	15,0	Sum [%]
Tz [s]	3,9	4,7	5,6	6,5	7,3	8,2	9,1	10,0	11,7	
0	0,00	0,00	0,00	0,00	0,00	0,00	0,00	0,00	0,00	0,00
1	6,69	12,65	10,53	5,37	2,01	0,55	0,15	0,04	0,00	37,98
2	1,23	5,05	7,86	6,76	3,95	1,65	0,62	0,21	0,02	27,35
3	0,21	1,48	3,59	4,44	3,53	1,97	0,93	0,38	0,05	16,57
4	0,03	0,38	1,33	2,21	2,25	1,58	0,89	0,43	0,07	9,16
5	0,01	0,09	0,43	0,93	1,18	1,00	0,66	0,36	0,07	4,74
6	0,00	0,02	0,13	0,35	0,54	0,55	0,42	0,26	0,06	2,32
7	0,00	0,00	0,04	0,12	0,22	0,27	0,23	0,16	0,05	1,09
8	0,00	0,00	0,01	0,04	0,08	0,12	0,12	0,09	0,03	0,49
9	0,00	0,00	0,00	0,01	0,03	0,05	0,05	0,05	0,02	0,21
10	0,00	0,00	0,00	0,00	0,01	0,02	0,02	0,02	0,01	0,09
Sum [%]	8,17	19,67	23,92	20,22	13,81	7,75	4,08	1,98	0,39	100,00

Figure 4.9: Wave scatter diagram based on empirical data of nautical zone 11 (North Sea) [96]

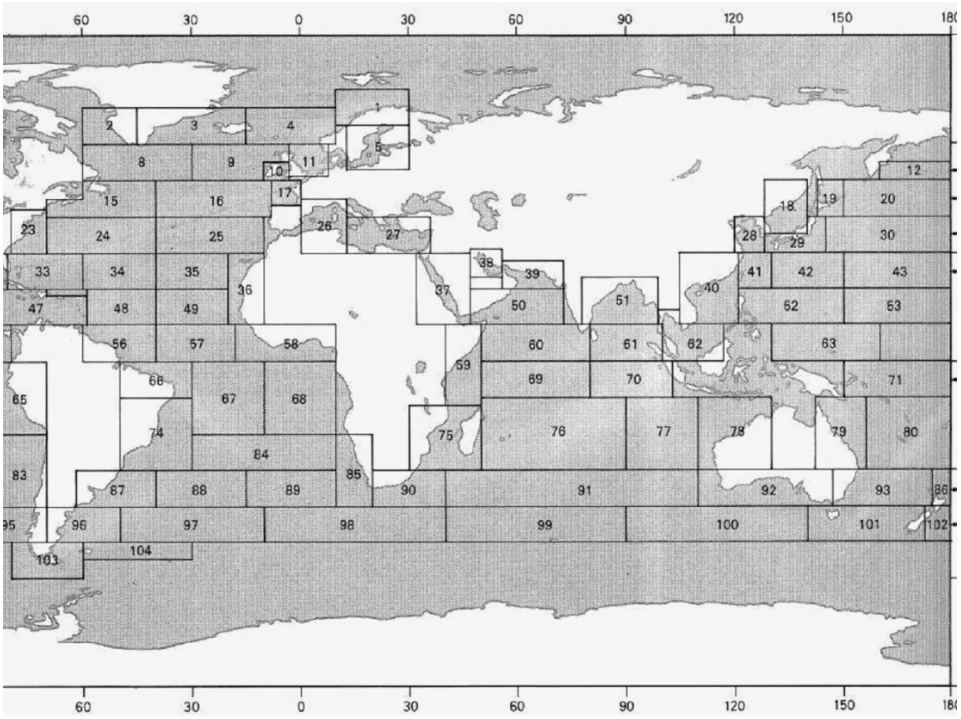

Figure 4.10: Nautical zones used for estimating long-term wave distribution parameters [96]

In Table 4.4, the different T_p are presented in the range of 5.0 to 15.0 seconds, based on the wave scatter diagram of Figure 4.9 and the hindcast data of Hornsea Wind Farm. The shorter wave periods around 5.0 to 8.0 seconds occur more frequently on the North Sea, due to the relatively small water depth. However, the larger wave periods are included in the case study to assess the dynamic behaviour for these environmental conditions to put the results of the shorter wave periods into perspective. Additionally, by simulating these larger wave periods on purpose, the critical conditions can be assessed.

Table 4.4: Simulated peak period T_p [s] based on hindcast data of Hornsea Wind Farm ([97], [99])

T_p [s]	5.0	6.1	7.2	8.3	9.4	10.6	11.7	12.8	15.0

Wind conditions
The NPD (Norwegian Petroleum Dictorate) wind speed spectrum is applied. Wind speed varies over height above mean water level (MWL), using a vertical wind variation factor based on the $\frac{1}{7}$ power law of the Oil Companies International Marine Forum (OCIMF) model for wind loads on vessels [100]. The wind speed at a height of 10 metres above MWL is calculated using:

$$v_w(10) = v_w(h)(10/h)^{\frac{1}{7}} \tag{4.17}$$

4.4. Conclusion

This chapter provides an answer to the subquestion: *"What is a suitable method for the assessment of operational limits for 2XL monopile installation?"*. The method consists of the methodology, which describes the framework of the thesis, the used tools, and the case study including input data. The methodology consists of definition of installation sequences and corresponding key positions, loading condition estimation and the generation of the hydrodynamic properties. The responses are analysed at relevant locations in terms of operational limits, which leads to a comparison between installation sequences and key positions. For the generation of hydrodynamic properties, HydroD is used. The model is set up in OrcaFlex, which also performs the simulations. The case study consists of a monopile, mission equipment and a vessel developed by Ulstein. The monopile has a mass of 2300 tonnes, a diameter of 11 metres and length of 100 metres. The mission equipment consists of a crane with a 5000 tonnes capacity and a pile gripper of 2000 tonnes. This case study is performed according to the conditions at the Hornsea Wind Farm on the North Sea: a water depth of 68 metres, a JONSWAP spectrum, and H_s of 2 and 3 metres. T_p is varied between 5.0 and 15.0 seconds, based on hindcast data and wave scatter diagram based on empirical data of the North Sea.

5

Model set-up

The set-up of the numerical simulations is described in this chapter. The model set-up covers the part of the flowchart (Figure 2.6) up to the analysis of motion responses. First, the preferred installation sequences are covered in Section 5.1. This section provides an answer to the subquestion: *"Which installation sequences are preferred for 2XL monopile installation?"*. For these sequences the loading conditions are established: this process is elaborated in Section 5.2. In combination with the environmental data, the hydrodynamic properties are generated, which is described in Section 5.3. In Section 5.4, choices regarding the modelling of the case study are clarified. Section 5.5 describes the set-up for the hydrodynamic damping for the loading conditions with a partly submerged monopile.

5.1. Installation sequences

The scope of this thesis is limited to the upending and lowering part of the installation sequence. The execution of upending and lowering depends on the storage method of the monopiles on deck. The monopiles are either transversely, longitudinally, or vertically stored on the deck. Transverse storage of monopiles on deck implies side installation. A higher number of monopiles can be transported by the vessel. However, the monopiles are hanging overboard. This method is elaborated in more detail in Section 5.2.1. Longitudinal storage results in stern installation of monopiles, which follows the installation concept of pipe layers. Stern installation is elaborated in Section 5.1.2. A third option is vertical placement of the monopiles. Upending of the monopile takes place in the port and not at the installation site. This method is not widely applied and consists as a concept [72]. Vertical placement is left out of scope to focus on the differences between side and stern installation, and differs by excluding upending at the installation site.

5.1.1. Side installation

The upending and lowering process is schematically represented in Figure 5.1. The upper part of the monopile is guided by the crane. The lower end of the monopile is placed into the pile gripper, which acts as a hinge, and upending frame. The upending frame prevents the monopile from sliding through the gripper. After upending, the upending frame is removed by rotating $90°$. The pile gripper is lowered towards to water surface and then the monopile is lowered. The heading of the vessel is $210°$ with respect to the wave direction. This provides a sheltered and shielded environment from waves and wind to lower the monopile towards the seabed.

5.1.2. Stern installation

The installation sequence for stern installation is similar to side installation. The schematic representation of stern installation is depicted in Figure 5.2. The crane is at the same location as for the side installation. The pile gripper is placed at the centre line of the vessel in front of the recess. The monopile is upended in the centre line of the vessel in a similar way as pipe-laying vessels. Stern installation provides a sheltered installation position and it creates a weather-vane effect. The heading of the vessel is in such a way that the wave direction is $180°$, according to the convention as presented in Figure 3.5.

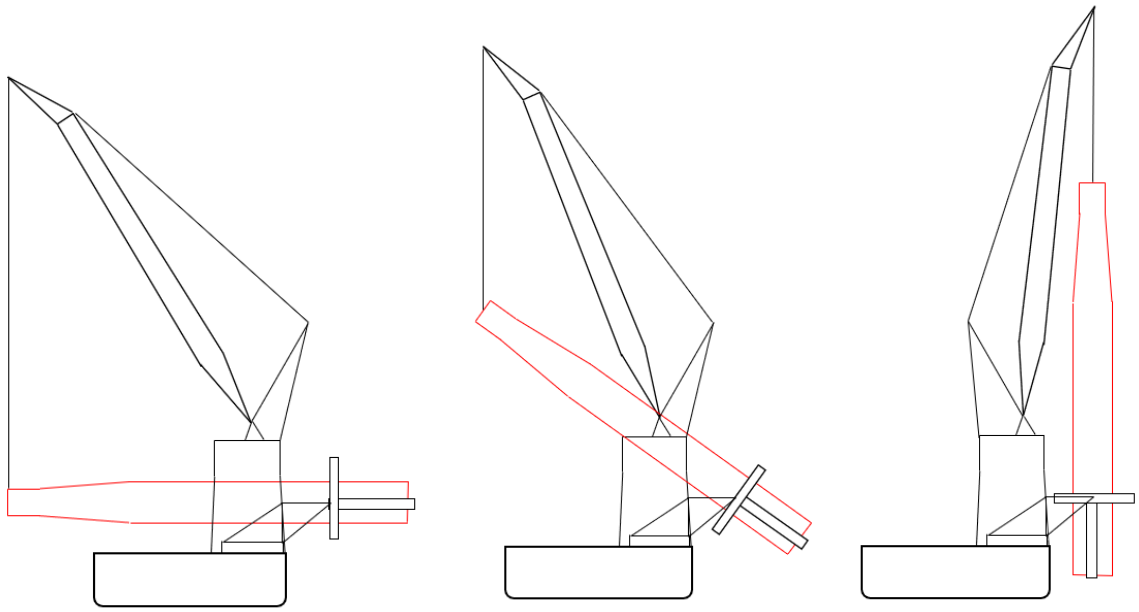

(a) Horizontal position

(b) Upending at an angle of 45 degrees

(c) End of upending

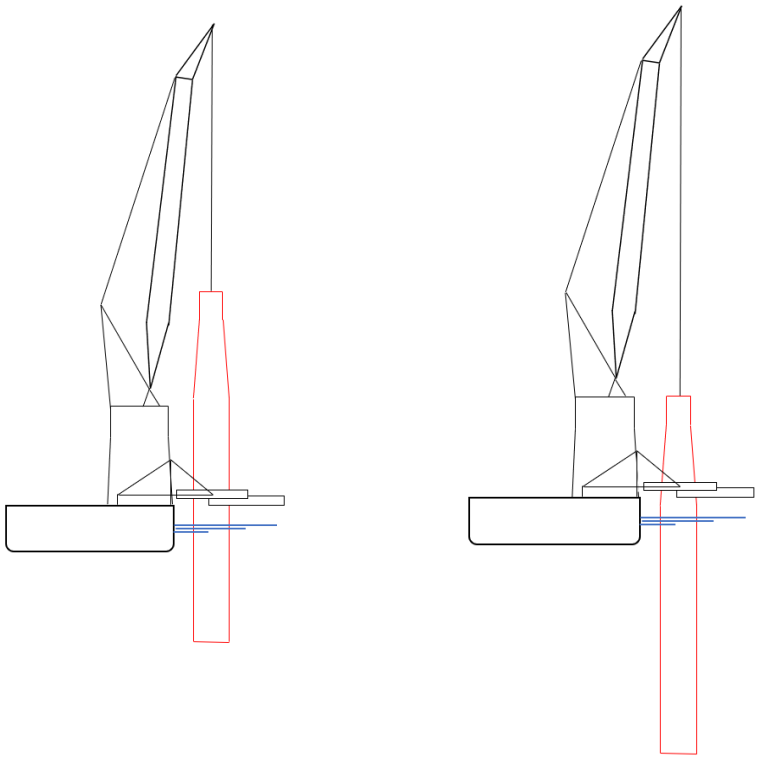

(d) Lowered at water depth of 35 metres

(e) Lowered at water depth of 65 metres

Figure 5.1: Stages of upending and lowering of a monopile towards the seabed for side installation

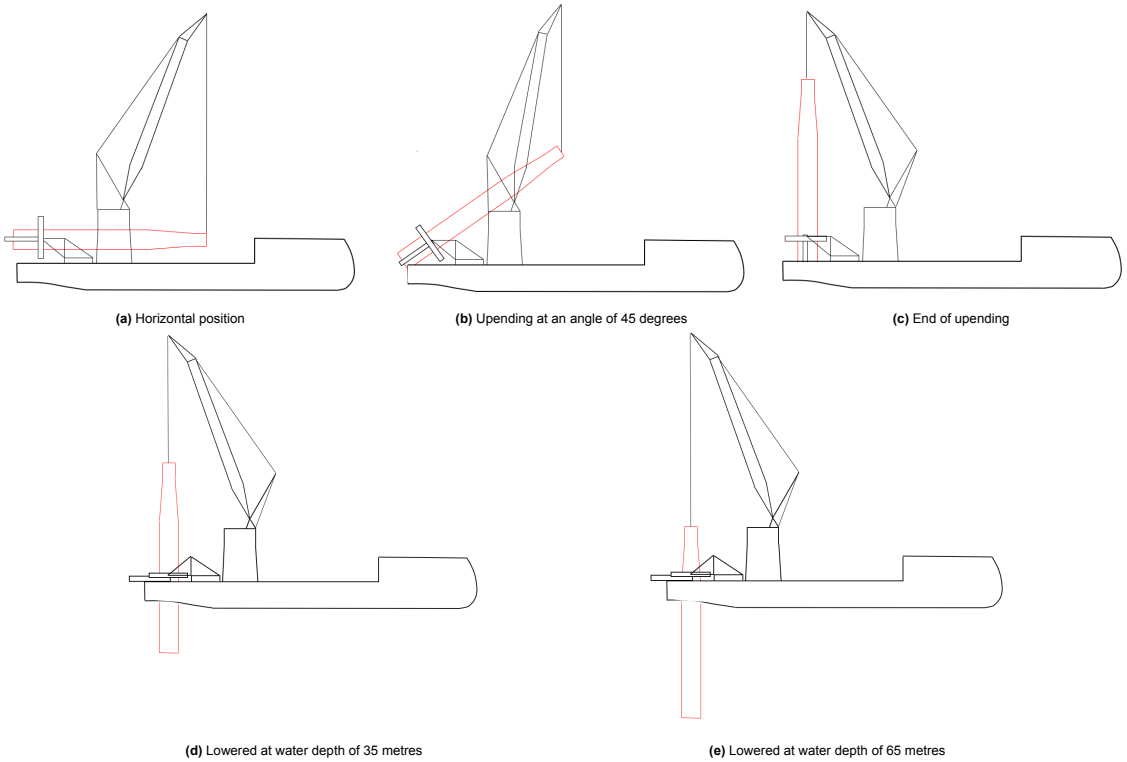

(a) Horizontal position **(b)** Upending at an angle of 45 degrees **(c)** End of upending

(d) Lowered at water depth of 35 metres **(e)** Lowered at water depth of 65 metres

Figure 5.2: Stages of upending and lowering of a monopile towards the seabed for stern installation

5.2. Loading conditions

The loading conditions corresponding to each stage of the installation sequence for side and stern installation are established. The loading condition depends on the position of the monopile, and are defined for stages depicted in Figure 5.1 and Figure 5.2. The lightship weight and deadweight are based on the loading conditions of the reference vessel HX118.

The loading conditions include the calculation of the mass moments of inertia, the Longitudinal Centre of Gravity (LCG), VCG, Transverse Centre of Gravity (TCG) and FSM, of each component of the lightship weight and deadweight, such as the crane and the monopile gripper, and the monopile. The loading conditions of a similar reference vessel are used as a starting point to obtain a first estimation of the loading conditions for each presented stage of side and side installation. These loading conditions are then adapted for the correct characteristics of mission equipment and monopile. This results in a centre of gravity and mass moment of inertia for the entire vessel and monopile in the specific condition. The calculation of inertia is simplified by only taking the Steiner terms into account. A second simplification is excluding the buoyancy of the partly submerged monopile. For side installation, not taking the buoyancy into account results in a maximum difference of 2% for the weight. For stern installation, the largest difference is about 5% of the FSM. These difference are assumed to be small enough to exclude the buoyancy of the monopile in the calculations for the loading conditions. The results of the loading conditions are applied in HydroD to obtain the hydrodynamic properties of the specific loading condition.

The loading conditions use specific coding. An example of a standard abbreviation is *GE-03-80%-LI: 5000 t @36m,90 degr* which implies:

GE-03-80%: Typical departure empty, consumable tanks are filled at 80%. GE is the abbreviation of general. *LI: 5000t, @ 36m, 90 degr*: It is specifically a lifting (LI) condition with the main crane. The load is 5000 tonnes, with a distance of 36 metres from the centre of rotation of the crane. The crane boom to starboard is 90 $^\circ$. In Section 5.2.1 and Section 5.2.2, the applied loading conditions are elaborated.

The reference loading conditions are then adjusted to have zero trim and list by changing the percentage the water ballast and anti-heeling tanks are filled at, using a nonlinear solver. The GRG nonlinear solver is a Generalised Reduced algorithm [101]. It is a nonlinear extension of the simplex method for linear programming. The VCG and FSM of the adapted tanks are adjusted, which is described in Section 5.2.3.

5.2.1. Side installation

The loading conditions are calculated based on data of existing loading conditions of the reference vessel. The loading conditions for side installation are presented in Table 5.1.

Table 5.1: Reference loading conditions for side installation

	Position MP	Reference loading condition	Final loading condition
1	Horizontal position	GE-03-80%-LI: 5000t @36m, 270 °	GE-03-80%-LI: 2300t@63.8m, 243 °
2	45 ° upended	GE-03-80%-LI: 5000t @36m, 270 °	GE-03-80%-LI: 2300t@ 50.7m, 235 °
3	Fully upended	GE-03-80%-LI: 5000t @36m, 90 °	GE-03-80%-LI: 2300t @31.6m, 159 °
4	Halfway water depth	GE-03-80%-LI: 5000t @36m, 90 °	GE-03-80%-LI: 2300t @31.6m, 159 °
5	3 metres above seabed	GE-03-80%-LI: 5000t @36m, 90 °	GE-03-80%-LI: 2300t @31.6m, 159 °

The loading conditions are then changed to the final loading conditions, as shown in Table 5.1. The final luffing and slewing angle are calculated based on the angle convention as depicted in Figure 3.5. The inertia corresponding to the used type of crane boom and slewing column at the current location at the vessel are adapted. The inertia is calculated based on the CoG of that object. The mass and dimensions of the MP are adapted to the values of the 2XL MP used in this thesis. For the stability calculation, the weight is placed at the crane tip instead of at the CoG of the monopile. Next, the TCG and LCG are set to have zero list and trim by using a non-linear solver varying the water ballast (and anti-heeling tanks). The corresponding VCG and free surface moment (FSM) are calculated. This estimation according to IMO rules is elaborated in Section 5.2.3.

5.2.2. Stern installation

The loading conditions for stern installation are established similarly to the loading conditions of side installation. The loading conditions for stern installation are presented in Table 5.2. The applied method for stern installation is identical to the method described in subsection 5.2.1 for side installation. The differences are the position of the monopile gripper and the position of the monopile.

Table 5.2: Reference loading conditions for stern installation

	Position MP	Reference loading condition	Final loading condition
1	Horizontal position	GE-03-80%-LI: 5000t @36m, 180 °	GE-03-80%-LI: 2300t@63.8m, 221 °
2	45 ° upended	GE-03-80%-LI: 5000t @36m, 180 °	GE-03-80%-LI: 2300t @27.9m, 247 °
3	Fully upended	GE-03-80%-LI: 5000t @36m, 0 °	GE-03-80%-LI: 2300t @47.8m, 303 °
4	Halfway water depth	GE-03-80%-LI: 5000t @36m, 0 °	GE-03-80%-LI: 2300t @47.8m, 303 °
5	3 metres above seabed	GE-03-80%-LI: 5000t @36m, 0 °	GE-03-80%-LI: 2300t @47.8m, 303 °

When the monopile is fully upended, the monopile is still in the frame of the pile gripper ring. This results in a level of submergence of 5.56 metres. The monopile is 35 metres submerged halfway the water depth, and 65 metres submerged when it is 3 metres above the seabed. These values are for both side and stern installation.

5.2.3. Free surface moment

The free surface moment is included in the estimation of the loading conditions. The free surface moment is estimated based on the IMO rules [102]. A tank that is not completely filled has a free surface of liquid. When the vessel heels, a free surface moment occurs because of the translation of the centre of gravity of the liquid. This free surface moment leads to a reduction of stability. The free surface moment is calculated for tanks with a capacity lower than 98 % of full condition. Based on the IMO rules, the residual of the liquid in empty tanks does not need to be taken into account since it does not

constitute a significant free surface effect. The free surface moment M_{fs} in $[mtonnes]$ is derived from the following formula [102]:

$$M_{fs} = V \cdot b \cdot \rho_{tank} \cdot k \cdot \sqrt{\delta} \tag{5.1}$$

The parameter k is based on the ratio of the maximum tank breadth b and the tank maximum height h, and on the heeling angle. The parameter δ is the permeability of the tank [%], which is set to 0.98, based on experience and knowledge of Ulstein.

5.3. Hydrodynamic properties

Hydrodynamic properties are generated in the software HydroD. Added mass and damping matrices, load and displacement RAOs, and multi-body analysis can be generated and performed. The hydrodynamical interaction between the vessel and the monopile is calculated. The interaction influences the hydrostatic and potential theory loads, such as first and second-order wave loads, stiffness, added mass and damping. The output of HydroD is provided for this thesis.

Sloshing

Sloshing of water occurs in structures such as moonpools and bays. The hull consists of a recess in which also sloshing occurs. This phenomenon is visible due to a peak for a certain period in the software of HydroD. This peak is checked with two methods to confirm the peak originates from the sloshing in the recess. The results are presented in Table 5.3.

The first check is executed by using the Merian formula, which originates from coastal engineering. The longitudinal period T_l in seconds and transversal period T_t in seconds are calculated using the Merian formula [103]:

$$T_l = \frac{2L_{recess}}{n\sqrt{gD_{recess}}} \tag{5.2}$$

$$T_t = \frac{2B_{recess}}{n\sqrt{gD_{recess}}} \tag{5.3}$$

with n the node number, L_{recess} the length of the basin, B_{recess} the width of the basin, and D_{recess} the depth of the basin, which are in this case the recess.

The second check is performed using the risk assessment of sloshing of BV [104]:

$$T_{l/r} = \frac{2 \cdot \pi}{\omega_n} \tag{5.4}$$

with:

$$\omega_n^2 = g \cdot \lambda_n \cdot \frac{1 + J_n tanh(\lambda_n h)}{J_n + tanh(\lambda_n h)} \tag{5.5}$$

and: ω_n the moonpool natural frequency, h water column height in the moonpool, g the gravity acceleration, $\lambda_n = \frac{n\pi}{l}$, n number of wave length, and J_n which is obtained by a graph provided by BV.

Table 5.3: Sloshing periods based on [103] and [104]

Bureau Veritas	**L**	**B**
$T_{l/r}$ [s]	6.02	4.89
Merian formula		
$T_{l/r}$ [s]	6.38	4.64

In conclusion, it is confirmed that the peak in response observed in HydroD originates from the sloshing phenomenon. The results of the Merian formula and the risk assessment of BV for the period in longitudinal and transversal direction are sufficiently close to each other. A relevant difference is that the

Merian formula assumes a basin or bay with a limited water depth, whereas in reality the water depth continues underneath the recess and thus the vessel. Additionally, a moonpool is a closed space both longitudinally and transversely, whereas the recess has one open side. Despite these differences, it still is concluded that this peak occurs due to the sloshing. To dampen this peak, a damping sheet of 3 % of the total potential damping is created in HydroD. The number is used as a rule of thumb and based on experience (C. Rossetti, personal communication, September 2023).

5.4. OrcaFlex model

The installation sequences including the generated hydrodynamic properties are set up in OrcaFlex. The multi-body system is modelled identically for side and stern installation except for the location of the monopile and pile gripper. The properties of the vessel, mission equipment and monopile are identical as well. This section describes the important modelling choices regarding the monopile and mission equipment.

5.4.1. Monopile

Depending on the position of the MP, the MP is modelled differently to incorporate all the relevant hydrodynamic information. When the MP does not have any water contact, the monopile is modelled as a line object, as presented in Figure 5.3. A line is a flexible linear element in OrcaFlex which can be used for ropes, chains, but monopiles as well. The chosen line type is a general pipe with the inner and outer diameter and structural properties inserted as defined in Section 4.3. When the MP is (partly) submerged, the monopile is modelled as a hybrid buoy-vessel-line object. The spar buoy accounts for the viscous drag and inertia regime, while the vessel accounts for the diffraction regime. The vessel object also includes the tip vortex damping derived from model tests and CFD tests, which is explained in more detail in Section 5.5. The vessel object is part of a multi-body group, together with the vessel itself. This multi-body group allows interaction between these two objects, such as wave shielding (Section 5.4.3). Additionally, the multi-body group defines properties such as the frequency dependent added mass and damping matrices of the monopile and the vessel, and the hydrostatic stiffness are also defined in this multi-body group. The line object acts as a sleeve and models the contact with the pile gripper ring. The vessel and line object are rigidly connected to the 6 DoF spar buoy. The hybrid modelling for the submerged monopile is shown in Figure 5.4.

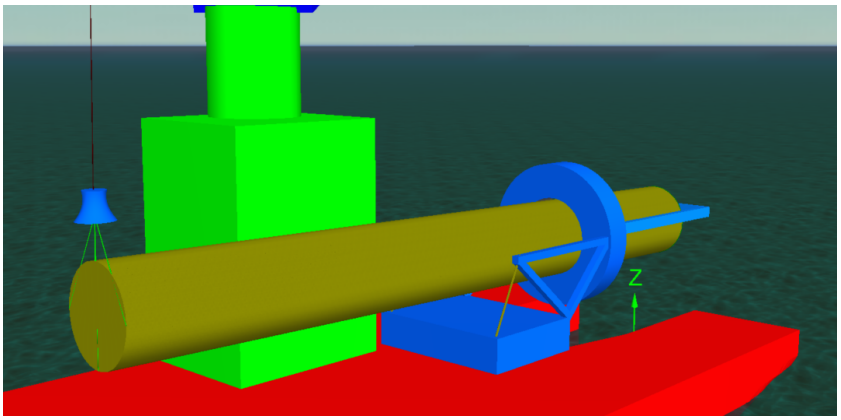

Figure 5.3: Modelling of monopile in OrcaFlex as line object for horizontal and upended monopile

The spar buoy creates the possibility to include the corresponding drag coefficient, added mass, slamming coefficients, and more accurately the buoyancy force. The spar buoy is discretised into multiple cylinders to better control the buoyancy force. The solver in OrcaFlex calculates the buoyancy by the wave slope above or below the centroid of the cylinder [105]. A more accurate estimation of the wave surface is obtained by having several centroids of cylinders as depicted in Figure 5.5.

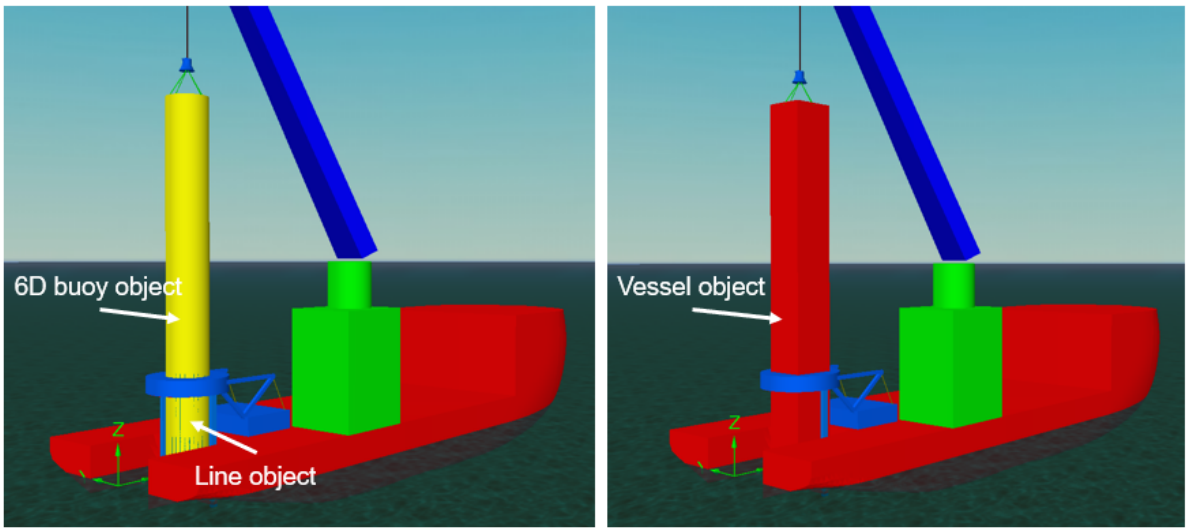

Figure 5.4: Modelling of monopile in OrcaFlex as hybrid buoy-vessel-line object for partly submergence of monopile

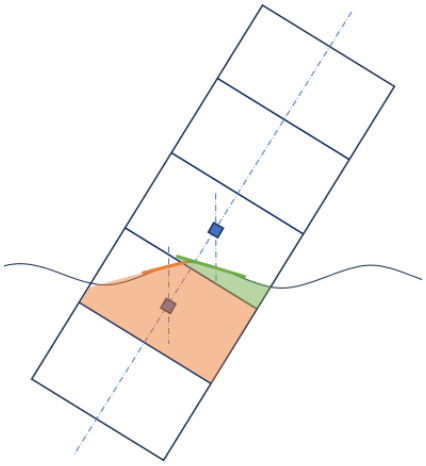

Figure 5.5: Wave slope estimation of OrcaFlex to calculate buoyancy based on [105]

The hydrodynamic loads on spar buoys are calculated with Morison's equation ([106], [107]). The added mass and drag forces are applied on the parts which are submerged. When the object is partly submerged, the forces are scaled to the proportion of cylinder volume of the submerged buoy. The interaction effects on the fluid forces between the vessel and the monopile are imported from HydroD. A special multi-body group is created to take these effects into account.

The Morison equation for a fixed object in an oscillatory flow is shown in Equation (5.6). The first addend represents the fluid inertia force, related to the water particle acceleration, while the second addend represents the drag force, related to the water particle velocity. For a cylinder with a diameter D Equation (5.6) is rewritten to Equation (5.7).

$$F = \rho \cdot C_m \cdot V \cdot \dot{u} + \frac{1}{2} \cdot \rho \cdot C_d \cdot A \cdot u \cdot |u| \tag{5.6}$$

$$F = \rho \cdot C_m \cdot \frac{\pi}{4} \cdot D^2 \cdot \dot{u} + \frac{1}{2} \cdot \rho \cdot C_d \cdot D \cdot u \cdot |u| \tag{5.7}$$

When the object itself also moves with a velocity $v(t)$, the Morison equation is rewritten to an equation with three addends (Equation (5.8): respectively the Froude-Krylov force, which is proportional to the

fluid acceleration relative to the earth, the hydrodynamic added mass force, which is proportional to the fluid acceleration relative to the body, and lastly the drag force:

$$F = \rho \cdot V \cdot \dot{u} + \rho \cdot C_a \cdot V \cdot (\dot{u} - \dot{v}) + \frac{1}{2} \cdot \rho \cdot C_d \cdot A \cdot (u - v)|u - v| \tag{5.8}$$

5.4.2. Mission equipment

The crane consists of a slewing column and a crane boom. The slewing column rotates, however the vertical position remains identical. Therefore, the slewing column is not separately modelled in terms of mass and mass moment of inertia, but included in the vessels mass and inertia. The crane boom however changes in the x, y, and z direction which affects the mass moment of inertia and the loading condition. The crane boom and crane hook are separately modelled. The crane hook is connected to the monopile with 4 springs. The crane hook has 6 degrees of freedom to model the behaviour of the crane hook as realistic as possible.

The crane boom, crane hook, and monopile gripper are separately modelled in OrcaFlex, due to the change of position of these mission equipment during the operation. This implies that a superstructure subtraction must be performed from the results of HydroD to have the correct mass, mass moments of inertia and centre of mass of the hull of the vessel. The inertia matrices I are shifted to a common origin (Equation 5.9), after which the structure matrix is subtracted [108]. When there is a rotation of the superstructure, the rotation matrices (Equation 5.12) first need to be applied. Lastly, the centre of gravity of the hull with respect to the common origin is calculated (Equation 5.14) [108]. This procedure is performed for both the crane boom and pile gripper.

$$I' = \begin{bmatrix} 1 & 0 \\ [\vec{\Delta}]_\times & 1 \end{bmatrix} I \begin{bmatrix} 1 & [\vec{\Delta}]_\times^T \\ 0 & 1 \end{bmatrix} \tag{5.9}$$

With 1 the 3x3 identity matrix, and $\vec{\Delta}$ the offset between the old origin and the new reference point.

$$[\vec{\Delta}]_\times = \begin{bmatrix} 0 & \Delta_z & -\Delta_y \\ -\Delta_z & 0 & \Delta_z \\ \Delta_y & -\Delta_x & 0 \end{bmatrix} \tag{5.10}$$

$$[\vec{\Delta}]_\times^T = -[\times\Delta]_x \tag{5.11}$$

When the structure has a rotation, then first the rotation matrices need to be applied before the structure matrix is transformed to a common origin. The rotation matrix accounting for roll, pitch, and yaw is presented in Equation 5.12 [109].

$$R = \Phi\Theta\Psi = \begin{bmatrix} 1 & 0 & 0 \\ 0 & cos(\phi) & sin(\phi) \\ 0 & -sin(\phi) & cos(\phi) \end{bmatrix} \begin{bmatrix} cos(\theta) & 0 & -sin(\theta) \\ 0 & 1 & 0 \\ sin(\theta) & 0 & cos(\theta) \end{bmatrix} \begin{bmatrix} cos(\psi) & sin(\psi) & 0 \\ -sin(\psi) & cos(\psi) & 0 \\ 0 & 0 & 1 \end{bmatrix} \tag{5.12}$$

The structure inertia matrix I_s is then rotated to use the same axes as the total inertia matrix:

$$I_s' = R \cdot I_s \cdot R^T \tag{5.13}$$

The centre of gravity for the hull relative to the common origin is calculated as follows, using the off-diagonal blocks of the inertia matrix [108]:

$$\vec{\Delta}_{hc} = \frac{1}{2}\frac{1}{m_h} \begin{bmatrix} {}^cI_h|_{26} - {}^cI_h|_{35} \\ {}^cI_h|_{34} - {}^cI_h|_{16} \\ {}^cI_h|_{15} - {}^cI_h|_{24} \end{bmatrix} \tag{5.14}$$

The contact between the pile gripper and monopile is relevant for the interface loads between these two objects. Four rollers with a constraint are applied to properly model this contact. The value for

the stiffness of the rollers is based on internal knowledge. The four rollers are shown in Figure 5.6. A drawing of the shape of the pile gripper ring is also included in the model, however this drawing does not have any physical properties and therefore does not influence the results.

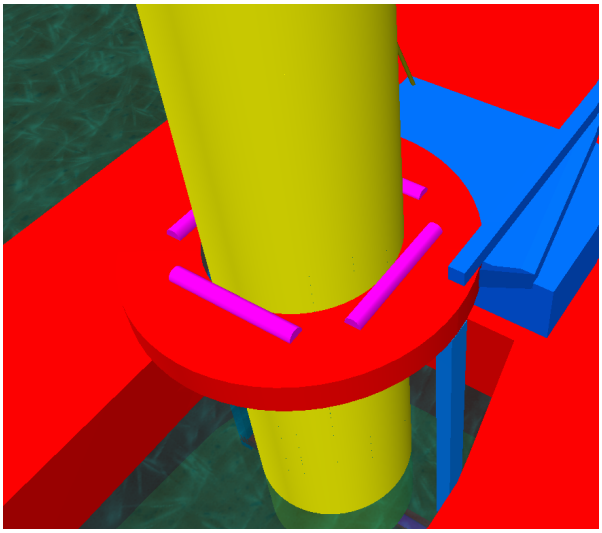

Figure 5.6: Modelling of pile gripper contact with monopile in OrcaFlex by four (pink) rollers with constraint

5.4.3. Wave shielding

Wave shielding is a phenomenon of diffraction of the incoming waves by the presence of a hull or object. For side installation, the monopile is lowered at the leeward side of the vessel. For stern installation, the monopile is lowered in the recess of the stern. The position and behaviour of the monopile is influenced by the presence of the vessel. The wave shielding reduces the overall dynamic forces that act on the subsea asset when it is lowered due to the decrease of the displacement, velocity and acceleration of the waves ([33], [73]). It is modelled in OrcaFlex by sea state RAOs defined for vessel objects in multi-body groups. These RAOs depend on the wave direction, wave frequency, velocity potential and velocity potential gradient, and are generated in HydroD. Shorter waves are more affected by shielding, because the vessel tends to follow the motion for longer wavesd. The hull of the vessel and the vessel object of the monopile are modelled in a multi-body group which allows to account for the interaction between these two objects, and therefore for wave shielding.

5.4.4. DP system

The horizontal motions and heading of the vessel are stabilised by a dynamic positioning system. Four soft spring lines represent the DP system which constrain the motion of the vessel in surge, sway and yaw. The natural period of the springs cannot interfere with the periods of the wave loads, therefore the stiffness is chosen to result in a large natural period. The exact value is chosen based on the knowledge of Ulstein.

5.5. Hydrodynamic damping

Hydrodynamic damping represents the dissipation of energy due to fluid-structure interaction. It consists of potential damping, viscous drag and tip vortex damping. Hydrodynamic damping is of importance for lowering surface-piercing cylinders, such as 2XL monopiles. A cooperation between Ulstein Design and Solutions, Huisman Equipment and Heerema aimed to assess the tip vortex damping for monopiles by conducting model tests and CFD tests. The schematic representation in 2D of the model decay test set-up is depicted in Figure 5.7a. The panel mesh of the monopile used for the damping calculation in WADAM, a by DNV developed hydrodynamic analysis program, by Ulstein is presented in Figure 5.7b. A general method is derived to compute the tip vortex damping of monopiles, depending on the diameter of the monopile. The tip vortex damping of monopiles is then included in the damping settings of the partly submerged monopile in OrcaFlex.

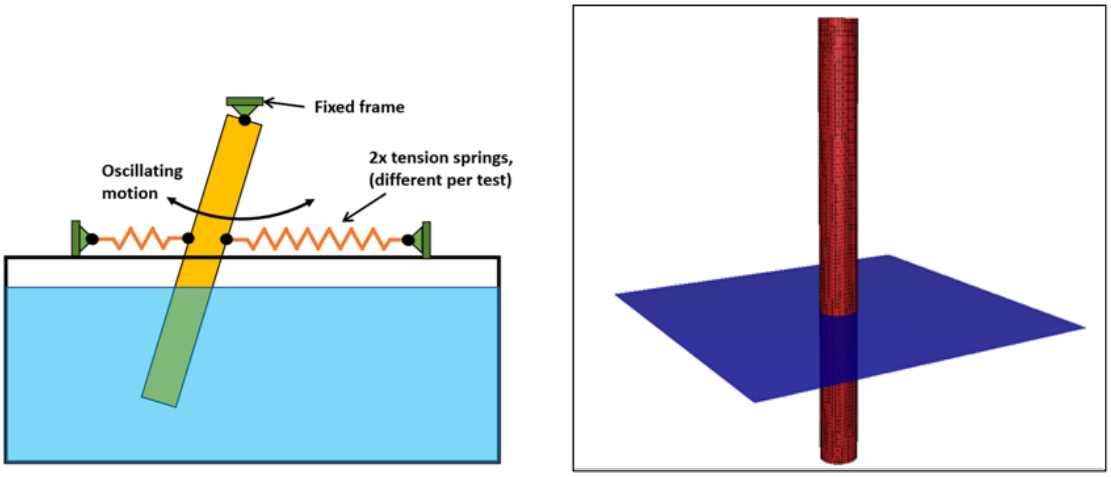

(a) Schematic 2D representation of model decay tests set-up performed by Huisman Equipment [11]

(b) WADAM panel mesh of the monopile used for the damping calculation by Ulstein [11]

Figure 5.7: Assessment of tip vortex damping by model tests and CFD calculations

5.6. Conclusion

This chapter provides an answer to the subquestion: *"Which installation sequences are preferred for 2XL monopile installation?"*. The installation sequence consists primarily of 5 loading conditions for both side and stern installation:

- Monopile placed horizontally on deck
- Monopile 45 ° upended
- Monopile fully upended
- Monopile half way water depth
- Monopile 3 metres above sea bed

These loading conditions include the beginning and ending of the upending and lowering phase, with a loading condition halfway the upending and lowering phase. For these situations, the loading conditions are calculated, taking into account the free surface moment of ballasting tanks. The hydrodynamic properties, such as added mass and damping matrices, load and displacement RAOs are generated by HydroD. These properties are then imported in the OrcaFlex files. For the loading conditions where the monopile is not submerged, the monopile is modelled as a line object. However, the submerged monopile is modelled as a hybrid line-buoy-vessel object. The line object models the contact with the pile gripper ring, while the buoy takes into account the viscous drag, inertia and buoyancy forces. Lastly, the vessel object of the model is needed to include the tip vortex damping. The tip vortex damping is part of the hydrodynamic damping and is derived from CFD tests performed by a combined effort of Ulstein, Huisman Equipment and Heerema. This model set-up is prepared and therefore the numerical simulations for different loading conditions are performed. These numerical simulations are elaborated in Chapter 6.

6

Numerical simulations

The numerical simulations are performed in OrcaFlex. These simulations consist of a static and a dynamic simulation. The static simulation is briefly elaborated in Section 6.1. The dynamic simulation is either a frequency-domain or time-domain solution, as covered in Section 6.2. Furthermore, this chapter describes the simulation approach, a time sensitivity analysis, and a comparison with a 3 hours time simulation in Section 6.2.3.

6.1. Static simulation

The static simulation provides the configuration used as a starting point for the dynamic simulation. The position and orientation of every object in OrcaFlex is found such that all forces and moments are in equilibrium by applying Newton's method. Due to the nonlinear nature of the models, the statics calculation is an iterative process and therefore consists of a line statics part and an entire statics part.

Firstly, only the statics of line objects are calculated. The degrees of freedom of all other objects are fixed. The goal of the determination of line statics is to provide an initial configuration for the entire system statics. In the first step various methods exist. For the falls, which are the line objects in the model, the catenary method is applied. The analytic catenary method allows the weight, buoyancy and drag of the object, but excludes bending stiffness and interaction with shapes. When the catenary method is accomplished, the full statics method is applied which uses the position of the catenary method to determine the equilibrium position now taking the bending stiffness and interaction with shapes into account. For the line object of the monopile, the spline method is applied. The line object is given an initial shape with multiple control points. The initial shape is based on a Bezier spline curve, which tries to follow the set of control points [110]. The smoothness of this curve is determined by the order of shape; the higher the order, the smoother the curve. The first and last control points are defined by the beginning and end of the line object and the curve is generated in between [111].

After the line statics calculation, all the degrees of freedom are released and an entire system statics is determined. It is possible to suppress certain degrees of freedom for objects in order to reach convergence more easily. During the dynamic simulation, all the degrees of freedom are then released again. It is however not preferred, because it might result in a transient at the start of the dynamic simulation causing issues later. With the position and orientation of every object determined, the model is prepared to perform the dynamic simulation.

6.2. Dynamic simulation

The dynamic simulation is either performed in the frequency domain or in the time domain. In the frequency domain, the dynamic response is solved at discrete frequencies. Frequency-domain simulations are in general faster than time-domain simulations. However, the analysis is linear and therefore nonlinearities in the model will be linearised. This implies that signigicant nonlinearities influence the accuracy and results of the simulation negatively. Multi-body interaction, such as the interaction between

the vessel and a monopile, implies nonlinearities. Therefore, time-domain simulations are necessary.

In the time domain, the equation of motion (Equation 7.6) based on Newton's second law is solved:

$$M(x,\ddot{x}) + C(x,\dot{x}) + K(x) = F_E(x,\dot{x},t) \tag{6.1}$$

with: $M(x,\ddot{x})$ the system inertia load, $C(x,\dot{x})$ the system damping load, $K(x)$ the system stiffness load, $F_E(x,\dot{x},\ddot{x})$ the external load, and $x,\dot{x},\ddot{x},t$ respectively the position, velocity, acceleration and the simulation time. The numerical integration methods to solve this differential equation are categorised into implicit (Section 6.2.1) and explicit (Section 6.2.2) methods. For both implicit and explicit methods different approaches exist, however OrcaFlex offers one approach for the implicit method and one approach for the explicit method. These integration schemes are covered in the next sections.

6.2.1. Implicit time-domain simulation

Implicit time-domain integration schemes involve the solution of the equation of motion at the end of each time step. Examples of implicit methods are the Backward Euler method and the Trapezoidal method [112]. A problem of the Backward Euler method is the high level of damping of high frequencies. The generalised-α methods offer the possibility to control the damping by changing the parameter α. This results in less damping and therefore more accuracy. However, it also implies a less stable result. OrcaFlex only offers the generalised-α integration scheme of Chung and Hulbert [113]. It is an iterative solution method which implies a longer computation time compared to the explicit integration scheme. However, it offers a relatively more stable method compared to the explicit method.

6.2.2. Explicit time-domain simulation

Various explicit time-domain methods exist, such as the Forward Euler and Runge Kutta 4 methods [112]. OrcaFlex only offers the semi-implicit Euler method. The equation of motion is first solved only locally at the beginning of the time step for the acceleration vector [114]. Next, it is integrated using semi-implicit Euler integration. This method calculates the state of the system with the derivative at the end of the time step, where the Forward Euler method uses the current derivative. The values of the position x, velocity $\dot{x}$ and acceleration $\ddot{x}$ at the end of the constant time step $(t + dt)$ are given by:

$$\dot{x}_{t+dt} = \dot{x}_t + dt\ \ddot{x}_t \tag{6.2}$$

$$x_{t+dt} = x_t + dt\ \dot{x}_{t+dt} \tag{6.3}$$

At the end of the time step the positions and orientations of each free body and line node are known and the process is repeated. The semi-implicit Euler method is a robust method. However, due to stability requirements, the time steps can be very short which results in long computation times.

For the numerical simulations in the time domain of this thesis, the implicit integration scheme, the generalised-α method with a constant time step is applied. The implicit integration scheme has a longer computation time. However, it is more stable than the explicit integration scheme, which probably needs shorter time steps due to stability requirements.

6.2.3. Simulation approach

The upending and lowering of a monopile is a nonstationary process. Two approaches to simulate nonstationary processes are proposed by Sandvik [115]:

1. Steady-state simulations in irregular waves of the most critical vertical positions of the object.
2. Simulations of a repeated nonstationary lowering process with different irregular wave realisations and for every simulation an analysis of the extreme response.

It was shown that the second approach, to have a repeated nonstationary lowering process, results in more realistic results compared to the steady-state simulations. The first approach creates a build-up of oscillation which is not observed in reality. However, for this Master's thesis, steady-state simulations in the time domain are applied. Steady-state simulations of different loading conditions are a relatively fast, effective and simple way of modelling an installation sequence, compared to modelling

a nonstationary version of the same installation sequence. By simulating different loading conditions of the installation sequence for various environmental conditions, the critical situations for different T_p and H_s can still be distinguished. For further research, setting up simulations with a nonstationary lowering process are recommended and interesting to analyse differences between the steady-state simulations and repeated nonstationary lowering processes.

The duration of the simulation is set at 1800 seconds, which is found to be a sufficient representative of a sea state reference period, which is 3 hours, which is explained in this section. Besides the actual simulation time of 1800 seconds, a build-up period of 50 seconds is applied, as shown in Figure 6.1. The build-up period provides a smooth build-up of sea conditions to avoid transients when the simulation starts.

Figure 6.1: Simulation time of the time-domain simulations solved with the generalised-α integration scheme

Due to the stability, the implicit time integration method is applied with a constant time step. A time step sensitivity analysis is conducted for 0.01, 0.10, and 1.00 seconds, as presented in Figure 6.2, Figure 6.3, and Figure 6.4. A trade-off between capturing all the relevant effects and the computational time led to a time step of 0.1 seconds. A larger time step results in less computational time, however the difference in results between 0.01 and 0.10 seconds is found to be small enough. In addition, the aim of this thesis is not to have the most accurate results, but to identify the critical behaviour during upending and lowering of the 2XL MP. Therefore, the a time step of 0.1 seconds is found to be sufficient.

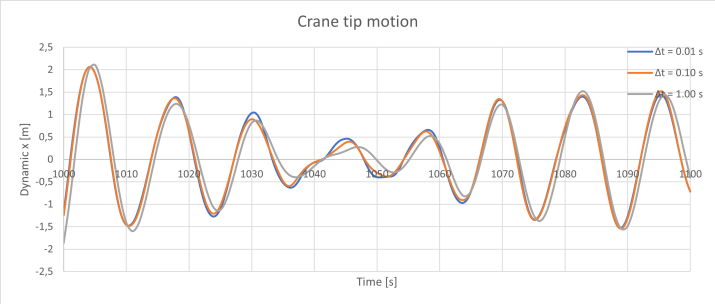

Figure 6.2: Dynamic x at the crane tip [m]

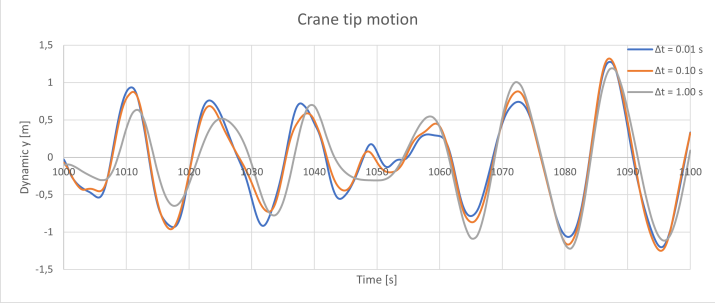

Figure 6.3: Dynamic y at the crane tip [m]

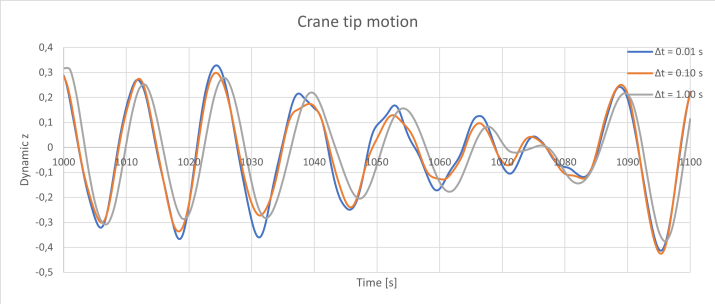

Figure 6.4: Dynamic z at the crane tip [m]

A sea state reference period takes 3 hours. For the numerical simulations a simulation time of 1800 seconds is set. In Figure 6.5, Figure 6.6, and Figure 6.7, a comparison between a simulation time of 1800 seconds and 3 hours are displayed for the loading condition where the MP is submerged for 5.56 metres, with a H_s of 2 metres and a T_p of 12.8 seconds. The total energy of the 3 hours run seems a bit higher for the dynamic x and y than for the 1800 seconds run. In addition, for the dynamic x and y, there are some differences in the curve of the graph due to possibly more scatter of waves, which are or are not in the simulation. For the dynamic y, the eigenfrequency of the MP seems more dominant, which explains the better correspondence compared to the dynamic x. In conclusion, the differences in spectral density are found to be negligible enough to continue with the 1800 seconds simulation times while also taking into account the longer computational time which is needed for 3 hours simulations.

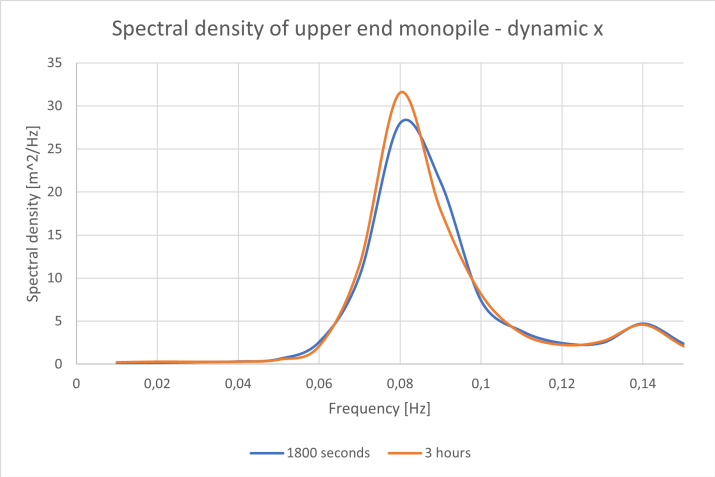

Figure 6.5: Dynamic x at the monopile tip [m]

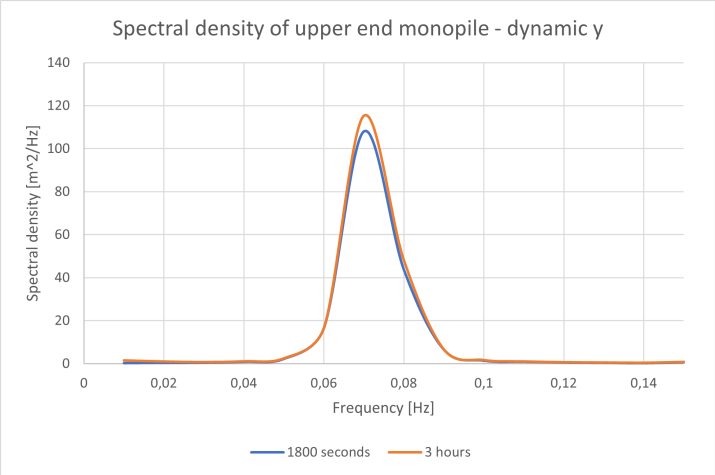

Figure 6.6: Dynamic y at the monopile tip [m]

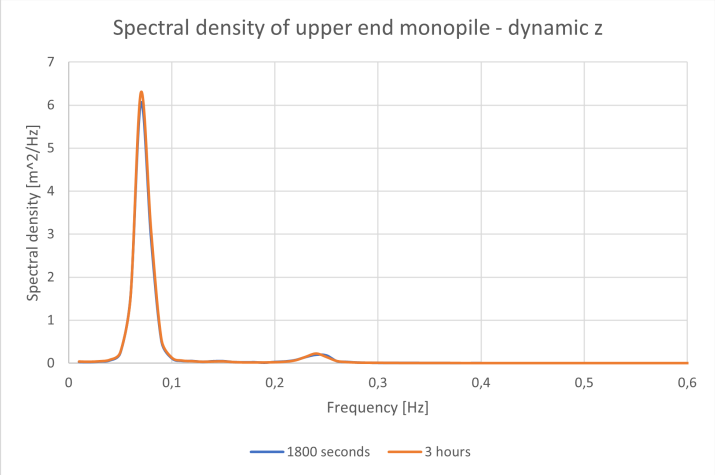

Figure 6.7: Dynamic z at the monopile tip [m]

6.3. Conclusion

This chapter describes the choices for the numerical simulations. The numerical simulation consists of a static simulation and a dynamic simulation. The static simulation forms the basis for the dynamic simulation. For this thesis, the dynamic simulation is performed in the time domain. The equation of motion is solved using a implicit time-domain integration scheme, the generalised-α integration scheme, with a time step of 0.1 seconds. The simulation time is 1800 seconds, which is found to be sufficient enough to represent a sea state reference period of 3 hours. In addition, there is a build-up time of 50 seconds to provide a smooth transition between the static and dynamic simulation. Lastly, the simulations are steady-state simulations for different positions of the monopile during the nonstationary process of upending and lowering of the monopile.

7

Validation and verification

This chapter covers the validation and verification of this thesis by answering the subquestion: *"How is the applied model verified and validated?"*. Verification is the procedure of which the goal is to proof that the used method is correctly used and therefore suitable for the research topic. Validation, on the other hand, is the procedure of proving that the outcomes of the research are true. For this specific thesis, a full-scale validation is not possible: comparable studies are not found for this application. Therefore, partial validation is applied. Parts of the study are validated to be able to assess the model accuracy. However, validation and verification is never a guarantee that the model is entirely correct and complete [116]. In Section 7.1, the loading conditions of the installation sequences are covered, in Section 7.2 the validation of HydroD is briefly described, the numerical simulations in OrcaFlex in Section 7.4, and finally the pendulum calculations are covered in Section 7.5. In Section 7.6 a concluding answer is provided including a reflection on the validation and verification process.

7.1. Loading conditions

The loading conditions are calculated based on a lightship weight estimate of the reference vessel. The specific properties of the mission equipment and the monopile are added to the loading conditions. The inertia of the lightweight components and the monopile only include the Steiner terms. For the crane, the entire inertia calculation is included. Another simplification is the exclusion of the buoyancy of the 2XL MP for the loading conditions with the monopile partly submerged.

The differences for excluding the buoyancy of the partly submerged, tapered monopile are calculated. For side installation and stern installation, the largest difference is in the total weight of the vessel with a difference of 0.50 % as shown in Table 7.1. The difference in radii of gyration remains below the 0.5 % for side and stern installation. The differences in LCG and TCG are certainly negligible, a difference of 0.00 %. The VCG has the largest difference for the 2XL 3 metres above seabed, 1.26 % for side installation and 2.99 % for stern installation. This is expected since the buoyancy is the largest in this loading condition. In conclusion, the effects of the buoyancy are sufficient small enough to neglect the buoyancy in the loading condition calculation.

Table 7.1: Difference [%] due to exclusion of buoyancy for the loading condition with a partly submerged, tapered monopile for side and stern installation

Side installation	Fully upended	Halfway water depth	$3m$ above seabed
Difference [%] in MP weight [t]	1.23 %	8.50 %	15.78 %
Difference [%] in total weight [t]	0.04 %	0.27 %	0.50 %
Stern installation	Fully upended	Halfway water depth	$3m$ above seabed
Difference [%] in MP weight [t]	1.23 %	8.50 %	15.78 %
Difference [%] in total weight [t]	0.04 %	0.24 %	0.45 %

The loading conditions are examined against design values which are used in the industry as check for the inertia calculations. These values depend on the type of vessel. Firstly, the I_{yy} should be equal to I_{zz} [117]:

$$I_{yy} = I_{zz} \tag{7.1}$$

with:

$$K_{yy} \geq 0.25 \cdot L_{vessel} \tag{7.2}$$

Furthermore, for crane vessels intended for this type of operation, the following constraint applies for K_{xx} (C. Rossetti, personal communication, August 2023):

$$K_{xx} \leq 0.50 \cdot B_{vessel} \tag{7.3}$$

For ships with an even transverse distribution of mass the approximate design value may be used [118], as presented in Equation 7.4. This value is not directly applicable on the reference vessel, but is included in this section to develop the understanding of these values.

$$K_{xx} = 0.38 \cdot B_{vessel} \tag{7.4}$$

whereas DNV states the following approximate design value [119]:

$$K_{xx} = 0.39 \cdot B_{vessel} \tag{7.5}$$

In Table 7.2 the radii of gyration, divided by either the width or length of the vessel, are displayed per loading condition for both side and stern installation. Equation 7.3 complies. The radii of gyration of the loading conditions do not comply with Equation 7.4 and Equation 7.5, which is expected, with the exception of the horizontally placed 2XL MP for side installation. It complies due to more evenly distributed mass, since the MP is horizontally and transversely placed on deck for that specific loading condition. For the other loading conditions the crane at starboard is one of the reasons the values are higher than Equation 7.4 and Equation 7.5. The values for K_{xx} are as expected between 0.38 and 0.50. Equation 7.1 is met, with exception for two loading conditions which are the transition between 0.27 and 0.28. An explanation is the rounding off of the values. All the loading conditions comply for the constraint of Equation 7.2.

Table 7.2: Ratio of radii of gyration and main dimension of the reference vessel for the loading conditions for side and stern installation

Side installation	Horizontal MP	$45°$ upended	Fully upended	Halfway water depth	3m above seabed
$\frac{K_{xx}}{B}$ [-]	0.38	0.40	0.46	0.44	0.45
$\frac{K_{yy}}{L}$ [-]	0.28	0.28	0.27	0.27	0.27
$\frac{K_{zz}}{L}$ [-]	0.28	0.27	0.27	0.27	0.27
Stern installation	Horizontal MP	$45°$ upended	Fully upended	Halfway water depth	3m above seabed
$\frac{K_{xx}}{B}$ [-]	0.43	0.44	0.43	0.49	0.50
$\frac{K_{yy}}{L}$ [-]	0.27	0.27	0.28	0.27	0.27
$\frac{K_{zz}}{L}$ [-]	0.27	0.27	0.28	0.28	0.27

Despite the simplifications in the loading condition calculation, such as excluding buoyancy and only taking into account the Steiner terms for the lightship weight estimate and the monopile, the radii of gyration comply in general with the approximate design values. An exception is visible for the K_{yy} and K_{zz}, but is explained as the transition from 0.27 to 0.28 in combination with the rounding off of the values.

7.2. Hydrodynamic properties

HydroD is a software package provided by DNV, a ship classification organisation. More information about HydroD is provided in Section 4.2.1. HydroD is developed by DNV and therefore also validated by DNV.

In Section 5.3, sloshing in the recess of the reference vessel is described. To verify the origin of this peak in frequency, it is verified with Merian's formula, originating from coastal engineering, and regulations of BV ([103], [104]). The relative differences of the longitudinally and transversely sloshing periods of approximately 5.6 % and 5.4 % are found to be small enough. Differences originate amongst others from the fact that Merian's formula is based on a basin with a certain water depth, where a recess or moonpool does not have bottom plating. The damping curves for respectively surge and sway of the vessel are generated by HydroD. For surge, the damping peaks at a frequency of approximately 0.183 Hertz, corresponding with a period of 5.46 seconds. For sway, the damping peaks at a frequency of 0.195 Hertz, corresponding with a period of 5.13 seconds. Comparing these values with the results of the Merian formula and the formula of BV, the values of BV and HydroD are closer to each other than for the Merian formula. However, the values of HydroD, the Merian formula, and the BV regulations are sufficiently close to each other to conclude that this peak originates from the sloshing effect.

The drag coefficient of the monopile is determined based on literature and based on CFD tests, as described in Section 5.5. The value of the drag coefficient based on literature was found to be too low, as it was expected to be between 0.25 and 0.50. Therefore, it was compared to the coefficients derived from the CFD tests which were found to be more reasonable.

The loading conditions, which are explained in the previous section, are processed in HydroD. Load and displacement RAOs are generated for the vessel for all six degrees of freedom for every loading condition for side and stern installation with its corresponding wave direction. The natural period of the vessel for heave, roll, and pitch can be visually derived. For stern installation with head waves, the absence of a peak in period for roll is particularly well visible, compared to the side installation method. For heave and pitch, the peak in period and order of amplitude corresponds for side and stern installation for these two loading conditions. In Appendix C, the RAOs are presented for all loading conditions. These graphs are used to verify the results in Chapter 8.

7.3. Wave shielding

The wave shielding is simulated with the sea state RAOs of vessel objects, as explained in Section 5.4.3. These RAOs are generated in HydroD and used as an input in OrcaFlex. A comparison of the wave height at the position of the monopile is made between CFD tests and the OrcaFlex simulations. The CFD tests are performed internally at Ulstein, for a wave height of 4.65 metres and a wave period of 7.02 and 10.91 seconds [120]. The wave direction is $210°$ for side installation. For stern installation, the wave direction is $165°$.

The wave height, wave period and wave direction of the CFD tests are implemented in the OrcaFlex files to enable a comparison. The loading condition of the fully upended monopile is used as a basis. Between the CFD and OrcaFlex are multiple modelling differences: the position of the monopile is slightly different for side and stern installation and the loading conditions are not identical. Furthermore, the hydrodynamic properties of the OrcaFlex simulation is based on a wave height of 2 metres.

The largest wave height of the CFD results is graphically derived, which is less accurate then for the OrcaFlex observed largest wave height which is extracted from the wave elevation dataset for every time step. The differences between the CFD results and OrcaFlex are below 25 %. For stern installation, it is shown that the reduction in wave height is larger compared to the CFD tests for the period of 7.02 seconds, whereas for the period of 10.91 seconds the CFD results show a larger reduction. For side installation, the CFD results show a larger reduction in largest observed wave height. It is concluded from both the CFD and OrcaFlex results that the wave height is less affected for the higher wave periods. For shorter wave periods, the reduction in wave height is larger. However, the difference in wave height reduction for side and stern installation is different for the two methods: based on the CFD results the

side installation provides a larger wave height reduction, and based on OrcaFlex the stern installation.

7.4. Numerical simulation

For the numerical simulation three types of validation are applied [116]:

- Sensitivity analysis validation
- Face validation
- Animation validation

For the time step of the numerical model, a sensitivity analysis is performed to determine the effect on the output. A more detailed elaboration is provided in Section 6.2.3. A trade-off is made between accuracy and computational time.

Similarly the simulation time is studied for a duration of 1800 seconds and 3 hours in Section 6.2.3 to determine the influence of the duration of the simulation. Differences are mostly observed in the dynamic x motion.

Face validation is the type of validation when knowledgeable professionals are asked whether the model is reasonable. For this thesis, there has been contact with a professional of OrcaFlex itself, who studied the input, such as physical characteristics, and simulation settings and provided the model of feedback. Within Ulstein, a hydrodynamic expert with a significant expertise of OrcaFlex also provided feedback on the numerical models.

Animation validation is another form of validation [121]. In OrcaFlex it is possible to graphically visualise the simulation when it runs over time. Different ways of applying this type of validation are possible: to check if things happen that cannot occur in real life, as a form of verification, or to see if displacements occur as intended.

7.5. Pendulum calculations

The multi-body behaviour of the crane boom with the monopile, rigging and crane hook result in resonance behaviour when the peak period of the wave coincide with the natural periods of system. The eigenfrequencies are determined to explain behaviour observed in the results. Firstly, the natural periods are determined with modal analysis in OrcaFlex in Section 7.5.1. Secondly, the natural periods are analytically derived for a simple pendulum, physical pendulum and double pendulum in Section 7.5.2.

7.5.1. Modal analysis

A modal analysis of the static simulation is performed in OrcaFlex for three different situations:

- Entire model including vessel and DP springs
- Crane with pile gripper and monopile
- Crane and monopile

The modal analysis in OrcaFlex is calculated for the undamped modes without added mass terms, after the static simulation. For one degree of freedom this, the differential equation is presented in Equation 7.6, which leads eventually to the calculation of the natural period T as described in Equation 7.7.

$$m \cdot \ddot{x}(t) = -k \cdot x(t) \tag{7.6}$$

$$T = 2 \cdot \pi \sqrt{\frac{m}{k}} \tag{7.7}$$

For multiple degrees of freedom, which is the case for the simulations, Equation 7.6 changes to, when also substituting the simple harmonic solution $x(t) = a \cdot sin(\omega t)$:

$$-\omega^2 \cdot \mathbf{M} \cdot \mathbf{x} = \mathbf{K} \cdot \mathbf{x} \tag{7.8}$$

The number of eigenfrequencies resulting from this equation equals the number of degrees of freedom of the model. For the modal analysis the added mass of vessel objects is neglected because of the frequency dependent added mass and damping data present in the simulation model.

For every loading conditions, the natural periods are presented in Appendix A. The natural periods of the system with and without pile gripper coincide partly. The pile gripper influences the natural periods of the considered system. However, for the analytical calculations, the effect of the gripper as a hinge, is neglected. When analysing the operational limits, the effect of the pile gripper needs to be included.

7.5.2. Analytical approach

The multi-body behaviour of the mission equipment and the monopile is also analysed analytically. The calculations start with the simple pendulum and then extending the calculations to the physical pendulum to include mass and inertia effects. Finally the double pendulum is calculated for the system including the falls, the crane hook and the monopile.

Simple pendulum

The simple pendulum is a mathematical model of a massless rod with a point mass at the end of the rod. The simple pendulum is depicted in Figure 7.1a with the characteristics of the 2XL MP applied. The mass of 2300 tonnes is applied at the end of the rod as a point mass. The angle θ is assumed to be small ($\theta \leq 15°$) and therefore the restoring force is directly proportional with the displacement. This implies the pendulum to be a simple harmonic oscillator. The linear natural period is presented in Equation 7.9.

$$T_n = 2\pi\sqrt{\frac{L_{MP}}{g}} = 2\pi\sqrt{\frac{100}{9.81}} = 20.06\ s \tag{7.9}$$

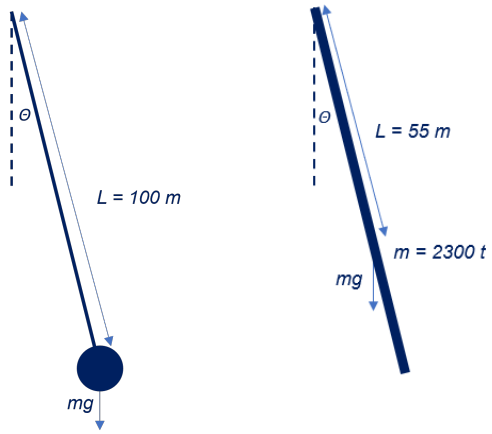

(a) Simple pendulum **(b)** Physical pendulum

Figure 7.1: Schematic representation of the simple and physical pendulum with the characteristics of the 2XL MP

Physical pendulum

A physical pendulum includes the inertia effects of the mass, including the Steiner term. In Figure 7.1b the physical pendulum is presented. The calculation of the natural period is presented in Equation 7.10 with the approximation of the I of the monopile as a small rod rotating about one of its ends in Equation 7.11.

$$T_n = 2\pi\sqrt{\frac{L}{g} + \frac{I}{M_{MP}gL}} = 2\pi\sqrt{\frac{55}{9.81} + \frac{7,666,666,667}{2,300,000 \cdot 9.81 \cdot 55}} = 21.57\ s \tag{7.10}$$

$$I \approx \frac{1}{3} \cdot m \cdot L_{MP}^2 \tag{7.11}$$

An increase of natural period of about 7.5 % is observed compared to the simple pendulum. The natural periods calculated for the simple and physical pendulum result in values slightly larger than 20 seconds. However, these values are not interesting for this case study. Resonance behaviour is observed when the natural period of the system equals the peak period of the environment. The peak period of the North Sea varies, although it is very unlikely to reach 20 seconds, as can be seen in Figure 4.9.

Double pendulum
A system of a double pendulum is also analysed. The system includes the characteristics of the falls of the crane, the crane hook and the 2XL MP. A schematic representation is presented in Figure 7.2.

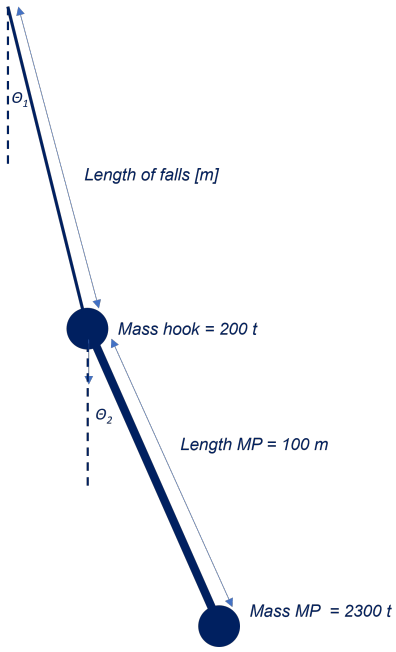

Figure 7.2: Schematic representation of the double pendulum with the characteristics of the falls, the crane hook, and the 2XL MP

For the double pendulum, there are two angles of inclination, θ_1 and θ_2. The small angle approximation is also applied for the double pendulum. The equation of motion (Equation 7.6) is solved similarly to the modal analysis, with the assumption that the solution is a sine-function. This results in Equation 7.8, which is an eigenvalue problem with two degrees of freedom.

$$\mathbf{K} \cdot \mathbf{x} = \lambda \mathbf{M} \cdot \mathbf{x} \tag{7.12}$$

The eigenvalue problem is solved using a Cholesky decomposition. The natural periods are calculated for multiple levels of submergence and graphically displayed in Figure 7.3. The two natural periods of the monopile do not coincide between 0 and 65 metres of submergence. The first and second natural period flip between 15 and 20 metres of submergence, because the natural period of the falls and the monopile, and therefore the rotation point, change over a different level of submergence. The difference between the natural periods increases when the monopile is more submerged.

In Appendix A, the modal analysis for every loading condition for side and stern installation is presented. Three situations are evaluated: the entire system, the system with the monopile and the mission equipment, and the monopile with the crane. Comparing the results of the double pendulum with monopile-crane system, it is visible that the natural periods of the double pendulum are in the same range as the first two modes of the modal analysis. However, the double pendulum calculations include the added mass, while the modal analysis excludes the added mass, since it is frequency-dependent. This causes, especially for the more submerged monopile, differences in natural period. When the monopile is more submerged, the added mass is larger. The rotation point shifts downwards, and the added mass shifts upwards over the length of the monopile [122]. These shifts reduce the distance between these two points and therefore reduces the inertia moment. The influence of the reduced arm is larger than the

increase in added mass, since the length is squared. Therefore, the mass matrix reduces, resulting in a decrease in natural period. This effect corresponds with the results of the double pendulum calculation. This trend is not visible in the modal analysis results, since the added mass is neglected and therefore the natural period of the crane-monopile system seems to increase. The difference in natural period between the double pendulum and the modal analysis also increases with a greater submergence of the monopile.

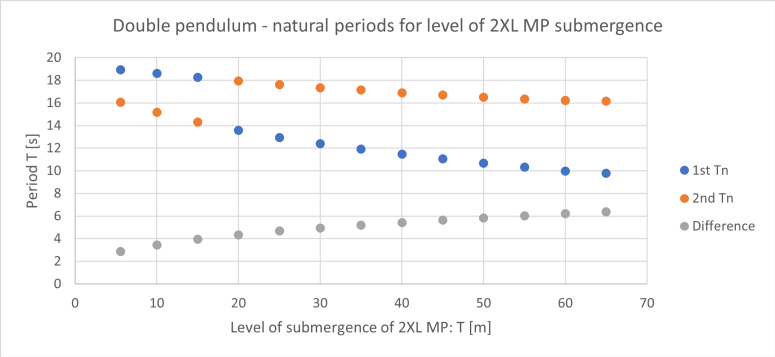

Figure 7.3: Natural periods for multiple levels of submergence of the monopile

7.6. Conclusion

This chapter provides an answer to the subquestion: *"How is the applied model verified and validated?"*. A full-scale validation is not possible since comparable studies are not found for this specific application. Therefore, parts of the methodology are validated. The loading conditions of the installation sequences are validated against design values of DNV and also supported by Gerritsma, Pinkster and Blom ([117], [118], [119]). The simplifications of neglecting the buoyancy of the partly submerged monopile and only taking the Steiner terms of the inertia calculation into account, lead to loading conditions that are considered accurate enough since the values are within the limits of the design values. The next stage in the methodology is the generation of the hydrodynamic properties in HydroD. HydroD is validated by DNV. Furthermore, the sloshing in the recess is double checked by BV regulations and the Merian formula originating from coastal engineering, and then compared to the damping curve of the vessel in OrcaFlex. The drag coefficient was first calculated based on literature, however the coefficient did not meet the expectations and was therefore secondly derived based on CFD tests.

The numerical simulations are also validated using partial validation. A sensitivity analysis is performed for the time step. A face validation is executed: a hydrodynamic expert within Ulstein and a software specialist of OrcaFlex provided iterative feedback on the (set-up of the) simulations. OrcaFlex provides a graphically presentation of the results which creates the possibility to also validate the results visually.

Finally, the behaviour of the monopile is validated by modal analysis of OrcaFlex and analytical pendulum calculations. The natural periods of the entire system, consisting of the vessel, mission equipment, and monopile, a system with only the mission equipment and the monopile, and thirdly only the monopile and crane, are extracted from OrcaFlex. The natural periods of the monopile are calculated according to the mathematical model of a simple and a physical pendulum. The effects of the falls and the crane hook with its mass and mass moments of inertia interacting with the monopile are also calculated applying the principle of the double pendulum. These values are used to verify the results.

Reflecting on the validation and verification of this thesis, the absence of a full validation and verification process implies in principle uncertainty about the validity and reliability of the results. Another possibility is to perform full-scale or model-scale experiments, but this is found financially and practically unrealistic within the scope of this thesis. However, this uncertainty is mitigated by performing a partial validation on stages in the methodology within the scope of this thesis. In addition, the aim of this thesis is not to obtain the most accurate results, but to be able to identify the critical key positions. Therefore, the partial validation for this thesis is found to be sufficient.

8

Operational limits

This chapter zooms in on the operational limits of each loading condition for side and stern installation and, therefore, answers the subquestion: *"What are the operational limits per installation sequence?"*. The operational limits are considered primarily for the crane tip and the pile gripper ring due to the economically valuable mission equipment and crane. After evaluating the forces at the crane tip and pile gripper ring, a follow-up question might be the displacement of the crane tip. For that reason, the upper end of the MP is included in Figure 8.1. The location of the pile gripper ring is either at starboard of the vessel for side installation or in the recess for stern installation. Human safety is explicitly not taken into account since it is another research topic. Therefore, the motion analysis at the bridge of the vessel is excluded.

The operational limits are based on the following key indicators:

- Roll and pitch angle at the crane tip in global x- and y-direction
- Dynamic amplification factor of the crane
- Dynamic utilisation factor of the crane
- Dynamic utilisation factor of the interface loads at the pile gripper ring in global x- and y-direction

In Section 8.1 the operational indicators for the crane tip are defined and discussed. In Section 8.2 the indicator for the pile gripper ring is covered. The results for side and stern installation expressed in terms of these key indicators are presented in Section 8.3, which also includes an analysis of a change in operational limits for the roll and pitch angle at the crane tip.

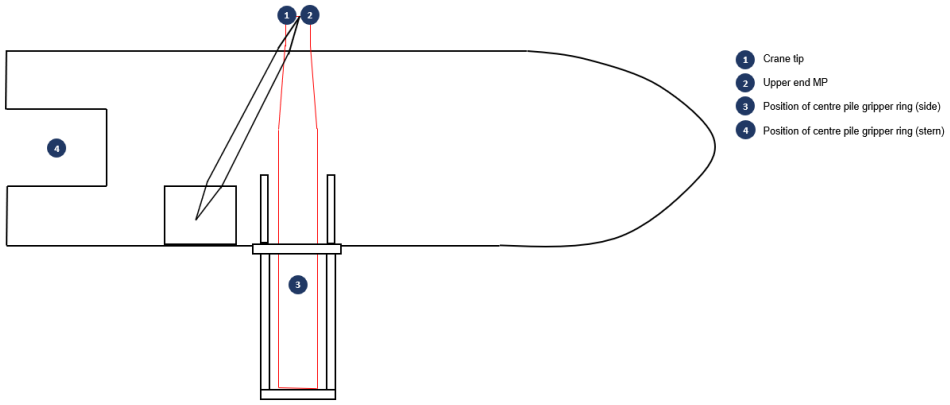

Figure 8.1: Locations for response analysis with the position of the pile gripper ring at starboard of the vessel for side installation and at the recess for stern installation

8.1. Crane tip forces

The crane tip forces in x-, y-, and z-direction in the global coordinate system are necessary to obtain the operational limits in terms of a roll and pitch angle at the crane tip, and the DAF and DUF of the crane tip. The roll and pitch angle are calculated with respectively F_x and F_y of the global coordinate system. The DAF and DUF are assessed using F_z of the global coordinate system.

Roll and pitch angle

The roll (ϕ_{crane}) and pitch angle (θ_{crane}) at the crane tip are the maximum allowable angles when hoisting or lifting a load, and are defined based on the global coordinate system of the vessel. The crane manufacturer uses the terms side and offlead, which are defined based on the crane coordinate system. The maximum values of the side and offlead are provided by the manufacturer of the crane.

The side lead of a crane consists of a static and dynamic part. The static side lead is the heeling of the crane. The dynamic part of the side lead is the dynamic angle between the vertical and the hoist tackle, resulting from swinging of the lifted load due to slewing and/ or drift-off of the vessel [123].

Similarly the offlead consists of a static and dynamic part. The static offlead is the trim of the crane. It is the angle between the crane slewing axis and vertical, as a result of the static inclination of the vessel, and is in plane of the boom. The dynamic offlead is the the dynamic angle between the vertical and the hoist tackle, as a result of swinging of the lifted load due to slewing and/or drift-off of the vessel, which is in plane of the boom [123].

For the crane with a maximum capacity of 5000 tonnes at a radius of 36 metres in horizontal plane, used in this case study, both the side and offlead have an angle of $3.5°$, including a maximum of $1°$ from the crane heel or trim [123]. For this crane capacity condition, the side and offlead are equal. Therefore, the maximum roll and pitch angle at the crane tip are also set to $3.5°$.

From the F_x and F_y of the crane tip, the roll and pitch angle are calculated to check whether the maximum limit is exceeded as presented in Equation 8.1 and Equation 8.2.

$$\phi_{crane} = \text{arctan}(\frac{F_y}{(M_{MP} + M_{rigging}) \cdot g}) \tag{8.1}$$

$$\theta_{crane} = \text{arctan}(\frac{F_x}{(M_{MP} + M_{rigging}) \cdot g}) \tag{8.2}$$

Dynamic Amplification Factor (DAF)

The DAF is a dimensionless ratio representing the dynamic hook load at the crane tip to its static hook force as described in Equation 8.3 and Equation 8.4.

$$DAF = \frac{Dynamic\ hook\ load}{Static\ hook\ load} \tag{8.3}$$

$$Static\ hook\ load = (M_{MP} + M_{rigging}) \cdot g \tag{8.4}$$

DAF is used for lifting operations to account for global dynamic effects [26]. This DAF should be determined by either specific analysis of the operation or by model testing. Depending on the location of the operation and the static hook load (SHL), the factor varies: offshore operations require higher DAFs compared to inshore or onshore, and for larger static hook loads the DAF becomes less. For this offshore marine operation with a 2XL MP, the maximum DAF is 1.15 based on the regulations of DNV [26].

Dynamic Utilisation Factor (DUF)

The DUF is the dimensionless ratio between the dynamic vertical force on the crane tip and the maximum crane capacity as presented in Equation 8.5. This factor is introduced due to cases when the mass of the lifted load is relatively low compared to the crane capacity, but the DAF is already close

to its maximum allowable limit. The DUF derived from the vertical dynamic crane tip force needs to be less than 1.00. The DUF is internally used at Ulstein and not described in literature.

$$DUF = \frac{Dynamic\ hook\ load}{Crane\ capacity \cdot g} \tag{8.5}$$

8.2. Pile gripper interface loads

The interface loads between the monopile and the pile gripper ring are considered as well. Generally, these interface loads are not governing compared to the DAF, DUF, and roll and pitch angle (J.D. Stroo, personal communication, December 2023). However, it is important to take these loads into consideration similarly to the crane tip forces. The pile gripper ring used for heavy lift crane vessels is a relatively novelty: only the Orion and Bokalift 2 have an operating pile gripper ring for the installation of monopiles as described in Chapter 3. Therefore, there are no explicit regulations according to a class society like DNV.

A DUF for the pile gripper ring is introduced in Equation 8.6 and Equation 8.7 to assess the lateral forces on the pile gripper ring. This DUF is the dimensionless ratio between the lateral force in the global coordinate system and the working load limit (WLL) in global x- and y-direction. The WLL for the pile gripper ring is not provided by the manufacturer for this case study. Based on industry experience of Ulstein, a suitable value is applied for global x- and y-direction, however this value depends on the specific pile gripper ring and should be provided by the manufacturer.

$$DUF_{pile\ gripper\ ring\ x} = \frac{F_x}{WLL} \tag{8.6}$$

$$DUF_{pile\ gripper\ ring\ y} = \frac{F_y}{WLL} \tag{8.7}$$

The DUF for the pile gripper is only applied when the MP is lowered. During the upending of the monopile, the pile gripper ring is not acting as a gripper. The mass of the MP is then divided between the crane and a steel cradle with a rubber pad on which the MP partly rests. This implies the DUF to be irrelevant for the loading conditions during the upending of the monopiles.

8.3. Results

The results are presented per key indicator and H_s. The key indicators are calculated based on crane tip forces and pile gripper contact forces, which are the Most Probable Maximum (MPM) for each T_p. The MPM is an extreme value statistic, based on the Rayleigh distribution. This implies the assumption that the force varies approximately linearly with the wave height, which is a variable of a stationary Gaussian process [124]. Table 8.1, Table 8.2, and Table 8.3 present in an overview for which loading conditions the maximum allowable limits are exceeded. Therefore, these tables provide an answer to the subquestion: *"What are the operational limits per installation sequence?"*. All the results, displayed in graphs for the MPM plotted against the T_p, for side and stern installation are attached in Appendix B.

8.3.1. Side installation

In Table 8.1 an overview of the operability per loading condition of the lowered MP is presented for side installation for a range of T_p between 5.0 and 15.0 seconds. This check is valid for the operational limits as presented in Section 8.1 and Section 8.2. A checkmark implies that that specific operational limit based on the MPM of the crane tip force or pile gripper force is not exceeded for the entire range of simulated T_p. When the allowable limit is exceeded, the corresponding spectral peak period is mentioned.

Based on Table 8.1, it is observed that the pitch angle, θ_{crane}, is limiting the operability. For the fully upended MP, the limits for the pitch angle is only exceeded at a T_p of 7.2 and 8.3 seconds. For the MP halfway the water depth, the pitch angle is first limiting and afterwards the pile gripper loads in x-direction, the DAF of the crane tip and finally the roll angle for H_s = 3 m. For T_p of 15.0 seconds for

H_s of 3 metres, the DUF of the pile gripper in y-direction is exceeded. When the MP is 3 metres above the seabed, the allowable limits are not exceeded.

For the fully upended monopile, the natural periods of the double pendulum calculation of Figure 7.3 are approximately 16 and 19 seconds. These values do not correspond with the displacement RAOs of the vessel for heave, pitch, and roll which peak around the 13 seconds, as visible in Appendix C.

The MP halfway the water depth experiences the largest responses for peak periods larger than 8.3 with in general a maximum response at 12.8 or 15.0 seconds. This corresponds with the natural period based on the double pendulum calculations in Figure 7.3, based on the level of submergence of the 2XL MP. In addition, the displacement RAOs of the vessel for heave, pitch, and roll peak around the period of 12.8 seconds. The RAOs and the natural period of the double pendulum reinforce the responses, thus the analysed forces, which eventually result in a peak in the operational limits. Lastly, it is important to consider that these long waves do not occur regularly on the North Sea based on the wave scatter diagram in Figure 4.9.

When the monopile is almost at the sea bed, the responses are below the allowable limits. The natural periods of the double pendulum of the rigging and 2XL MP are outside the range of the peak of the displacement RAOs of the vessel. The motion behaviour of the monopile is damped by the wave loads. The responses due to behaviour of the multi-body system do not exceed the operational limits.

Table 8.1: Operability with a maximum roll angle and pitch angle of $3.5°$, maximum crane tip DAF of 1.15, crane tip DUF of 1 and pile gripper DUF for x- and y-direction of 1 for range of T_p between 5.0 and 15.0 seconds for a fully upended 2XL MP, a 2XL MP halfway water depth, and 2XL MP 3 metres above seabed for side installation

Side installation		H_s = 2 m	H_s = 3 m	H_s = 2 m	H_s = 3 m	H_s = 2 m	H_s = 3 m
		Fully upended		*Halfway water depth*		*3 m above seabed*	
Crane tip	Roll angle [°]	✓	✓	At 12.8 s	> 10.6 s	✓	✓
	Pitch angle [°]	✓	At 7.2, 8.3 s	> 9.4 s	> 8.3 s	✓	✓
	DAF [-]	✓	✓	✓	≥ 10.6 s	✓	✓
	DUF [-]	✓	✓	✓	✓	✓	✓
Pile gripper	DUF_x [-]	✓	✓	> 10.6 s	> 9.4 s	✓	✓
	DUF_y [-]	✓	✓	✓	At 15.0 s	✓	✓

In Table 8.2 a table with the operability check for the upending stage is presented, solely for the crane tip, for the horizontal position of the MP and the MP $45°$ upended for both side and stern installation.

The pitch angle is limiting for side installation for the horizontally placed and $45°$ upended 2XL MP. For the horizontally placed MP, the vessel RAOs experience a maximum around the range of $12 - 15$ seconds. These maxima correspond with the course of the graphs as displayed in Appendix B. For the upended MP, the roll angle is additionally exceeded at 15.0 seconds for side installation and at 12.8 seconds for H_s of 3 metres for stern installation.

Table 8.2: Operability with a maximum roll and pitch angle of 3.5 °, maximum crane tip DAF of 1.15, and crane tip DUF of 1 for range of T_p between 5.0 and 15.0 seconds for a horizontal placed and $45°$ upended 2XL MP for side installation and stern installation

Crane tip	H_s = 2 m	H_s = 3 m	H_s = 2 m	H_s = 3 m	H_s = 2 m	H_s = 3 m	H_s = 2 m	H_s = 3 m
	Side installation		*Side installation*		*Stern installation*		*Stern installation*	
	Horizontal position		*45° upended*		*Horizontal position*		*45° upended*	
Roll angle [°]	✓	✓	At 15.0 s	At 15.0 s	✓	✓	✓	At 12.8 s
Pitch angle [°]	>10.6 s	>10.6 s	>11.7 s	>10.6 s	✓	✓	✓	✓
DAF [-]	✓	✓	✓	✓	✓	✓	✓	✓
DUF [-]	✓	✓	✓	✓	✓	✓	✓	✓

8.3.2. Stern installation

Finally, a third operability overview is shown in Table 8.3 for the cases with an MP during the lowering phase for stern installation. The allowable limits are similar to side installation. The pitch angle is governing the allowable limits for the lowering stage as it is first exceeded for a fully upended MP and the MP halfway water depth. For the fully upended MP, only the maximum pitch angle is exceeded, and only at the spectral peak period of 7.2 seconds. A peak in the displacement and load RAOs of the MP is visible around 6 seconds, which explains the increase in response for the smaller T_p in the range of $5.0 - 7.2$ seconds. For the MP halfway the water depth, the pitch angle is limiting as first, after that the roll angle, and finally the DUF for the pile gripper and the DAF for the crane tip. The displacement and loads RAOs of the monopile are the largest in the range of $12 - 15$ seconds, which explains the increase in response at these larger spectral peak periods. The MP 3 metres above seabed does not exceed the operational limits, similarly to the side installation. The load and displacement RAOs of the monopile are at a maximum around 21 seconds, which is outside the range of the spectral peak periods.

It is observed that similarly to the side installation sequence, the MP halfway water depth exceeds the most limits, but only for larger T_p. This observation corresponds with the natural period of the double pendulum of 12.8 seconds in combination with the peak of RAOs of the MP and the displacement RAOs of the vessel for heave and pitch. The vessel RAO is neglible for roll for head waves, which is the case for stern installation.

The operational limits during upending are presented in Table 8.2. Only the roll angle is exceeded at 12.8 seconds, which is the only case without a limiting the pitch angle. For stern installation, the pitch angle is restricted due to the position of pile gripper ring and the MP placed longitudinally in the centre line. However, a roll angle is possible, which explains the exceedence for the largest simulated H_s for the upended MP. The loading condition with the horizontally placed MP complies for every key indicator.

Table 8.3: Operability with a maximum roll and pitch angle of $3.5°$, maximum crane tip DAF of 1.15, crane tip DUF of 1 and pile gripper DUF for x- and y-direction of 1 for range of T_p between 5.0 and 15.0 seconds for a fully upended 2XL MP, a 2XL MP halfway water depth, and 2XL MP 3 metres above seabed for stern installation

Stern installation		H_s = 2 m	H_s = 3 m	H_s = 2 m	H_s = 3 m	H_s = 2 m	H_s = 3 m
		Fully upended		*Halfway water depth*		*3 m above seabed*	
Crane tip	Roll angle [°]	✓	✓	>9.4 s	>9.4 s	✓	✓
	Pitch angle [°]	✓	At 7.2 s	>8.3 s	>8.3 s	✓	✓
	DAF [-]	✓	✓	✓	At 11.7, 12.8 s	✓	✓
	DUF [-]	✓	✓	✓	✓	✓	✓
Pile gripper	DUF_x [-]	✓	✓	> 10.6 s	> 9.4 s	✓	✓
	DUF_y [-]	✓	✓	✓	>11.7 s	✓	✓

8.3.3. Comparison side and stern installation

The 5 loading conditions of side and stern installation differ from the wave direction and the position of the monopile compared to the vessel. Other than that, the loading conditions are analogous and this is particularly visible during the lowering stage, for instance for the fully upended MP and the MP halfway the water depth for the pitch angle as shown in Figure 8.2. The other graphs are displayed in section B.1 and section B.2. However, the responses during the upending stage show differences due to the change in position of the pile gripper ring and the monopile.

Upending stage

The roll and pitch angle are the key indicators that are exceeding the maximum allowable limits during upending. The DAF and DUF of the crane tip are not exceeding limits for both installation methods, since the monopile also partly rests on a cradle. During upending the pitch angle is not exceeding the allowable pitch angle, however for the side installation it happens. For stern installation, the monopile is placed in the centre line of the vessel. The pile gripper constrains the behaviour of the monopile so the pitch angle for stern installation is smaller during upending than for side installation. During side installation, chaotic double pendulum behaviour occurs when the monopile is in horizontal position, when the the spectral peak period corresponds with natural period of the vessel .

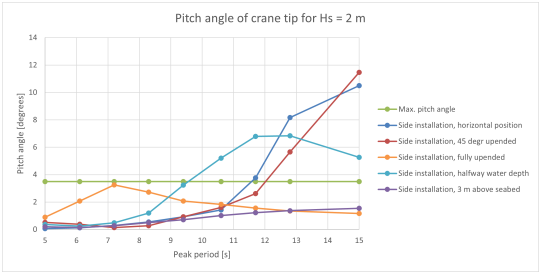

(a) Side installation

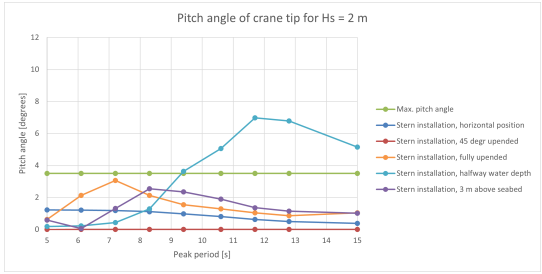

(b) Stern installation

Figure 8.2: Pitch angle [°] for H_s = 2 metres for side and stern installation with a maximum allowable limit of 3.5 °

Lowering stage

During the lowering stage, the pitch angle is governing for every loading condition. The case with the fully upended MP does not exceed the allowable limits for H_s = 2 metres. In addition, the pitch angle is only exceeded at 7.2 and 8.3 seconds for H_s = 3 metres. The RAOs of the monopile are at its maximum in the range of $5.0 - 8.0$ seconds.

The case with the MP halfway the water depth exceeds most limits compared to the other 2 loading conditions during lowering, starting from a T_p of 8.3 seconds for both side and stern installation. The natural frequency of the double pendulum coincides with the RAOs of the vessel and the spectral peak period, resulting in exceedence of operational limits in the range of $12 - 15$ seconds. The roll angle for the MP halfway water depth is exceeded for a smaller T_p compared to side installation. For both installation methods, the DUF of the pile gripper in x- and y-direction is exceeded.

The case with the MP 3 metres above seabed does not exceed the allowable limits for both installation methods. The RAOs of the MP are outside the range of the T_p and the RAOs of the vessel. However, for stern installation, there is a maximum in response for the roll and pitch angle visible at 8.3 seconds, and corresponding to that for the DUF of the pile gripper in x- and y-direction. This is still underneath the allowable limits, however, in the vessel RAOs graphs for this loading condition there is a local maximum visible.

8.3.4. Change of maximum roll and pitch angle

The operational limits are dependent on the choice of crane capacity condition, provided by the manufacturer, and therefore the maximum allowable limits. For this case study, the pitch angle with an angle of 3.5°, is in general limiting the operation. A capacity condition with a maximum roll and pitch angle of 6° can also be applied. A higher value for the maximum roll and pitch angle implies a lower safe working load for an increasing radius of the crane boom in the horizontal plane. Therefore, the maximum crane capacity reduces, which causes an increase in the DUF of the crane. Figure 8.3 shows the results for the pitch angle for side and stern installation. In Appendix B.3 and Appendix B.4 the results for the roll angle, pitch angle and DUF of the crane tip are shown. The DAF of the crane tip and the DUF of the pile gripper ring in x- and y-direction remain unchanged.

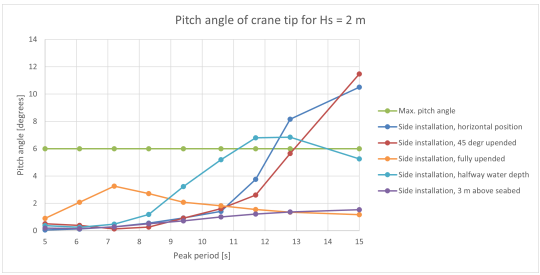

(a) Side installation

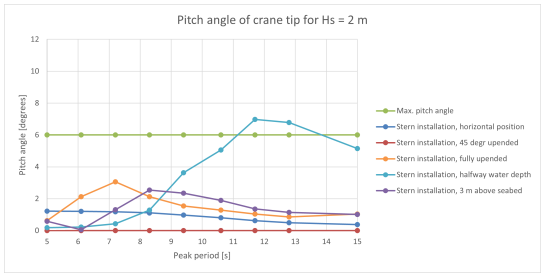

(b) Stern installation

Figure 8.3: Pitch angle [°] for H_s = 2 metres for side and stern installation with a maximum allowable limit of 6 °

For side installation, for an H_s of 2 metres, the upending stage is exceeding the allowable limit of 6 ° for the larger T_p. The MP halfway the waterdepth exceeds at 11.7 and 12.8 seconds for side installation. For stern installation, the loading condition with the monopile halfway the water depth also exceeds for 11.7 and 12.8 seconds. For the DUF of the crane tip, the loading conditions with the largest crane radius are affected the most. For side installation, the upending phase is the most affected, and for stern installation the lowering phase. However, the DUF remains under the allowable limit of 1.00. In conclusion, a higher pitch angle results in an increase in operability, especially for larger T_p. The DUF is negatively affected by a larger roll and pitch angle, since the crane capacity is reduced for larger crane radii, but the DUF is not exceeding the allowable limit. With an increase in the maximum allowable roll and pitch angle, the pitch angle is not anymore explicitly exceeded as first. The situation with the monopile halfway water depth is in general still exceeding the most allowable limits. The DUF of the pile gripper in x-direction for both side and stern installation becomes more relevant, since it is exceeded for the same range of T_p.

8.4. Conclusion

This chapter provides an answer to the subquestion: *"What are the operational limits per installation sequence?"*. The operational limits for both side and stern installation are provided in Table 8.1, Table 8.2, and Table 8.3. These tables are based on the maximum limits of 3.5° roll and pitch angle, a maximum DAF of 1.15 and maximum DUF of 1.00 for the crane tip, and finally a maximum DUF for the pile gripper of 1.00 for the global x- and y-direction.

During the upending stage, the allowable pitch angle is exceeded for side installation. The allowable pitch angle is not exceeded for stern installation, due to the longitudinal position of the monopile and pile gripper ring. For stern installation, the MP is restrained by the gripper. Despite the gripper, the motion of the monopile in global x-direction is still possible for side installation due to its different position. For stern installation, the roll angle is once limiting when the MP is 45° upended for an H_s of 3 metres. Due to the longitudinal position of the MP and gripper, larger responses and thus larger forces in y-direction are possible, resulting in a larger roll angle.

For the lowering stage, the pitch angle is limiting for both side and stern installation. The fully upended monopile experiences a peak in responses for smaller T_p in the range of $5.0 - 7.2$ seconds, since the maxima of the load and displacement RAOs of the monopile correspond with these spectral peak periods. These peak periods frequently occur on the North Sea. The monopile halfway the water depth experiences the largest responses for the pitch and roll angle in the range of T_p between 12.0 and 15.0 seconds. The maxima of the vessel RAOs for heave, pitch and roll coincide with the natural period of the double pendulum behaviour of the rigging and the monopile. However, these wave periods are large and do not occur regularly on the North Sea, since the majority of the wave periods is around the 5-8 seconds based on hindcast data. The monopile 3 metres above seabed does not exceed the operational limits of any key indicator for side and stern installlation.

The pitch angle is limiting in general, except for stern installation during upending. However, the maximum allowable angle of 3.5° is for the load curve with a maximum capacity of 5000 tonnes and a radius of 36 metres in the horizontal plane. Larger angles for roll and pitch are allowed, with a change in crane capacity corresponding with the crane boom radius in horizontal plane, according to the provided load curves of the crane. A maximum roll and pitch angle of 6° increases the operability, with the allowable limit of the pitch angle exceeded for a larger T_p. For side installation, the roll angle does not exceed the limit. For stern installation, the roll angle exceeds only for an H_s of 3 metres. The DUF of the crane tip also stays underneath the allowable limit of 1.00. In conclusion, a larger pitch and roll angle is possible while staying underneath the crane capacity for the crane radius in horizontal plane.

9 Discussion

This chapter emphasizes the relevance of this thesis in section 9.1, the limitations of this research in section 9.2, and finally the recommendations for further research in section 9.3.

9.1. Relevance of the results

Monopiles are becoming larger in size and weight, and are located further offshore, in deeper waters. This development implies that more 2XL MPs are installed by HLVs. Dynamic behaviour of the multi-body system of the vessel, crane, monopile, and pile gripper in combination with environmental conditions becomes more relevant, which is modelled for different installation sequences including a newly derived tip-vortex damping to more accurately model the hydrodynamic damping of the 2XL MP. This thesis provides insight in the governing allowable limits of side and stern installation for different loading conditions. In addition, this thesis visualises motion and thus forces responses trends for different T_p during upending and lowering of the 2XL MP which ultimately leads to a better understanding of the operability of 2XL MP installed from HLVs.

9.2. Limitations of the results

This study has limiting factors concerning the results. The model includes first order wave loads, but excludes second order wave loads. However, added mass and damping matrices are frequency dependent. For this case study, the water depth is 68 metres. Shallow water effects might occur, in particular for longer waves. The current is excluded, which particularly affects the cases during lowering when the monopile is partly submerged. The response are analysed in terms of MPM which assumes that the variable is a Gaussian process and, in this case, the forces vary linearly with the waves. However, for shallow water, this assumption may not always be accurate. Lastly, the model approach of steady state simulation results in an unrealistic build-up of oscillation.

9.3. Recommendations for further research

Recommendations are suggested for further research for different stages of the methodology, which are categorised in Section 9.3.1, Section 9.3.2, and Section 9.3.3.

9.3.1. Installation sequences

Side and stern installation are covered in this thesis, with the monopile stored at deck in horizontal position. This implies upending offshore for side and stern installation and less deck space for storage of monopiles for stern installation. Vertical storage of monopiles aboard does not require upending offshore, which reduces extra handling time offshore and it increases the possibility to store more monopiles aboard. Therefore, it is relevant to analyse the operational limits of lifting a vertical stored 2XL MP. Lowering the 2XL MP remains identical to either side or stern installation.

9.3.2. Model set-up

In the model set-up simplifications are applied to be able to easier identify the effects or critical behaviour. However, simulating a more realistic model, with for instance directional wave spreading or current, adds value as a follow-up study.

Wave spreading is not considered in the current model set-up: only wave direction is applied. This allows to clearly observe differences in shielding effects. However, in reality, there is not one wave direction, and a combination of wave direction is present. The effect of shielding is then less.

Current is not applied in this thesis. Including current in the model set-up is interesting for the lowering process and is expected to have a larger influence if the monopile is more submerged. For the identification of the critical behaviour due to resonance of the multi-body system it is not the main focus. However, the level of influence on the multi-body system behaviour is interesting as a follow-up question.

Slamming coefficients consist of a water entry coefficient and a water exit coefficient. These coefficients are relevant for loading conditions where the lower end of the monopile is near or in the splash zone. For the water entry coefficient a value of 5.15, based on DNV regulations for cylinders, is applied. The water exit coefficient is neglected, since the effect is considered small. The water exit coefficient is due to the combination of time and contribution to the thesis, not implemented. To increase the accuracy of the model, it can be applied in further research. However, the effect is expected to be small.

9.3.3. Numerical simulations

The numerical simulations are solved with an implicit time-integration scheme. A recommendation for further research is to study the differences between the explicit and implicit time domain integration scheme.

In Section 6.2.3 two approaches are presented to simulate a nonstationary process. For this thesis the approach of steady-state simulations of five positions of the 2XL MP is applied. The simulation time of each loading condition is 1800 seconds, which creates an unrealistic oscillation build-up. To further investigate the behaviour of the multi-body system, a repeated nonstationary simulation is recommended of the upending and lowering process.

10

Conclusion

This concluding chapter answers the main question which is presented in the introduction of this thesis: ***"How do side and stern installation of 2XL monopiles from heavy lift crane vessels compare in terms of operational limits during the upending and lowering stage?"***. Supporting subquestions are formulated to eventually answer the main question. The subquestions are first answered, whereafter the main question is covered.

"Why are monopiles widely applied as foundation for offshore wind turbines, and which physical phenomena are relevant concerning the operational limits of monopile installation?"
Monopiles are the most widely applied support structures because of relatively low costs, simplicity and ease of installation. However, the water depth can be a limiting factor. Approximately 88% of the planned fixed foundations are monopiles. The identification of critical events during marine operations, such as monopile installation, is obligatory in the planning phase by classification societies. The critical events are identified by assessing the operational limits. These limits are the allowable limits of sea states and motion responses and therefore include H_s, T_p, and wave direction. A critical event of an installation operation is the lowering phase of the asset according to multiple studies. The multi-body system of the vessel, crane, and asset induces interaction between the structures and pendulum effects of the asset might occur. Furthermore, rocking motions and slamming and snap forces while passing the splash zone are also possibly critical effects.

"What are the state-of-the-art installation methods for 2LX monopile installation?"
Monopiles are installed from jack-up vessels or floating vessels (monohulls, SSCVs, sheerlegs). Jack-up vessels are stable platforms, but these vessels are limited in terms of water depth, suitable seabed, and crane capacity. Floating vessels are less constrained to water depths and positioning requires less time compared to jack-up vessels. However, the dynamic behaviour of the vessel, crane, and monopile is more important due to the larger motions. Monopiles are transported to the location of the wind farm on board, by either the installation vessel itself (shuttling strategy), by a feeder vessel or the monopile can be wet-towed. When the monopile is transported on board, the monopile can either be longitudinally, transversely, or vertically stored. Vertical storage of monopiles on deck is still in the concept phase. The start of the installation of the monopile is the upending of the monopile, which can be done by a specialised pile gripper device, an upending frame, or a crane. Other strategies, such as the use of an upending trolley, are more useful for floating vessels with a fixed hoist. The hoisting of the upper end of the monopile can be done by multiple types of lifting tools, which are in constant development, such as combinations of grippers and upending tools. During the lowering of the monopile, hydrodynamic wave loads induce motion of the monopile and the vessel. The gripper device controls the horizontal motions. This gripper is fixed or motion-compensated. Other concepts of installation methods exist, such as stern installation or ballasting for vertical transfer, although these methods are not regularly applied. Stern installation with the monopiles longitudinally placed on deck is in development and currently becoming one of the state-of-the-art installation methods with multiple companies being engaged in this method. However, the dominant installation method remains side installation with the monopiles placed transversely on deck.

"What is a suitable method for the assessment of operational limits for 2XL monopile installation?"
A general framework is created to assess the operational limits. This framework consists in general of the definition of the installation sequence, the establishment of the loading conditions, the generation of the hydrodynamic properties, and the assessment of the operational limits. The installation sequences corresponding to the installation method suitable for 2XL monopiles, need to be defined. From the installation sequence, the loading conditions are derived. These loading conditions depend on the stages of the studied installation method and form the basis of the generation of the hydrodynamic properties in HydroD. Together with the characteristics of the case study, the hydrodynamic properties are an input for the numerical simulations perfomed in OrcaFlex. The relevant forces of the mission equipment are extracted from OrcaFlex and are used to calculate the operational limits per loading condition and per installation sequence. In the methodology, iterative loops are included to ensure the calculations of the loading conditions and hydrodynamic properties lead to a floating equilibrium of the vessel, mission equipment, and monopile.

This methodology is applied on a case study. Hornsea Wind Farm, located on the North Sea, with a water depth of 68 metres, is chosen as a basis for the environmental conditions. The JONSWAP spectrum is applied. The wave conditions are varied for H_s of 2 and 3 metres and for T_p in a range of 5.0 to 15.0 seconds. Monopiles with a length of 100 metres, diameter of 11 metres and a mass of 2300 tonnes are installed from a vessel developed by Ulstein. The mission equipment consists of crane with a capacity of 5000 tonnes and a pile gripper frame.

"Which installation sequences are preferred for 2XL monopile installation?"
For 2XL MP installation, side and stern installation are preferred. The model set-up consists primarily of 5 loading conditions for both side and stern installation:

- Monopile placed horizontally on deck
- Monopile 45° upended
- Monopile fully upended
- Monopile half way water depth
- Monopile 3 metres above sea bed

For these situations, the loading conditions are calculated, taking into account the free surface moment of ballasting tanks. The hydrodynamic properties, such as added mass and damping matrices, load and displacement RAOs, are generated by HydroD. These properties are then imported in the OrcaFlex files. For the loading conditions where the monopile is not submerged, the monopile is modelled as a line object. However, the submerged monopile is modelled as a hybrid line-buoy-vessel object. The line object models the contact with the pile gripper ring, while the buoy takes into account the viscous drag, inertia and buoyancy forces. Lastly, the vessel object of the model is needed to include the tip vortex damping. The tip vortex damping is part of the hydrodynamic damping and is derived from CFD tests performed by a combined effort of Ulstein, Huisman Equipment and Heerema. This model set-up is prepared and therefore the numerical simulations for different loading conditions are performed.

"How is the applied model verified and validated?"
A full-scale validation is not possible since comparable studies are not found for this specific application. Therefore, parts of the methodology are validated. The loading conditions of the installation sequences are validated against design values of DNV and also supported by Gerritsma, Pinkster and Blom ([117], [118], [119]). The hydrodynamic properties are generated in HydroD, which is validated by DNV. Furthermore, the sloshing in the recess is double checked by BV regulations and the Merian formula originating from coastal engineering. These sloshing values are then compared to the period corresponding to the peak in the damping curve of the vessel for surge and sway.

For the numerical simulations, a sensitivity analysis is performed for the time step. Face validation is applied by a hydrodynamic specialist within Ulstein and software specialists of OrcaFlex which both provided iterative feedback. The visual representation of the simulation opts for graphical validation.

Finally, the behaviour of the monopile is also validated by modal analysis of OrcaFlex and analytical pendulum calculations. The natural periods of the entire system and parts of the system are calculated. The natural periods of the monopile are calculated according to the mathematical model of a simple and a physical pendulum. The effects of the crane hook with its mass and mass moments of inertia interacting with the monopile are also calculated applying the principle of the double pendulum, for various levels of MP submergence. The results of the analytical double pendulum calculation are in the same range as the first two modes of the modal analysis for the system of the monopile and the crane. However, there are differences due to the simplifications of the analytical calculation and the exclusion of added mass in the modal analysis.

The partial validation for this thesis is found to be sufficient, despite the absence of a full validation. On multiple stages within the methodology, different validation methods, as described previously, are applied to be able to assess the main question of the thesis.

"What are the operational limits per installation sequence?"
The operational limits for both side and stern installation are provided in Table 8.1, Table 8.2, and Table 8.3. These tables are based on the maximum limits of 3.5° roll and pitch angle at the crane tip, a maximum DAF of 1.15 and maximum DUF of 1.00 for the crane tip, and finally a maximum DUF for the pile gripper of 1.00 for the global x- and y-direction. Based on these limits, the pitch angle is limiting for side and stern installation during lowering. During upending, the allowable pitch angle is exceeded for side installation. The maximum pitch angle is not exceeded for stern installation, due to the longitudinal position of the pile gripper and monopile. The monopile is then restrained by the gripper. Despite the gripper, the motion of the monopile in x-direction is still possible for side installation. For stern installation, the roll angle is once limiting when the MP is 45° upended for H_s. Due to the position of the MP and gripper, larger responses and thus larger forces in y-direction are possible. For the fully upended monopile, maxima in responses are experienced for the shorter T_p, since the RAOs of the monopile have a maximum in the range of $5.0 - 7.2$ seconds. The monopile halfway the water depth experiences the largest responses of roll and pitch angle at the crane tip for the range T_p around 12.8 seconds. The maximum in the vessel RAOs for heave, pitch and roll coincides with the natural period of the double pendulum behaviour of the rigging and the monopile. However, these wave periods are large and have a very small chance of occurring on the North Sea, since the majority of the wave periods are around the $5 - 8$ seconds based on the wave scatter diagram and hindcast data of the North Sea. The monopile 3 metres above seabed does not exceed the operational limits for side and stern installation for an H_s of 2 and 3 metres.

The pitch angle in limiting in general, however, the maximum allowable angle of 3.5° is for the load curve with a maximum capacity of 5000 tonnes and a radius of 36 metres in the horizontal plane. Larger angles for roll and pitch angle are allowed for different crane capacity conditions. In such a case, the crane capacity then reduces for the same radius. With a maximum allowable angle of 6° for roll and pitch at the crane tip, the operability in terms of the roll and pitch angle increases, and the maximum DUF of 1.00 at the crane tip is not exceeded, despite the reduction in crane capacity.

"How do side and stern installation of 2XL monopiles from heavy lift crane vessels compare in terms of operational limits during the upending and lowering stage?"
Concluding, the pitch angle is generally governing the operational limits for both side and stern installation except during the upending of the monopile with stern installation. For stern installation, during upending, the roll angle can be governing, due to the longitudinal position of the monopile.

During upending, the differences in operational limits between side and stern installation are clearly visible: pitch angle is limiting the operation only for side installation and not for stern installation. The operability during upending is larger for stern installation. However, during the lowering stage, both installation sequences show a similar course in the key indicators plotted against the spectral peak periods.

For the fully upended MP, the shorter spectral peak periods are critical due to the maximum in RAOs of the monopile. These periods coincide with the spectral peak periods that have a larger chance of

occurring on the North Sea. However, the most critical loading condition is the MP halfway the water depth, the operational limits are most exceeded for both installation sequences, for T_p in the range of $12.0 - 15.0$ seconds. The spectral peak period coincides with the natural period of the double pendulum system of the crane hook and the monopile, and in addition with the natural period of the vessel for heave, pitch, and roll. On the other hand, these operational limits are exceeded for T_p in the range of $12.0 - 15.0$ seconds, which are long waves which do not occur frequently on the North Sea. When the monopile is almost at the seabed, the operational limits are not limiting the operation for both side and stern installation. The natural period of the monopile is then outside of the range of the spectral peak period and the natural period of the vessel.

In conclusion, the stern installation shows a larger operability window during upending compared to side installation. During the lowering stage, the operability differs per loading condition. For the fully upended monopile, stern installation has a larger operability window based on these allowable limits. The loading condition with the monopile halfway the water depth has a larger operability window for side installation compared to stern installation. The results for the monopile 3 metres above seabed are underneath the allowable limits for both side and stern installation. Considering both the upending and lowering phase of 2XL monopiles from heavy lift crane vessels, stern installation shows promising results in terms of operability.

References

[1] Ulstein International A.S. - Ulstein Design & Solutions B.V. *Future Trends Offshore Wind - Rev 2.3*. Tech. rep. 2019.

[2] International Energy Agency. *Offshore Wind Outlook 2019*. Tech. rep. International Energy Agency, 2019.

[3] DNV. *Energy Transition Outlook - The rise of renewables*. 2022. URL: https://www.dnv.com/energy-transition-outlook/rise-of-renewables.html (visited on 01/11/2024).

[4] F. Kühn et al. *How to succeed in the expanding global offshore wind market*. 2022. URL: https://www.mckinsey.com/industries/electric-power-and-natural-gas/our-insights/how-to-succeed-in-the-expanding-global-offshore-wind-market (visited on 11/23/2023).

[5] L. Li, Z. Gao, and T. Moan. "Response Analysis of a Nonstationary Lowering Operation for an Offshore Wind Turbine Monopile Substructure". In: *Journal of Offshore Mechanics and Arctic Engineering* 137 (2015).

[6] L. Li, Z. Gao, and T. Moan. "Operability Analysis of Monopile Lowering Operation Using Different Numerical Approaches". In: *International Journal of Offshore and Polar Engineering* 26.2 (2016), pp. 88–99.

[7] L. Li. "Dynamic Analysis of the Installation of Monopiles for Offshore Wind Turbines". PhD thesis. Norwegian University of Science and Technology, 2016.

[8] M. Chen et al. "Dynamic Analysis and Extreme Response Evaluation of Lifting Operation of the Offshore Wind Turbine Jacket Foundation Using a Floating Crane Vessel". In: *Journal of Marine Science and Engineering* (2022).

[9] M. Zou et al. "A constant parameter time domain model for dynamic modelling of multi body system with strong hydrodynamic interactions". In: *Ocean Engineering* (2023).

[10] Huisman Equipment B.V. *Pile drag model tests*. Tech. rep. Huisman Equipment B.V., 2022.

[11] A. Pistidda, D. Vis, and C. Rossetti. *Monopile Hydrodynamic damping*. Tech. rep. Huisman Equipment, Ulstein Design, Solution B.V., and Heerema Engineering Solutions, 2023.

[12] DNV. *Support structures for wind turbines*. Høvik, Norway: Det Norske Veritas AS, 2021.

[13] M.J. Kaiser and B. Snyder. *Offshore Wind Energy Installation and Decommissioning Cost Estimation in the U.S. Outer Continental Shelf*. Tech. rep. Minerals Management Service, 2010.

[14] W. Musial, S. Butterfield, and B. McNiff. *Midwest Research Institution*. Tech. rep. Energy from offshore wind, 2006.

[15] Aker Solutions. *Design and Construction of Jackets*. n.d. URL: https://www.akersolutions.com/what-we-do/fixed-and-floating-solutions/jacket-designs/ (visited on 02/12/2024).

[16] Y.E. Liu. "Monopile Forever: Overcoming the Technical Boundaries of Monopile Foundations in Deep Waters". Master's Thesis. Delft University of Technology, 2021.

[17] L. Ramírez et al. *Offshore Wind in Europe*. Tech. rep. WindEurope, 2020.

[18] Gemini Windpark. *Monopiles | Transition Pieces*. 2015. URL: https://www.geminiwindpark.nl/monopiles--transition-pieces.html (visited on 03/30/2023).

[19] Acteon. *Fixed Wind Foundations: An independent concept screening approach*. 2021. URL: https://acteon.com/blog/fixed-wind-foundation-selection/ (visited on 03/30/2023).

[20] S. Subramanian et al. "Early Engagement in FEED to Overcome Engineering Challenges - Delivering Fast Track EPC projects". In: *Abu Dhabi International Petroleum Exhibition and Conference*. 2019.

[21] Equinor. *Hywind Tampen*. 2022. URL: https://www.equinor.com/energy/hywind-tampen (visited on 02/23/2023).

[22] Equinor. *Floating Wind*. 2023. URL: https://www.equinor.com/energy/floating-wind (visited on 02/23/2023).

[23] G.E. Barter, A. Robertson, and W. Musial. "A systems engineering vision for floating offshore wind cost optimization". In: *Renewable Energy Focus* 34 (2020), pp. 1–16.

[24] Wind Power Engineering. *Excipio Energy unveils new hybrid floating offshore wind platform*. 2019. URL: https://www.windpowerengineering.com/excipio-energy-unveils-new-hybrid-floating-offshore-wind-platform/ (visited on 03/30/2023).

[25] W. Guachamin Acero et al. "Methodology for assessment of the operational limits and operability of marine operations". In: *Ocean Engineering* 125 (2016), pp. 308–327.

[26] DNV. *ST-N001: Marine operations and marine warranty*. Høvik, Norway: Det Norske Veritas AS, 2021.

[27] J.M.J. Journée and W.W. Massie. *Offshore Hydromechanics*. 2th ed. Delft, the Netherlands: Delft University of Technology, 2008.

[28] DNV. *RP-N101: Risk management in marine and subsea operations*. Høvik, Norway: Det Norske Veritas AS, 2021.

[29] C. Naden, International Organization for Standardization. *Offshore windfarms set to flywith new standards for their ports*. 2015. URL: https://www.iso.org/news/2015/06/Ref1968.html (visited on 03/23/2023).

[30] L. Li et al. "Splash zone lowering analysis of a large subsea spool piece". In: *Marine Structures* 70 (2020).

[31] Z. Gao et al. "Numerical simulation of marine operations and prediction of operability using response-based criteria with an application to installation of offshore wind turbine support structures". In: *Marine operations specialty symposium* (2016).

[32] F. Solaas et al. "Dynamic forces and limiting sea states for installation of GRP protection covers". In: *International Conference on Ocean, Offshore & Arctic Engineering* (2017).

[33] A.M. Amer, L. Li, and X. Zhu. "Dynamic Analysis of Splash-zone Crossing Operation for a Subsea Template". In: *Sustainable Marine Structures* 4.2 (2022), pp. 18–39.

[34] DNV. *Lifting appliances used in subsea operations*. Høvik, Norway: Det Norske Veritas AS, 2021.

[35] DNV. *RP-N103: Modelling and analysis of marine operations*. Høvik, Norway: Det Norske Veritas AS, 2021.

[36] R. Gordon, G. Grytøyr, and M. Dhaigude. "Modeling Suction Pile Lowering Through the Splash Zone". In: *Proceedings of the ASME 32nd International Conference on Ocean, Offshore and Arctic Engineering* (2013).

[37] SCR (Steel Catenary Riser). *Encyclopedia of Ocean Engineering*. Singapore: Springer, 2022.

[38] O.A.J. Peters and L.J.M. Adegeest. "Motion Monitoring and Decision Support during Heavy Lift Transport". In: *Proceedings of the ASME 2010 29th International Conference on Ocean, Offshore and Arctic Engineering* (2010).

[39] Kongsberg Maritime. *Vessel Motion Monitor - VMM*. 2023. URL: https://www.kongsberg.com/maritime/products/vessel-reference-systems/motion-and-heading-sensors/vessel-motion-monitor/ (visited on 11/24/2023).

[40] Wise group. *Vessel Motion Monitoring Systems (VMMS)*. 2023. URL: https://wisegroupsystems.com/systems/vessel-motion-monitoring-systems-vmms/ (visited on 11/24/2023).

[41] Y. Guo, H. Wang, and J. Lian. "Review of integrated installation technologies for offshore wind turbines: Current progress and future development trends". In: *Energy Conversion and Management* 255 (2022).

[42] IRO. *Monopile installation completed at Arcadis Ost 1 offshore wind farm*. 2022. URL: https://iro.nl/nl/nieuws-en-pers/monopile-installation-completed-at-arcadis-ost-1-offshore-wind-farm/ (visited on 03/19/2023).

[43] A. Buljan. *Steelwind Dispatches First Batch of XXL Monopiles for Gode Wind 3 Offshore Wind Farm*. 2023. URL: https://www.offshorewind.biz/2023/02/28/steelwind-dispatches-first-batch-of-xxl-monopiles-for-gode-wind-3-offshore-wind-farm/ (visited on 03/31/2023).

[44] Jan de Nul. *Jan de Nul Kicks Off Orsted's Borkum Riffgrund 3 Offshore Wind Farm Construction*. 2024. URL: https://www.jandenul.com/news/jan-de-nul-kicks-orsteds-borkum-riffgrund-3-offshore-wind-farm-construction (visited on 01/11/2024).

[45] The Offshore Wind Foundations Alliance. *Offshore wind foundations: building a sustainable future*. 2021. URL: https://media.graphassets.com/8KQEKo4mSilsy1gYCI2I (visited on 03/20/2023).

[46] J.W. Nielsen. *DMI Ocean Models [HBM]*. 2022. URL: https://ocean.dmi.dk/models/hbm.uk.php (visited on 02/24/2023).

[47] Van Oord Offshore Wind. *Offshore installation vessel Aeolus*. Tech. rep. Van Oord Marine Ingenuity, 2018.

[48] DEME Group. *Innovation*. 2023. URL: https://www.deme-group.com/technologies/innovation (visited on 03/30/2023).

[49] Jan de Nul Group. *Vole au Vent*. Tech. rep. Jan de Nul Group, 2020.

[50] Cadeler. *Technical Specifications Windfarm Installation Vessel (WIV) Wind Orca*. Tech. rep. Cadeler, 2021.

[51] F.M. Birkeland. "Numerical Simulation for Installation of XL Monopile for Offshore Wind Turbine". Master's Thesis. Norwegian University of Science and Technology, 2016.

[52] Bureau Veritas. *The conversion projects boosting offshore energy*. 2022. URL: https://marine-offshore.bureauveritas.com/magazine/conversion-projects-boosting-offshore-energy (visited on 02/24/2023).

[53] Heerema Marine Contractors. *Aegir - Fast-moving Heavy Lift Vessel*. Tech. rep. Heerema Marine Contractors, 2021.

[54] Boskalis. *Equipment sheet - Bokalift 1*. Tech. rep. Boskalis, 2021.

[55] Boskalis. *Equipment sheet - Bokalift 2*. Tech. rep. Boskalis, 2022.

[56] Jan de Nul Group. *Les Alizés*. Tech. rep. Jan de Nul Group, 2020.

[57] DEME Group. *Orion*. 2023. URL: https://www.deme-group.com/technologies/orion (visited on 03/30/2023).

[58] Seaway 7. *Seaway Strashnov*. Tech. rep. Seaway 7, 2021.

[59] Seaway 7. *Seaway Alfa Lift*. Tech. rep. Seaway 7, 2022.

[60] Z. Jiang. "Installation of offshore wind turbines: A technical review". In: *Renewable and Sustainable Energy Reviews* 139 (2021).

[61] Heerema Marine Contractors. *Sleipnir - HMC Equipment*. Tech. rep. Heerema Marine Contractors, 2020.

[62] Saipem. *Saipem 7000*. Tech. rep. Saipem, n.d.

[63] Heerema Marine Contractors. *Thialf - HMC Equipment*. Tech. rep. Heerema Marine Contractors, 2020.

[64] Van Oord Offshore Wind. *Heavy lift installation vessel Svanen*. Tech. rep. Van Oord Marine ingenuity, 2018.

[65] Van Oord. *Van Oord's hefschip Svanen is aangekomen bij windpark Kriegers Flak*. 2020. URL: https://www.vanoord.com/nl/updates/van-oords-hefschip-svanen-aangekomen-bij-windpark-kriegers-flak/ (visited on 03/22/2023).

[66] A. Durakovic. *Wärtsilä Gear for Bokalift 2*. 2020. URL: https://www.offshorewind.biz/2020/02/24/wartsila-gear-for-bokalift-2/ (visited on 02/24/2023).

[67] Seaway7. *Seaway Alfa Lift - Seaway 7*. 2023. URL: https://www.seaway7.com/vessels/seaway-alfa-lift/ (visited on 02/24/2023).

[68] Heerema. *Aegir | Heerema*. 2022. URL: https://www.heerema.com/fleet/aegir (visited on 02/24/2023).

[69] S.A. Herman. *Offshore wind farms - Analysis of Transport and Installation Costs*. Tech. rep. TNO, 2002.

[70] J. Tjaberings, S. Fazi, and E. Ursavas. "Evaluating operational strategies for the installation of offshore wind turbines substructures". In: *Renewable and Sustainable Energy Reviews* 170 (2022).

[71] Cosco Shipping Heavy Transport. *Cosco Shipping Specialized awarded transportation contract of monopiles for Moray West Offshore Wind Farm*. 2022. URL: https://coscoht.com/cosco-shipping-specialized-awarded-transportation-contract-of-monopiles-for-moray-west-offshore-wind-farm/ (visited on 02/27/2023).

[72] Vuyk Engineering. *VERticale: future-proof installation vessel for offshore wind | Vuyk Engineering Rotterdam*. 2022. URL: https://vuykrotterdam.com/projects/verticale-future-proof-installation-vessel-for-offshore-wind/ (visited on 02/27/2023).

[73] L. Li et al. "Analysis of lifting operation of a monopile for an offshore wind turbine considering vessel shielding effects". In: *Marine Structures* 39 (2014), pp. 287–314.

[74] T.W.A. Vehmeijer and R.C.L. Boelens. "Vessel and method for upending a monopile of an offshore wind turbine". U.S. pat. WO 2022/096523 A1. Nov. 3, 2021.

[75] Knud E. Hansen. *Mono-pile Upending Trolley*. 2023. URL: https://www.knudehansen.com/reference/mono-pile-upending-trolley/ (visited on 03/31/2023).

[76] OER International. *Test Monopile Upending and Lifting Tool successfully completed*. 2022. URL: https://ocean-energyresources.com/2022/07/17/test-monopile-upending-and-lifting-tool-successfully-completed/ (visited on 03/01/2023).

[77] IQIP. *Flanged Pile Upending Tool*. 2023. URL: https://iqip.com/products/lifting-equipment/flanged-pile-upending-tool/ (visited on 03/17/2023).

[78] B. Zhang et al. "Design and Experiment of a Lifting Tool for Hoisting Offshore Single-Pile Foundations". In: *Machines* 9.29 (2021).

[79] Huisman Equipment. *Motion Compensated Pile Grippers*. 2023. URL: https://www.huismanequipment.com/nl/products/renewables/offshore_wind/motion-compensated-pile-grippers (visited on 03/01/2023).

[80] A. Elkadi. *New pile installation method for offshore wind monopiles*. 2023. URL: https://www.deltares.nl/en/projects/new-pile-installation-method-offshore-wind-monopiles/ (visited on 03/01/2023).

[81] IQIP. *Blue Piling Technology - Pile driving - IQIP*. 2023. URL: https://iqip.com/products/pile-driving-equipment/blue-piling-technology/ (visited on 04/21/2023).

[82] C. Moormann, F. Kirsch, and V. Herwig. "Vergleich des axialen und lateralen Tragverhaltens von vibrierten und gerammten Stahlrohrpfählen". In: *Proceedings 34 Baugrundtagung* (2016).

[83] J.D. Stroo. "A vessel and method configured to install a foundation structure". U.S. pat. WO 2023/001493 A1. Jan. 26, 2023.

[84] E.B. Rosenboom. "Stern vs Side installation of Monopiles from floating vessels". Master's thesis. Delft University of Technology, 2022.

[85] J. Haugvaldstad and O.T. Gudmestad. "Testing of a new transport and installation method for offshore wind turbines". In: *IOP Conference Series: Materials Science and Engineering* 700 (2019).

[86] A. Sarkar and O.T. Gudmestad. "Study on a new method for installing a monopile and a fully integrated offshore wind turbine structure". In: *Marine Structures* 33 (2013), pp. 160–187.

[87] DELFTship maritime software. *DELFTship: Visual hull modelling and stability analysis*. n.d. URL: https://www.delftship.net/ (visited on 02/01/2024).

[88] Orcina Ltd. *OrcaFlex key features and technical specification*. 2022. URL: https://www.orcina.com/orcaflex/specification/ (visited on 03/30/2023).

[89] M.A.R. Irkal, S. Nallayarasu, and S.K. Bhattacharyya. "CFD approach to roll damping of ship with bilge keel with experimental validation". In: *Applied Ocean Research* 55 (2016), pp. 1–17.

[90] ITTC. *Recommended procedures - Numerical estimation of roll damping*. Tech. rep. International Towing Tank Conference, 2011.

[91] Orcina Ltd. *Data: Constraints*. n.d. URL: https://www.orcina.com/webhelp/OrcaWave/Content/html/Data,Constraints.htm#RollDampingAsPercentOfCritical (visited on 07/10/2023).

[92] Orcina Ltd. *General data: Dynamics*. 2022. URL: https://www.orcina.com/webhelp/OrcaFlex/Content/html/Generaldata,Dynamics.htm (visited on 04/06/2023).

[93] Ulstein. *HX118 heavy lift crane vessel design*. n.d. URL: https://ulstein.com/vessel-design/hx118 (visited on 05/04/2023).

[94] R.M. Isherwood. "A revised parameterisation of the Jonswap spectrum". In: *Applied Ocean Research* 9.1 (1987), pp. 47–50.

[95] K.E. Thomsen. *Offshore wind: a comprehensive guide to succesful offshore wind farm installation*. Academic Press, 2014.

[96] DNV. *Environmental conditions and environmental loads*. 2021.

[97] S. Brans. "Applyng a Needs Analysis to promote Daughter Craft for year-round access to far-offshore wind turbines". Master's thesis. Delft University of Technology, 2021.

[98] MetOcean Solutions. *Mean significant wave height*. 2020. URL: https://app.metoceanview.com/hindcast/.

[99] J. Jiao et al. "Reproduction of ocean waves for large scale model seakeeping measurement: The case of coastal waves in Puerto Rico and Virgin Islands and Gulf of Maine". In: *Ocean Engineering* 153 (2018), pp. 71–87.

[100] Oil Companies International Marine Forum. *Prediction of Wind and Current Loads on VLCCs*. London, United Kingdom: Witherby and Co., 1994.

[101] L.S. Lasdon et al. "Design and Testing of a Generalized Reduced Gradient Code for Nonlinear Programming". In: *ACM Transactions on Mathematical Software* 4.1 (1978), pp. 34–50.

[102] International Maritime Organization. *Effect of free surface of liquids in tanks*. 2022. URL: https://imorules.com/GUID-A33918B2-CC1D-4250-96B6-37B19E8A41A3.html (visited on 10/08/2023).

[103] C.H. Mortimer. "Lake Hydrodynamics". In: *Internationale Vereinigung für Theoretische und Angewandte Limnologie: Mitteilungen* 20.1 (1974), pp. 124–197.

[104] BV. *Guidelines for Moonpool Assessment*. Tech. rep. Bureau Veritas - Marien and Offshore Division, 2016.

[105] Orcina Ltd. *Knowledge Base Article: Discretisation of Spar Buoys in OrcaFlex*. Tech. rep. Orcina, 2018.

[106] Orcina Ltd. *6D buoy theory: Spar buoy and towed fish drag*. n.d. URL: https://www.orcina.com/webhelp/OrcaFlex/Content/html/6Dbuoytheory,Sparbuoyandtowedfishdrag.htm#SparBuoyTheoryDragForces (visited on 12/08/2023).

[107] J.R. Morison et al. "The Force Exerted by Surface Waves on Piles". In: *Journal of Petroleum Technology* 2 (5 1950), pp. 149–154.

[108] Orcina Ltd. *Knowledge Base Article: Explicit modelling of floater superstructures*. Tech. rep. Orcina, 2019.

[109] D.T. Greenwood. *Advanced Dynamics*. Cambridge University Press, 2006.

[110] P. de Casteljau. *Mathématiques et C.A.O. Tome 2: Formes à pôles*. Paris, France: Hermes, 1985.

[111] Orcina Ltd. *Line statics: spline*. n.d. URL: https://www.orcina.com/webhelp/OrcaFlex/Content/html/Linestatics,Spline.htm (visited on 01/14/2024).

[112] C. Vuik et al. *Numerical Methods for Ordinary Differential Equations*. Second edition. Delft Academic Press, 2016.

[113] J. Chung and G.M. Hulbert. "A time integration algorithm for structural dynamics with improved numerical dissipation: the generalized-α method". In: *Journal of Applied Mechanics* 60.2 (1993), pp. 371–375.

[114] Orcina Ltd. *Dynamic Analysis: Time domain solution*. n.d. URL: https://www.orcina.com/webhelp/OrcaFlex/Default_Left.htm#StartTopic=html/Generaldata,Logging.htm%7CSkinName=Web%20Help (visited on 12/15/2023).

[115] P. Chr. Sandvik. "Estimation of Extreme Response from Operations Involving Transients". In: *Proceeding of the 2nd Marine Operations Specialty Synpmosium (MOSS)* (2012).

[116] C. Yin and A. McKay. "Model Verification and Validation Strategies and Methods: An Application Case Study". In: *The 8th International Symposium on Computational Intelligence and Industrial Applications* (2018).

[117] prof. ir. J. Gerritsma. *Hydromechanicca 4 - Scheepsbewegingen, sturen en manoeuvreren*. Dictate. TU Delft - Werktuigbouwkunde en Maritieme Techniek, sectie Scheepshydrodynamica, n.d.

[118] ir. J. Pinkster and ing. C.J. Bom. *MT2431 Geometrie en Stabiliteit II*. Dictate. TU Delft - Faculteit 3mE Maritieme Techniek, 2016.

[119] DNV. *Rules for classification of Ships - Part 3 Chapter 1 - Hull structural design - Ships with length 100 metres and above*. Høvik, Norway: Det Norske Veritas AS, 2016.

[120] J.D. Stroo. *Presentation: U-stern CFD in waves Rev 04*. Presentation. Ulstein Design and Solutions B.V., 2022.

[121] J.P.C. Kleijnen. "Verification and validation of simulation models". In: *European Journal of Operational research* 82 (1995), pp. 145–162.

[122] M. Dam. "Monopile installation assessment". Master's Thesis. Delft University of Technology, 2017.

[123] Huisman Equipment. *Technical Specification - TMC 270000-5000*. Tech. rep. Huisman Equipment BV, 2021.

[124] Orcina Ltd. *Results: Extreme value statistics results*. n.d. URL: https://www.orcina.com/webhelp/OrcaFlex/Content/html/Results,Extremevaluestatisticsresults.htm (visited on 01/17/2023).

A

Modal analysis

The contents of this appendix are excluded from the repository due to confidentiality reasons.

B

Additional results

The additional results in this appendix are presented for side and stern installation.

B.1. Side installation

Results of the operational limits for side installation for a maximum roll and pitch angle of $3.5\,^{\circ}$, maximum DAF of 1.15, and a maximum DUF of 1.00.

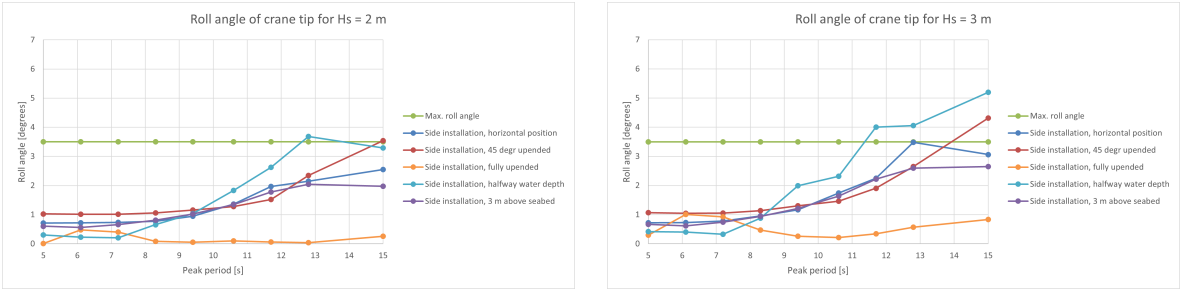

(a) H_s = 2 m **(b)** H_s = 3 m

Figure B.1: Roll angle [°] for side installation

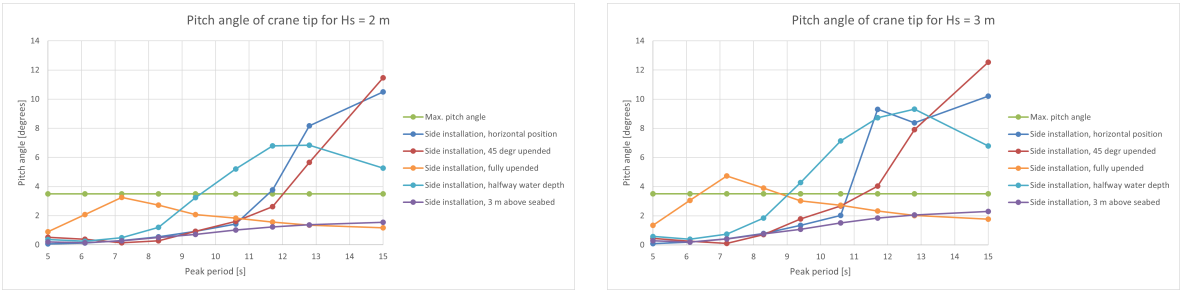

(a) H_s = 2 m **(b)** H_s = 3 m

Figure B.2: Pitch angle [°] for side installation

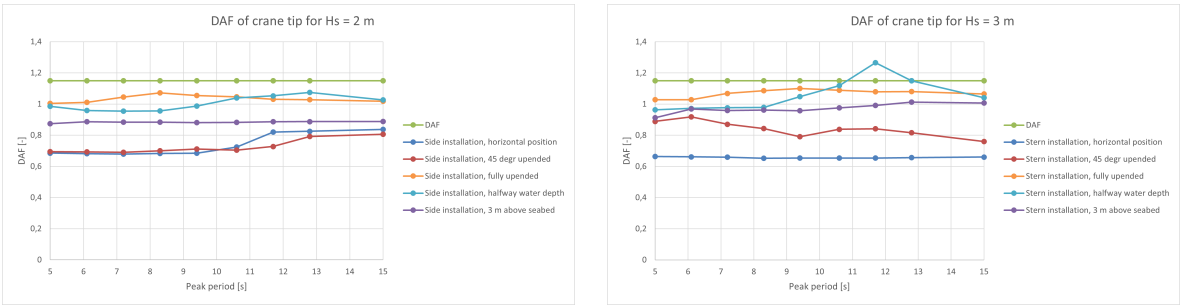

(a) H_s = 2 m **(b)** H_s = 3 m

Figure B.3: DAF of crane tip [-] for side installation

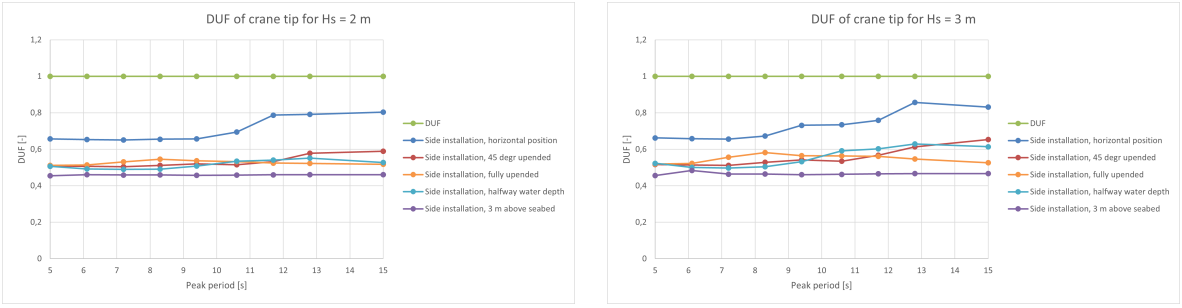

(a) H_s = 2 m **(b)** H_s = 3 m

Figure B.4: DUF of crane tip [-] for side installation

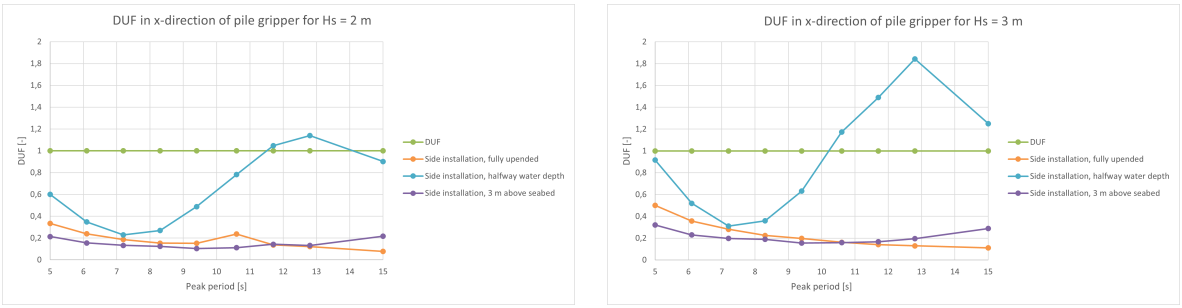

(a) H_s = 2 m **(b)** H_s = 3 m

Figure B.5: DUF of pile gripper in x-direction [-] for side installation

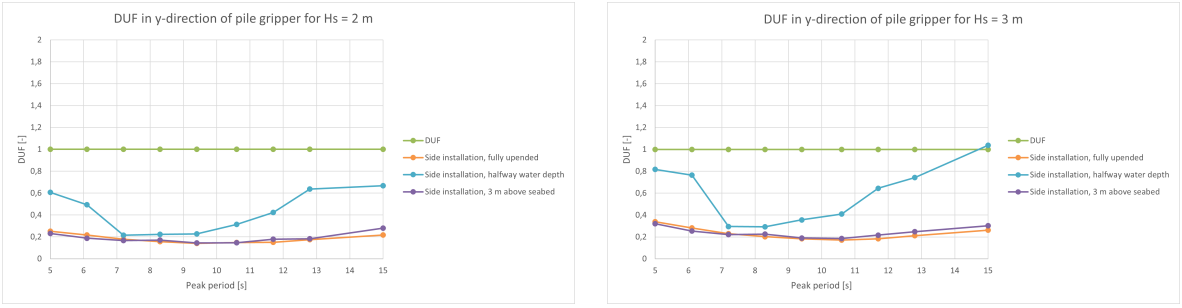

(a) H_s = 2 m **(b)** H_s = 3 m

Figure B.6: DUF of pile gripper in y-direction [-] for side installation

B.2. Stern installation

Results of the operational limits for stern installation for a maximum roll and pitch angle of 3.5 °, maximum DAF of 1.15, and a maximum DUF of 1.00.

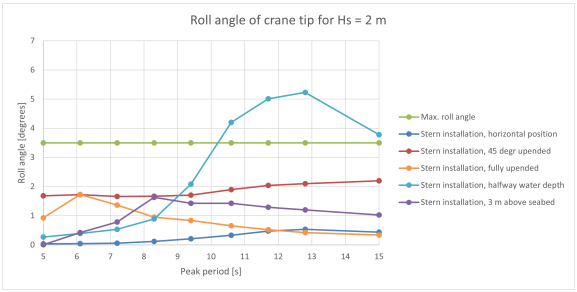

(a) H_s = 2 m

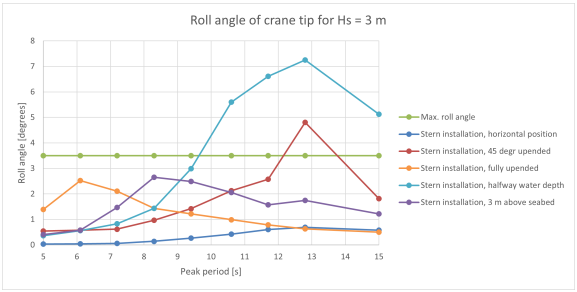

(b) H_s = 3 m

Figure B.7: Roll angle [°] for stern installation

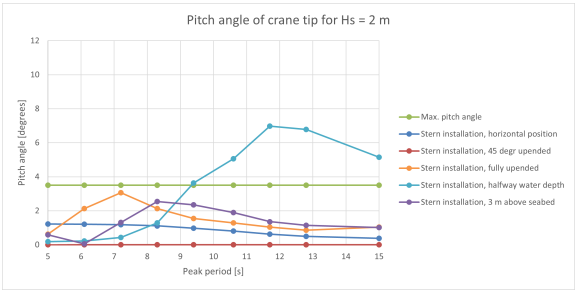

(a) H_s = 2 m

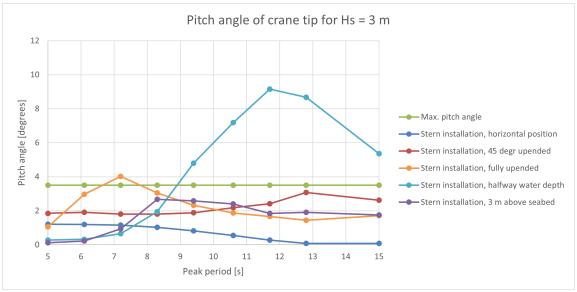

(b) H_s = 3 m

Figure B.8: Pitch angle [°] for stern installation

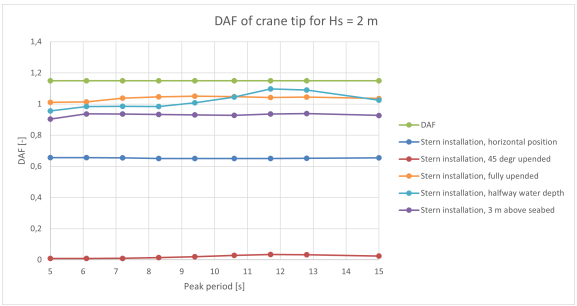

(a) H_s = 2 m

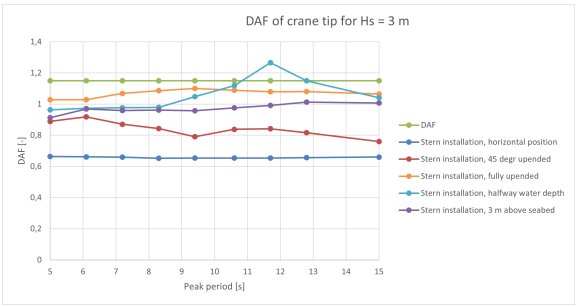

(b) H_s = 3 m

Figure B.9: DAF of crane tip [-] for stern installation

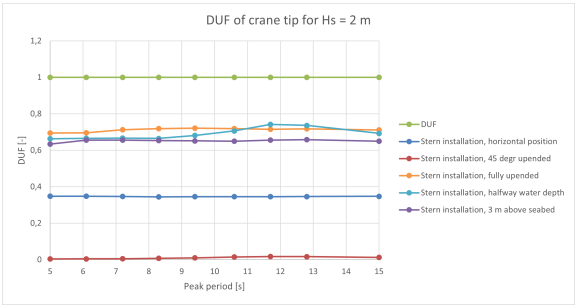

(a) H_s = 2 m

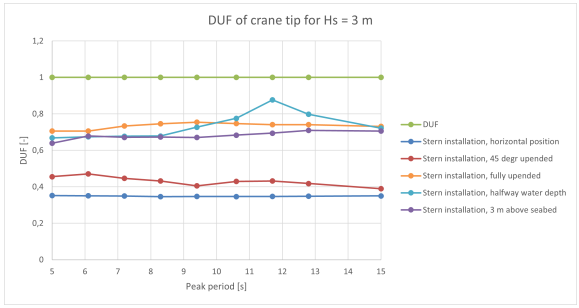

(b) H_s = 3 m

Figure B.10: DUF of crane tip [-] for stern installation

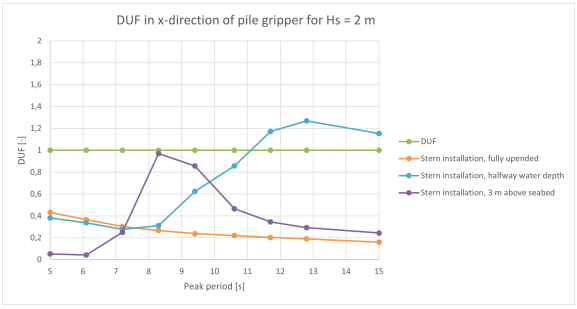

(a) H_s = 2 m

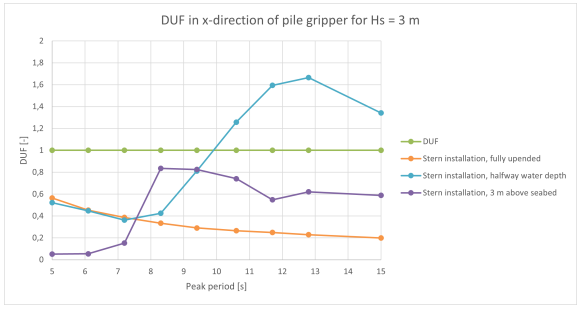

(b) H_s = 3 m

Figure B.11: DUF of pile gripper in x-direction [-] for stern installation

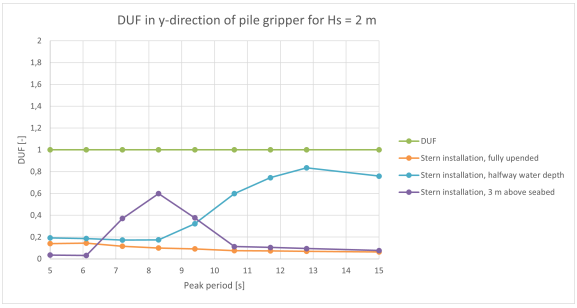

(a) H_s = 2 m

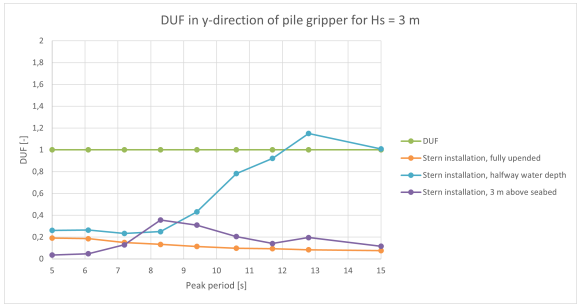

(b) H_s = 3 m

Figure B.12: DUF of pile gripper in y-direction [-] for stern installation

B.3. Side installation - max. pitch angle of 6 °

Results of the operational limits for side installation for a maximum roll and pitch angle of 6.00 ° and a maximum DUF of 1.00. The DAF of the crane tip and the DUF of the pile gripper ring is not affected compared to Appendix B.1 and therefore not included in this appendix.

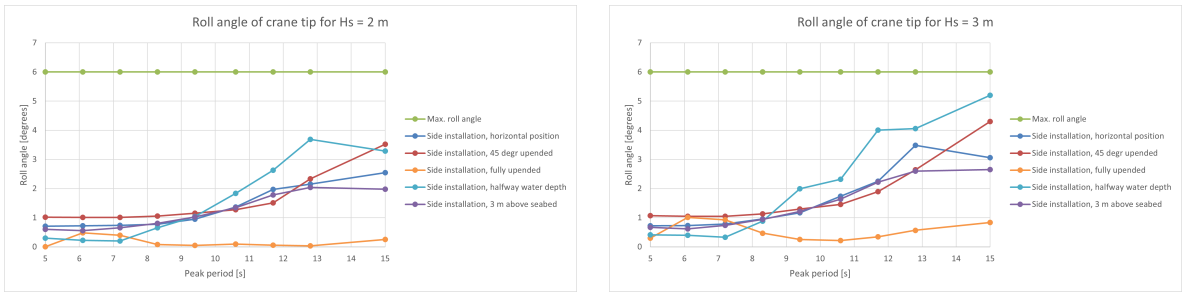

(a) H_s = 2 m **(b)** H_s = 3 m

Figure B.13: Roll angle [°] for side installation

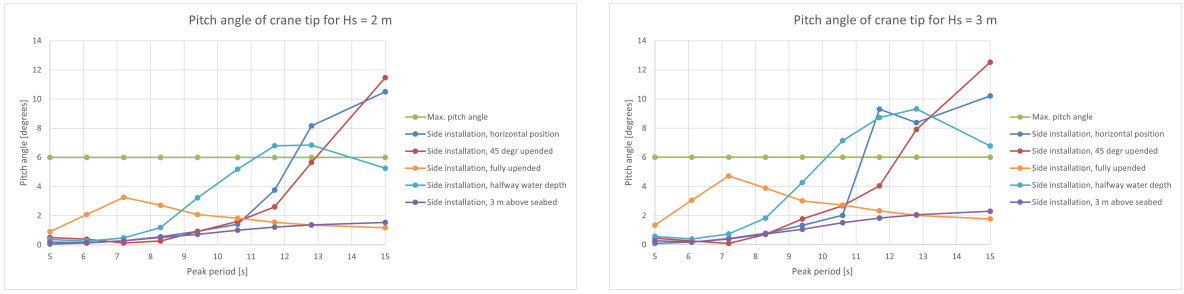

(a) H_s = 2 m **(b)** H_s = 3 m

Figure B.14: Pitch angle [°] for side installation

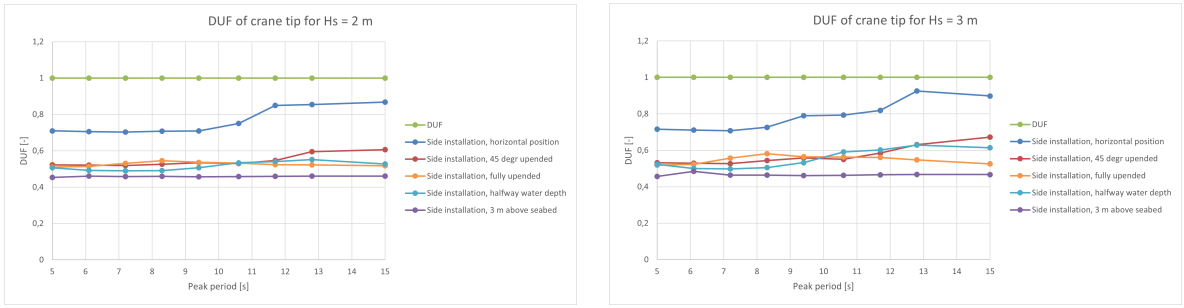

(a) H_s = 2 m **(b)** H_s = 3 m

Figure B.15: DUF of crane tip [-] for side installation

B.4. Stern installation - max. pitch angle of 6 °

Results of the operational limits for stern installation for a maximum roll and pitch angle of 6.00 ° and a maximum DUF of 1.00. The DAF of the crane tip and the DUF of the pile gripper ring is not affected compared to Appendix B.2 and therefore not included in this appendix.

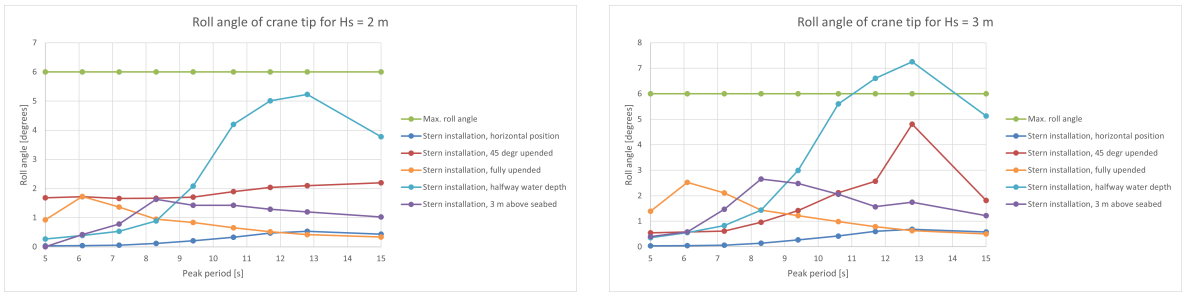

(a) H_s = 2 m **(b)** H_s = 3 m

Figure B.16: Roll angle [°] for stern installation

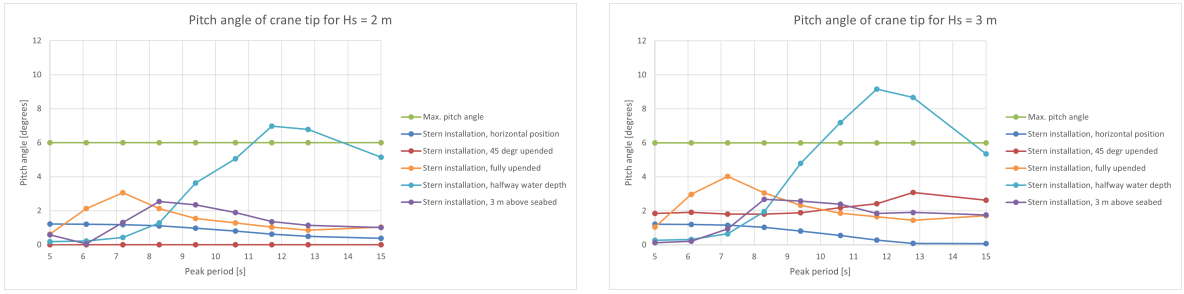

(a) H_s = 2 m **(b)** H_s = 3 m

Figure B.17: Pitch angle [°] for stern installation

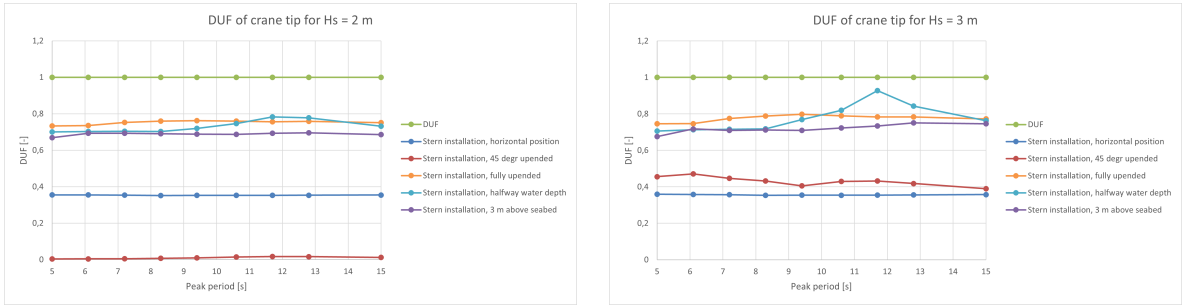

(a) H_s = 2 m **(b)** H_s = 3 m

Figure B.18: DUF of crane tip [-] for stern installation

C

Load and displacement RAOs

The contents of this appendix are excluded from the repository due to confidentiality reasons.